Cortico-Cortical Evoked Potentials to Probe Neuroplasticity: Methodological Considerations and Contextualization

Lila Hart Levinson

A dissertation submitted in partial fulfillment of
the requirements for the degree of

Doctor of Philosophy

University of Washington

2024

Reading Committee:
Jeffrey Ojemann,Chair
Steve Perlmutter, Chair
David Perkel

Program authorized to offer degree:
Neuroscience

University of Washington

Abstract

Cortico-Cortical Evoked Potentials to Probe Neuroplasticity:

Methodological Considerations and Contextualization

Lila Levinson

Co-Chairs of the Supervisory Committee:
Jeffrey Ojemann
Neurological Surgery

Steve Perlmutter
Physiology and Biophysics

Neuroplasticity is the set of processes that allow the brain to adapt to changing conditions, needs, and inputs. It is fundamentally important for learning, memory formation, habit formation, and recovery after a brain injury. While neuroplasticity has been characterized at the cellular level, much remains to be discovered about neuroplasticity in the living, human brain. The more we understand about neuroplasticity, the better equipped we will be to leverage neuroplasticity as a clinical tool for recovery after ischemic strokes and other injuries.

To study neuroplasticity in living humans, we need a way to measure connections in the brain and changes to those connections over time. Cortico-cortical evoked potentials (CCEPs) are one possible metric. CCEPs are stereotyped waveforms that can be recorded throughout the cortex in response to electrical stimulation at a single cortical site. They are a metric of effective connectivity and are interpreted as the sum of monosynaptic and polysynaptic inputs from a stimulated site to the neurons at a recording site. This makes them a useful tool for causal, directional inference about neural pathways. More directly, CCEPs measure the brain's response to electrical stimulation. Electrical stimulation is a proposed method for inducing neuroplasticity in the aftermath of a stroke, and as a stim-

ulation response metric, CCEPs may be particularly useful in tracking the efficacy of such treatments.

However, much remains unknown about the physiological underpinnings of CCEPs and the relationship between CCEPs and the functional and behavioral outputs of the brain. This limits conclusions that can be drawn from CCEP results. In this thesis, I address some basic, unanswered questions about CCEPs. I collected CCEP data in consenting human patients implanted with stereo-electroencephalography (sEEG), electrocorticography (ECoG), and/or deep brain stimulation (DBS) electrodes for intractable epilepsy or Parkinson's Disease. I quantitatively examine methodological considerations when choosing a data collection and analysis strategy. I also use other metrics of brain connectivity to contextualize CCEPs and work towards a clearer interpretation of their mechanisms and roles.

I found that sEEG CCEP results can be influenced by methodological choices including data processing techniques, the number of trials of data collected, the quantification approach, and the period over which CCEPs are collected. This work collectively demonstrates the importance of carefully considering and fully reporting all CCEP methodology. Additionally, I found that CCEPs are not always stable between recording sessions on multiple days, indicating that long-term studies utilizing CCEPs will need to account for potential variability and supporting the hypothesis that CCEPs may be brain state dependent. I also found little similarity between CCEPs and various established metrics of resting state functional connectivity (rsFC), which suggests that CCEPs measure network processes not captured by traditional rsFC analysis.

This dissertation aims to advance our understanding of CCEP mechanisms and functional significance by systematically approaching basic questions of methodological considerations and context that have often been overlooked. By more fully characterizing CCEPs, I also aim to lay the groundwork for studies to use CCEPs to measure neuroplasticity.

Contents

List of Figures

List of Tables

Chapter 1

Introduction

The brain is incredibly flexible. When your body or your environment change, your brain can reorganize to meet your new needs. Brains can reorganize by modifying the structure of neurons, the connections between neurons, and the behaviors produced when neurons fire [117]. This unique adaptability is called neuroplasticity, and is vital for learning new skills [38, 147, 157, 167, 196], forming and accessing memories [13, 61], and recovering from brain injuries, including strokes [137, 138, 44, 173].

In a stroke, part of the brain stops working. Depending on where the injury is located and other factors, this can make it harder to perform everyday tasks, regulate emotions, and/or move certain areas of the body [2, 140, 159, 186]. When stroke survivors regularly practice these lost functions in rehabilitative therapy, they can trigger neuroplasticity, allowing their brains to adapt to these new conditions [137, 138, 44, 173]. However, natural neuroplasticity alone is often not enough. Only about 15% of stroke survivors fully recover from stroke-related physical disability, even with rehabilitative therapies [80].

What if we could give neuroplasticity an extra boost to improve those odds? One way to do this would be to use electrical stimulation through devices implanted in the brain. With these devices, we could "engineer neuroplasticity," focusing and strengthening brain reorganization after a stroke or another injury to promote maximal recovery [132, 91, 71].

To create this technology, we will need to find the most effective ways of delivering electrical stimulation, which means we need to understand more about how the brain responds to stimulation. This requires accurate, meaningful ways of measuring how stimulation alters the connections in the brain. With these measurements, we will be able to assess how effectively stimulation triggers neuroplasticity and the kinds of reorganization it can induce.

In this dissertation, I investigate evoked potentials (EPs), one way of measuring connections in the brain and how they change during neuroplasticity. EPs are distinct responses that can be seen throughout the brain after stimulation is delivered [122]. They are a direct

way of measuring how a living organism's brain responds to electrical stimulation. However, EPs can be difficult to interpret, and the interpretation might change depending on the steps we take to collect and process the data.

I explore the neural basis of EPs, contributing to our understanding of the underlying connectivity of the human brain. I focus on how different approaches to analyzing EP data can affect results and how other types of measurements can complement and contextualize EPs. By rigorously and systematically approaching these basic questions, I aim to lay groundwork for future studies of engineered neuroplasticity.

1.1 Neuroplasticity and Injury Recovery

Brains are busy places, and the neurons that make up our brains need energy to keep everything working smoothly. That energy comes from oxygen, delivered by the blood. During a stroke, oxygen-rich blood can't make it to certain areas of the brain. Without their energy supply, the neurons in these areas will die.

At first, only neurons very close to the most oxygen-deprived areas of the brain will die. As they die, they send out electrical and chemical alarms to nearby cell signaling damage. As these signals spread outwards from the site of the stroke, cell death will also spread within a certain radius, with the most dead cells closest to the center of the injury [177].

Information needs to travel between different areas of the brain for us to accomplish basic tasks like moving and speaking. When neurons die in a stroke, they can no longer relay this kind of information, disrupting these basic functions. This is why stroke survivors often have disabilities after their injuries, and why rehabilitation therapy is commonly prescribed.

During rehabilitation, stroke survivors repeatedly practice activities that have become harder since their injuries. As they practice, their brains begin to adjust to their new conditions of life, and these activities may slowly become easier [137, 138, 44, 173]. This is neuroplasticity at work — the brain is reorganizing itself in ways both large and small.

Neuroplasticity includes both structural and functional components. Structural neuroplasticity has to do with physical changes in the neurons, like partially damaged neurons growing back and forming new connections. Functional neuroplasticity has more to do with the ways the neurons behave. Although both structural and functional neuroplasticity may happen in parallel, I will focus on the functional changes to neurons associated with rehabilitation neuroplasticity.

One example of functional neuroplasticity is the strengthening of pathways that have been spared in an injury. As we learn and practice activities to form habits, we can trigger neuroplasticity to build strong connections among different areas of the brain [24, 135, 141].

These connections are like information highways that allow signals to pass efficiently through networks. A stroke is like damage to the highway that makes it difficult or impossible for information to get through the damaged brain area, meaning brain areas that were previously strongly connected may no longer have those connections. After a stroke, signals need to travel on less efficient routes (more like surface streets than like highways). However, as a stroke survivor practices the tasks that require information to travel this way, these longer routes can become more efficient, re-strengthening the connections that were lost in the injury [3, 21]. As these connections become strong and efficient again with ongoing practice, the stroke survivor may be able to regain some of the function that was initially lost.

Another related neuroplasticity process is functional remapping, which happens when functions associated with an area of the brain that was damaged during an injury find new homes elsewhere in the brain. Nudo et al. demonstrated this type of reorganization in a 1996 study in which squirrel monkeys were trained to retrieve food from small wells using their fingers and subsequently given strokes in an area of the brain that controls finger movement [138]. After intensive rehabilitation therapy, areas of the monkeys' brains previously associated with control over the elbow and shoulder muscles took over finger and hand control functions which were lost in the stroke [138]. Along with these changes, the monkeys improved at the food retrieval tasks.

The process of neuroplasticity occurs naturally during rehabilitation therapies, but it is often not enough to fully compensate for the functions lost during a stroke [80]. This is where engineered neuroplasticity may provide additional opportunities for improving recovery outcomes. Engineered neuroplasticity could include interventions to put the brain in an optimal state for strengthening existing pathways and functionally remapping. It could also potentially allow clinicians to focus the process of neuroplasticity by "suggesting" pathways for information and areas of the brain to take over lost functions and reinforcing change along these possible routes.

A previous clinical trial in stroke patients piloted the use of electrical stimulation to induce neuroplasticity and, thus, recovery. This trial, called EVEREST, showed early promise in a small study [85] but yielded mixed results in a subsequent larger study [107]. EVEREST was terminated when it did not reach anticipated milestone, so we still do not have strong evidence that stimulation-induced neuroplasticity will be an effective treatment for stroke. The limitations of the EVEREST study, as well as the outline of a proposed new clinical trial, are discussed further in Section 1.6. To understand the theoretical underpinnings of EVEREST and other engineered neuroplasticity studies, we will first review existing research of neuroplasticity from the level of neurons up to the level of living human brains.

1.2 Functional neuroplasticity at the level of neurons

Changes in the functions of neurons underlie the changes in neural circuits and mapping associated with neuroplasticity. In his 1949 book, The Organization of Behavior, psychologist Donald Hebb described a model of cellular neuroplasticity that is still a guidepost for research into the subject. Hebb's model suggests that if two areas of the brain are activate in the same processes enough times, those areas will become more strongly connected [78].

Evidence supporting this model emerged over the following decades, and experiments have uncovered different processes that fall under the umbrella of neuroplasticity. Many foundational neuroplasticity experiments examined this model at the level of individual neurons [14, 48, 12]. These experiments isolated a single synapse — a junction connecting one neuron to the other. Generally, synapses are one-way — neuron A sends signals to neuron B, but neuron B doesn't send signals to neuron A at the same synapse.

Action potentials are the basis of communication at a synapse [11]. During an action potential, a neuron very briefly "turns on," or fires, then "turns off" again. But action potentials are more complicated than an on/off button. They are complex signals involving both electrical and chemical changes to a neuron [11].

When neuron A fires an action potential, it passes on those electrical and chemical changes to neuron B. If the changes are large enough to meet a set of biophysical conditions, neuron B will fire an action potential. One action potential from neuron A may not make neuron B cross that threshold, but when neuron A fires a string of action potentials, the changes may accumulate enough to make neuron B fire.

To isolate just one synapse, researchers can take advantage of the electrical properties of neurons. They look for two neurons under a microscope and insert electrodes with ultrafine tips into the neurons. The electrodes record electrical changes in the neurons. These recordings show when each neuron fires an action potential and the changes that don't meet the threshold to fire an action potential. Those changes appear as a distinct signature in neuron B called an excitatory post-synaptic potential (EPSP). The voltage of the EPSP is a measure of how strong the synapse is. If neurons A and B are strongly connected, the EPSP will be large and may even result in an action potential, indicating a strong synapse. Smaller EPSPs indicate weaker synapses.

The electrodes inside the neurons can use electrical stimulation to cause changes in the neurons as well as record them. By introducing a small amount of electric current into a neuron through the electrodes, experimenters can make enough change (depolarize the neuron enough) to meet the threshold for that neuron to fire an action potential [87]. The electrodes can also adjust the electrical properties of a neuron (hyperpolarize the neuron) to

prevent it from firing.

These micro-electrodes provide the three main tools of neuroplasticity experiments — recording (measuring how the voltage of the neurons changes over time), stimulation (causing one or both neurons to fire action potentials at specific times), and a metric of how strongly the neurons are connected (EPSPs and action potentials).

Foundational neuroplasticity experiments used these tools to test hypotheses about the mechanisms that can drive neuroplasticity. Based on natural firing patterns in the brain, experimenters developed patterns of stimulation in neuron A and/or neuron B. In their experiments, they then delivered that stimulation and measured if there were any changes in the strength of the synapse using EPSPs and action potentials. Most experiments followed a three-part format. After isolating a single synapse, they measured the size of EPSPs in neuron B after action potentials in neuron A to establish how strong the synapse was before any manipulation. Then, they delivered their pattern of stimulation to one or both neurons. Finally, they measured EPSPs again to see if the strength of the synapse had changed after the stimulation.

Experiments using this three-part approach identified long-term potentiation (LTP) as one process that can produce neuroplasticity in a synapse. Bliss and Lømo demonstrated that by making neuron A fire many times in quick succession, they could strengthen the synapse between neurons A and B [14]. Dudek and Bear demonstrated the opposite effect, which they called long-term depression (LTD). LTD happens when neuron A is forced to fire very infrequently, making the synapse weaker [48].

Bi and Poo observed another mechanism of neuroplasticity, which they called spike-timing dependent plasticity (STDP) [12]. In their experiment, they controlled when both neurons fired. First, they forced neuron A to fire, waited for various intervals up to about 100 milliseconds, then made neuron B fire. They found that if neuron B fired within about 20 milliseconds of neuron A, EPSPs got larger, indicating that the synapse got stronger [12]. They also tested what happened at these delays if neuron B fired before neuron A. Again, they saw an effect if the neurons fired within about 20 milliseconds of one another, but this time the EPSPs got smaller, indicating a weakening of the synapse [12].

While these experiments can help guide approaches to engineering neuroplasticity in human brains, the methods they used were best suited to examining cells in petri dishes, anesthetized lab animals, or slices of brain tissue, where it is possible to isolate a single synapse. It is very difficult to isolate a single synapse in a living, human brain. Instead of looking at individual neurons, human neuroplasticity experiments tend to look at larger areas of brain. The connections between brain areas are more complex than the connections in one synapse, which has made it harder to identify stimulation patterns that can create

neuroplasticity than at the level of single neurons.

To study neuroplasticity at this larger scale, we can still use the three-part format of measuring the strength of connections, delivering stimulation, and then seeing if the connection strength changed. But we need counterparts of the three tools that single-synapse studies use — a way to record brain activity, a way to stimulate the brain, and a way to measure how strongly different areas of the brain are connected. The following sections examine tools to accomplish these three goals in a living, human brain.

1.3 Measuring brain activity

The plasticity experiment described thus far look at one synapse in relative isolation, with full control over both neurons. This is very difficult to achieve in a living human brain [143], which has billions of neurons, each with an average of 7000 synaptic connections [144].

While we can't easily measure a single synapse in the human brain, we can study larger areas using implanted electrodes. Implanting electrodes in the brain is a highly invasive procedure done in certain clinical scenarios. One population of patients who often have electrodes implanted are people with epilepsy that is not responding to medications and who are candidates for surgical removal of the area of the brain where seizures are originating [25, 53, 54, 101]. These patients are implanted with electrodes on the surface of the brain (electrocorticography, ECoG) and/or penetrating into the brain (stereo-electroencephalography, sEEG). Patients typically remain in the hospital for about a week after implant, while neurologists, epileptologists, and surgeons collect data on their seizures and determine if surgical removal of abnormal tissue will be possible. During that week of observation, many patients consent to take part in research studies. Most of the data presented in this dissertation come from studies run during that period in research participants implanted with penetrating sEEG electrodes, with some data from ECoG electrodes as well.

sEEG electrodes are embedded in cylindrical shafts of 0.8-2mm in diameter [126]. Each shaft, or probe, contains 4-16 electrodes, each about 2mm long and spaced so that their centers are 5-10mm apart. Probes are implanted through small burr holes drilled in the patient's skull. Their length allows them to span the many layers of the human brain and reach anatomical structures below the surface. In contrast, ECoG consists of larger, disc-shaped electrodes that are placed directly onto the surface of the brain and are therefore unable to record from these deeper areas.

Each sEEG electrode records neurons in approximately a 5mm3 sphere around it [49, 113], likely encompassing activity from hundreds of thousands of neurons. sEEG recordings can't tell us whether a certain neuron is firing at any given moment, but the principle of

recording electrical activity is still similar as at the level of individual neurons. Essentially, the electrodes record the net electrical output of many, many nearby synapses. If interpreted properly, these data can tell us how active this small area of the brain is. Recordings can be done at many sites simultaneously — patients typically have 100+ electrodes implanted at a time — and comparing the resulting signals across areas can also give us information about networks of interconnected activity across the brain.

1.4 Stimulating the brain

In addition to recording the brain, sEEG electrodes, like the electrodes used to measure individual synapses, can use electrical stimulation to change the activity of nearby neurons, although on a much larger scale than their microscopic counterparts [181]. Depending on the parameters used and the position of the electrodes, electrical stimulation delivered through sEEG electrodes can increase and/or decrease the likelihood of nearby neurons firing [15]. The likelihood of firing increases when the stimulation changes a neuron's electrical properties to be more like the state the neuron needs to be in to fire. The likelihood decreases when the stimulation causes the neuron to get farther from that state. This will depend on what part of the neuron is stimulated, how the neuron is oriented relative to the electrode [102], and the electrical properties of the stimulation [160], including the configuration and polarity.

Stimulation configuration refers to the path that electrical charge follows after it is put into the brain. That current needs somewhere to go, and there are two main categories of configuration for dealing with this. One is monopolar stimulation, in which stimulation is sent out through a single electrode then passes through tissue to a grounding electrode that is located far away, generally in a region that is not of interest. This grounding electrode completes the circuit by returning the current to the stimulating device, but it plays a passive role in the stimulation process. The alternative is bipolar stimulation in which two electrodes, usually neighboring electrodes, play an active role. In bipolar stimulation, the electric current stays in closed circulation between the two electrodes, keeping the neuron activation more localized [136]. Electrical stimulation can also be delivered with either a positive or negative current (cathodic and anodic stimulation, respectively), with cathodic stimulation tending to affect deeper areas of the brain than anodic stimulation [160]. Other properties of stimulation that can affect neural activation include the amount of current delivered [75, 76] and the time over which the current is delivered [77].

As the neurons near the stimulation site fire, they activate other neurons that they are connected to via synapses. This gives us the opportunity to measure the networks of connections spreading out from the stimulation site (see Section 1.5). If a large enough

amount of electrical current is delivered via stimulation, enough neurons may fire throughout a network to produce an observable behavioral output. Depending on the area that is stimulated, this could include muscle movements, disruptions in the patient's ability to speak, and the patient "feeling" sensations like they are being touched [93, 33]. Systematically delivering high current stimulation across different brain areas and measuring reports of sensations or changes in behavior has long been a tool for mapping functions onto cortical areas [149]. Clinical teams may also perform functional mapping during neurosurgery to ensure that they do not remove or damage tissue associated with vital functions such as language [115, 190, 179]. In epilepsy patients, clinical mapping is often done during the observation interval between electrodes being implanted and surgery to remove the area where seizures are originating.

Electrical stimulation through implanted electrodes is also becoming more common for treating a variety of diseases. Deep Brain Stimulation (DBS) was initially developed for treating Parkinson's Disease by stimulating in the brain areas that are largely responsible for the movement-related symptoms of Parkinson's [185]. Implanting DBS devices in other areas of the brain is also promising treatment for depression [92, 189], obsessive-compulsive disorder [65, 114], and chronic pain [162, 63], among other conditions. Despite the efficacy of these therapies, the basic mechanisms of DBS are not completely understood. DBS is explored more fully in Chapter 4 of this thesis.

The foundational neuroplasticity experiments discussed in Section 1.2, required electrodes that could record and stimulate neurons, but also a third component — metrics of the strength of connections between neurons. In these experiments, EPSPs and action potentials were typically the metrics of choice. Electrical stimulation provided two distinct functions in these experiments. It was used to induce neuroplasticity, but it was also used to trigger and measure EPSPs and action potentials. Likewise, the large-scale stimulation methods discussed in this section, in combination with the recording methods discussed in Section 1.3, can be used to induce neuroplasticity and to measure connections in the brain.

1.5 The effects of stimulation: evoked potentials

The connections that can be measured with sEEG and ECoG recording and stimulation are not connections between neuron A and neuron B, as in previous experiments. Because of the scale of these electrodes, they instead measure connections between larger areas of the brain. We can think of these sites as site A and site B, analogous to neurons A and B but composed of hundreds of thousands of neurons. Stimulation at neuron A caused an EPSP or an AP at neuron B. Likewise, by essentially scaling up the same protocol and stimulating

at site A, we can observe a large-scale analog of an EPSP called an evoked potential (EP — this acronym pulls from the E and the *second* P of EPSP) at site B.

As discussed in the previous section, stimulation through a bipolar pair of sEEG electrodes at site A will cause nearby neurons to fire. Each neuron will pass this signal along to many other neurons that it is connected to via synapses. If many synapses connect site A to site B, near a different electrode, neurons at site B will likely receive these signals and fire in response. When the connections from site A to site B are strong enough, the recorded signal at site B will have a distinct electrical signature that keeps a consistent shape every time site A is stimulated. This electrical signature is the EP. EPs grossly resemble responses in the brain to sensory inputs such as light and touch [109]. Stimulation to measure EPs happens at a much lower intensity (i.e., with less electrical current) that stimulation used for clinical mapping.

While EPSPs last on the order of milliseconds, EPs last longer, on the order of hundreds of milliseconds [122]. During that time, the electrical signal at site B will increase and decrease one or more times, creating peaks and valleys, which are called EP components. Measuring the height of the peaks and valleys can give us a sense of how strongly site A is connected to site B. Higher peaks and/or lower valleys are generally interpreted to mean a stronger connection, reflective of many synapses carrying information from site A to site B [97].

The earliest components of EPs typically occur within 20ms of stimulation [120, 99]. It is hypothesized that these components reflect pathways involving only one synapse (i.e., monosynaptic), with neurons originating in site A directly signaling to neurons in site B [120, 99]. The earliest component is therefore often of interest in EP studies, as it is interpreted as the most direct measure of connectivity [122, 120]. Even though many neurons are firing at once in response to electrical stimulation, there is some variability in the timing of firing, which means even this fast component lasts longer than a single EPSP would, leading to the distinctive broad, blunt peak of an EP [120].

After this early response, there are often additional peaks and valleys lasting for approximately 500ms, a timescale that cannot be explained by the fast activity of individual synapses. Rather, these later components are interpreted as the signals sent through longer pathways involving more than one synapse (i.e., polysynaptic) [120, 99]. Evidence from animal studies suggests that some of these pathways may go through the thalamus, a structure deep in the brain that is involved in processing and relaying signals [168]. It is also possible that the slower components reflect activity from neurons that were stimulated such that the signals did not travel forwards (towards a synapse) but traveled away from the synapse instead [120, 99]. If these neurons were primarily located near site B, the electrodes could

pick up on this antidromic (backwards-moving) activation. However, in animal experiments, this type of activation was rarely observed [57].

Multi-component EPs likely reflect a sum of all these pathways, including monosynaptic, polysynaptic, and antidromic signaling and signaling via the thalamus. As previously discussed, many studies measure the amplitude, or height, of EP peaks and troughs as an indirect metric of the strength of the connections between sites A and B. Variations on this include measuring the difference between consecutive peaks and troughs. Another measure of the size of EPs is a root mean squared, which is a normalized measure of the area under the curve of one or more components. To describe EPs more fully, it is also common to look at the latency of peaks and troughs, or the time that passes between stimulation onset and the component reaching its maximum. For a review of literature using each of these metrics, see Appendix A.

It is important to note that while most EPs exhibit multiple components, the timing and shape of these components can also vary greatly between recording sites [128]. This means that trying to measure individual components and connect them to specific physiological responses has limited utility when interpreting EPs across the brain. The root mean square is a useful metric when accounting for this variability because it can be measured without defining component peaks and valleys. Recent work has also investigated other metrics that could describe the shape and size of EPs without assuming anything about the component makeup [128, 164].

Physiological responses to electrical stimulation in the brain have been observed since the middle of the twentieth century [154, 155, 66], but Matsumoto et al. introduced EPs as a tool for probing brain connectivity in the early 2000s [122, 120]. EPs have since become commonly used in research with epilepsy patients and other populations with implanted electrodes [190, 99, 104, 180]. In addition to using EPs to map networks associated with functional outputs such as language [122, 180] and movement [120, 88], EPs have also been used to investigate properties of the brain associated with epilepsy [105, 161, 52, 100, 51]. They have also been piloted as a tool for clinicians to identify the area of the brain where seizures are located [75, 195, 194, 94, 90, 72] and to map the functions of brain areas during neurosurgery [115, 190]. EPs have also been used to track changes in brain connections in preliminary studies of engineered neuroplasticity [97, 20, 192].

1.6 Neuroplasticity in living human brains

Human neuroplasticity studies, like cellular studies, tend to follow a three-part structure. First, EPs are measured to estimate the baseline level of connection between the two sites.

Then, something is done that might induce neuroplasticity. EPs are then measured again to see if the level of connection changed as a result.

Experiments in humans and nonhuman primates have attempted to replicate neuron-level neuroplasticity findings as directly as possible, using similar patterns of stimulation. For example, instead of making a neuron fire quickly many times as in LTP, Keller et al. delivered fast electrical stimulation to one area of the brain [97]. They saw both increases and decreases in EP size after this fast stimulation depending on the locations of sites A and B. This is less consistent than cellular LTP, reflecting the higher complexity and lower ability to control the experiment in a living human brain. Human [20] and nonhuman primate [192] studies have also seen changes in EPs after STDP-like electrical stimulation, though again their findings were not as straightforward as in neurons. Increases and decreases in EP size after LTP-, LTD-, or STDP-like stimulation don't necessarily mean that LTP, LTD, and STDP are happening at the synapses connecting site A to site B. The many complex pathways, both monosynaptic and polysynaptic, connecting the sites make it difficult to draw conclusions about the mechanisms underlying this change. But large-scale plasticity experiments drawing from what is known about neuron-level plasticity can reveal overall features of neuroplasticity in a living human brain. This can point us towards ways to harness neuroplasticity for medical treatments.

As briefly discussed in Section 1.1, the EVEREST trials provided mixed results about the potential efficacy of electrical stimulation for engineered neuroplasticity following a stroke [85, 107]. Notably, EVEREST relied primarily on only one of the three tools outlined in Sections 1.3-1.5 — electrical stimulation. Recordings of brain activity, taken with noninvasive imaging tools rather than electrodes, guided the areas chosen for stimulation in each patient, but stimulation was not adjusted based on the activity of the brain at any given time. EPs were not used. The primary measurement of if neuroplasticity was occurring was if the patients' ability to move improved over time. While functional improvement is the desired ultimate outcome of engineered neuroplasticity therapies, it is not the most sensitive measurement of change and gives little direct information about what may be happening in the brain.

Our research group has proposed a new clinical trial studying electrical stimulation for stroke rehabilitation, building on the findings of EVEREST. This new proposal takes advantage of the opportunities for recording brain activity and measuring connections using EPs. Unlike the EVEREST study, which delivered stimulation at set intervals, we propose a methodology where stimulation is triggered by recorded changes in ongoing activity in the brain. We hypothesize that features of the recording can indicate when the brain may be at its most excitable — that is, when the neurons near the stimulation site are most likely to respond and their signals are most likely to get carried to the recording sites [83, 133,

134, 163]. If we deliver stimulation timed to correspond with peak excitability, we expect more targeted neuroplasticity induction than if we used stimulation that is not triggered by these peaks. Additionally, we plan to use EPs to track changes in the connectivity of the brain, not just in its functional outputs. A study in monkeys using a similar stimulation protocol caused short-term strengthening of CCEPs, suggesting that this is a viable metric of changes in cortical connectivity for this study [192]. This will give us more insight into the consequences of our stimulation and the mechanisms underlying any neuroplasticity that is induced. It will also provide more data about the relationship between EPs and brain functions by giving us the opportunity to test if changes in EPs are associated with any changes in behavior or recovery.

While the proposed study will deepen our understanding of EPs, the fact that EPs themselves are incompletely understood also provides a challenge when designing effective human neuroplasticity experiments and interpreting their results. As a tool primarily used in experiments with human clinical patients, where data collection opportunities are rare and time is precious, many fundamental aspects of EPs are understudied. Methods for measuring EPs and processing EP data are inconsistent across studies, and it is unclear how these inconsistencies could affect results. As discussed in in Section 1.5, the physiological mechanisms and meanings of EPs are not clear. To help fill these gaps in the methods and interpretation of EPs, I investigate the impact of different EP methods and try to contextualize EPs using other ways of measuring connections between brain areas.

1.7 Outline of dissertation and its goals

In this dissertation, I will lay vital groundwork for future studies of engineered neuroplasticity after strokes and other brain injuries. I will also explore the tools we use to study neuroplasticity and fundamental connectivity in living human brains.

In this introduction, I have used the general term evoked potential, which does not imply anything about the areas of the brain where either the stimulation or recording happen. However, the focus of this dissertation is EPs that are both evoked and measured in the cortex. The cortex includes most of the surface of the brain as well other areas involved in some of our more advanced functions. EPs evoked and measured in the cortex are referred to as cortico-cortical evoked potentials (CCEPs). Chapters 2, 3, and 5 focus on CCEPs. Chapter 4 focuses on EPs that are evoked outside of the cortex but measured in the cortex.

The first section of the dissertation deals with methodological considerations around CCEPs — that is, the process of collecting, analyzing, and measuring CCEPs in humans. While CCEPs are a relatively common research tool, there is wide variability in the way they

are used and a fundamental lack of understanding of how this variety can impact results.

In Chapter 2, I examine how the basic processing that most CCEP data goes through can impact the final measurements that we take from the CCEPs. While I offer a general set of guidelines for choosing a processing strategy, the point of this chapter is not to suggest a definitive, optimal strategy for CCEP processing. Rather, it is to highlight the importance of fully considering and reporting all processing steps taken with CCEP data to maximize interpretability and comparability across studies.

I discuss additional methodological questions in Chapter 3, all related to variability in individual trials that measure CCEPs. The number of trials used in CCEP studies varies widely through the literature, from as few as 10 to over 1000. I investigate how the number of trials used in a CCEP study can impact results and suggest that using 50 trials balances the requirements for stability and reliability of results against the clinical time constraints. In addition, I demonstrate that quantifying CCEPs using individual trials rather than a trial average can be advantageous in terms of stability and reliability, especially when few trials are available. Finally, I demonstrate that there is often a significant difference between CCEP trials measured on different days, suggesting that there may be natural fluctuation in CCEPs over time.

The second part of my dissertation examines EPs in the context of the rest of the brain. By comparing EPs to other, more established metrics of brain function, I hope to be able to better interpret what exactly EPs are measuring. In Chapter 4, I look at EPs measured in the cortex in response to DBS in patients who are being treated for Parkinson's Disease. Using stimulation parameters like those used in clinical DBS, I demonstrate the existence of two separate EPs — one ongoing during stimulation, and one immediately after stimulation onset. I show that these two types of EP have different relationships with ongoing brain activity, suggesting that they may be caused by different neural processes. This finding may provide insight into how and why DBS therapies work in treating Parkinson's Disease.

Finally, Chapter 5 compares CCEPs to other measurements of connectivity between different areas of the brain. Many of these other metrics have been linked to functional outputs and behaviors, so knowing which metrics are most like CCEPs could be indirect evidence tying CCEPs to those outputs and behaviors. I planned to compare findings in sets of patients who received stimulation in different anatomical areas of the brain to see if overlap between CCEPs and other metrics was location specific. However, results were highly inconsistent between subjects, including between subjects with similar stimulation sites, making such an analysis difficult. Although I did not establish any clear connections between CCEPs and other metrics of connectivity, this in and of itself may be useful for elucidating what CCEPs are — and are not — measuring.

Chapter 2

Data Processing Techniques Impact Quantification of Cortico-Cortical Evoked Potentials

Cortico-cortical evoked potentials (CCEPs) are a common tool for probing effective connectivity in intracranial human electrophysiology. As with all human electrophysiology data, CCEP data are highly susceptible to noise. To address noise, filters and re-referencing are often applied to CCEP data, but different processing strategies are used from study to study. We systematically compare how common average re-referencing and filtering CCEP data impacts quantification. We show that common average re-referencing and filters, particularly filters that cut out more frequencies, can significantly impact the quantification of CCEP magnitude and morphology. We identify that high cutoff high pass filters (greater than 0.5Hz), low cutoff low pass filters (less than 200Hz), and common average re-referencing impact quantification across subjects. However, we also demonstrate that the presence of noise may impact CCEP quantification, and preprocessing is necessary to mitigate this. We show that filtering is more effective than re-referencing or averaging across trials for reducing most common types of noise. These results suggest that existing CCEP processing methods must be applied with care to maximize noise reduction and minimize changes to the data. We do not test every available processing strategy; rather we demonstrate that processing can influence the results of CCEP studies. We emphasize the importance of reporting all processing methods, particularly re-referencing methods. We propose a general framework for choosing an appropriate processing pipeline for CCEP data, taking into consideration the noise levels of a specific dataset. We suggest that minimal gentle filtering is preferable.

2.1 Introduction

Evoked potentials (EPs) are stereotyped electrophysiological responses to stimulus, and can measured in vivo in humans, either extracranially or intracranially. Cortico-cortical evoked potentials (CCEPs) are EPs seen in response to electrical stimulation and are a measure of effective connectivity between broad areas of the brain. This stimulation is typically delivered directly to the cortex [55, 99, 104] or subcortex [45, 50] using electrocorticography (ECoG) or stereo-electroencephalography (sEEG) electrodes in humans. CCEPs have stereotyped morphology and can be seen throughout the brain (Fig. 2.1A) [99, 104]. In humans and nonhuman primates, CCEPs have confirmed and validated functional connectivity networks [59, 79, 98, 174], engendered new insights underlying the organizational structure of the brain [29, 122, 165], and been used as a baseline metric of brain state in testing of plasticity-inducing stimulation paradigms [86, 97].

However, there is great variability in the methodologies employed by CCEP studies, making it difficult to compare results across studies. While CCEP data collection (Section 2.1.1) and quantification (section 2.1.2) generally adhere to common protocols, across the literature the intermediate step of data processing prior to quantification (Section 2.1.4; Fig. 2.2) is highly variable. This study directly assesses the impact of different processing techniques on the quantification of CCEPs, highlighting the importance of consistency in data processing and proposing a common framework for processing CCEP data.

2.1.1 CCEP data collection protocols

For human subjects research, CCEP studies are typically performed in clinical populations who have temporary surgically implanted intracranial electrodes (e.g., commonly for clinical monitoring of medically intractable epilepsy). To measure CCEPs, bipolar stimulation is delivered between two adjacent ECoG or sEEG contacts at a low frequency, typically $\leq$ 1Hz. Stimulation may be monophasic [16, 79] or biphasic [86, 99, 97] with a duration of 100μs to 1ms per phase. Often, experiments alternate or otherwise divide trials to use each contact within the stimulation pair as the cathode [100, 120]. Stimulation amplitude also varies but is typically in the range of 5-10mA and is either tailored per patient [86, 100, 120, 164] or is held constant across all patients [29, 55, 79, 98, 99]. Often, jitter is introduced in the interval between stimulation pulses [86, 97], mitigating the potential impact of repeated stimulation at a constant frequency, which has been shown to change CCEP amplitude [97].

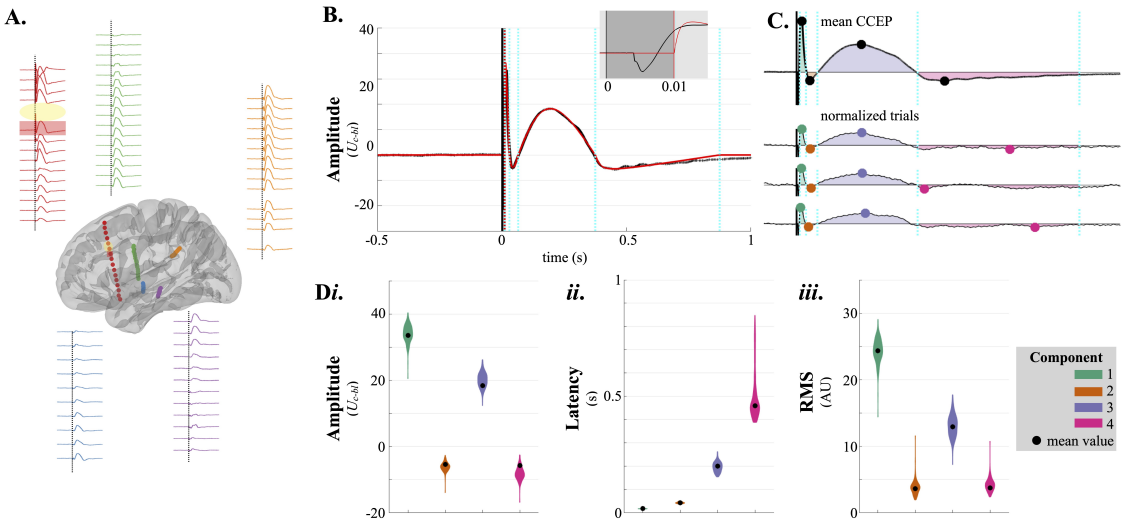

Figure 2.1: Overview of CCEP morphology and quantification. (A) CCEPs from stimulation electrode pair (yellow oval) were measured at all contacts of several sEEG probes implanted throughout the brain (example: Subject 4, mean over all trials for channels on 5/14 electrode probes shown; see Table 1 for electrode placement information for all subjects). (B) For each recording site and recording session, we construct a mean CCEP by averaging over trials (example: Subject 4, session 1, average over 202 trials, recording electrode immediately inferior to stimulation pair on the same probe; all subsequent examples unless otherwise stated are from this CCEP). A multi-component model is fit to this mean, excluding the first 10ms (dark shading), to identify 1-4 CCEP components separated by zero-crossings (indicated by cyan vertical lines). (C) From the mean (upper) and each trial (lower; 3 trials shown), each identified CCEP component is quantified. Component peak or trough amplitude (circles) and latency (horizontal lines), as well as RMS (normalized area under the curve, shaded) are computed. (D) Using trial-level quantification, distributions of amplitude (i), latency (ii), and RMS (iii) are constructed for each component. These can be compared to the quantification from the mean of trials (black circles). U_{c-bl}: channel-wise normalized units with baseline subtraction; AU: arbitrary units.

2.1.2 CCEP quantification and interpretation

CCEP morphology is typically characterized by multiphasic responses in the first 500ms after stimulation and can be seen throughout the cortex (Fig. 2.1A). The phases, or components, of these responses have been characterized previously and are consistent between studies [55, 99, 104]. CCEP components alternate polarities (peaks and troughs). Their borders are usually defined at points between peaks and troughs where the electrical potential crosses above or below the baseline voltage level (zero-crossings). The most common metrics used to characterize CCEPs include the amplitude of a peak or trough (or the peak-to-trough amplitude of consecutive components), the time between the stimulation onset and this peak or trough (latency), and the quadratic mean (root mean squared; RMS) of the component signal between zero-crossings [151]. Amplitude and RMS measure CCEP magnitude, while latency, zero-crossings, and polarity describe morphology. CCEP quantification metrics have been compared elsewhere [151].

CCEPs with greater magnitudes are interpreted as indicating stronger directional connectivity from the stimulation site to the recording site relative to CCEPs with smaller magnitudes (i.e., when neurons fire at the stimulation site, they are more likely to trigger peri-synaptic potentials at the recording site) [99, 122, 191]. Differing waveform morphologies across recording sites likely reflect various connectivity influences for instance laminar microcircuitry, macroscale connections and both antidromic and orthodromic activation of distinct pathways [99, 102, 127].

CCEPs are usually quantified after averaging over stimulation trials (Fig. 2.1B and 2.1C-upper; Fig. 2.2), with trial counts ranging from tens to hundreds [97]. The same metrics may also be examined in individual trials (Fig. 2.1C-lower; Fig. 2.2), which presents advantages for statistical testing – rather than a single CCEP measurement at each site, it generates a distribution of measurements (Fig. 2.1D; Fig. 2.2). However, the quality of single trial results depends largely on noise levels in the data.

2.1.3 Noise and the necessity of data processing

As human CCEP experiments are typically performed in clinical environments, experimenters are challenged by the impact of non-biological noise and artifacts present in recordings. Noise can be introduced by subject movement or the slight shift of electrodes over the brain surface, as well as by nearby electrical equipment. DC offset leads to nonzero centering of voltage, and low-frequency drift causes slow changes in the baseline voltage over the course of a recording. We will refer to DC offset and low-frequency drift as "low-frequency noise." Electrical line noise (60Hz in the US, 50Hz in Europe) and its harmonics introduce

high-amplitude, non-neural oscillations. Finally, there may be noise in high-frequency power bands (>200Hz) that are generally not associated with neural signals in electrophysiology (Fig. 2.2C) [17, 156]. This may come from multiple sources, including but not limited to sampling/digitization noise and white noise, which will affect high frequencies more substantially than low frequencies due to the 1/f dropoff in frequency contributions of neural signals [17]. For convenience, we will group these noise sources under the category of "high-frequency noise."

Additionally, the application of electrical stimulation produces large, transient artifacts in the data, which can be orders of magnitude larger than the signals of interest, due to electrical coupling between the stimulating and recording electrodes. These factors can impact the accuracy of CCEP quantification, so processing steps are often taken to reduce noise.

2.1.4 Data processing methods

To mitigate the impact of noise on CCEP results, especially if few trials are available due to experimental time constraints, a variety of processing methods are used. These include artifact removal, filtering, re-referencing, normalization, and baseline correction.

Artifact removal

Large electrical artifacts after stimulation may obscure short-latency CCEP components, so the first 10ms post-stimulation is typically excluded from analysis [16, 55, 86, 99, 97]. Electrical artifacts also may introduce edge-like artifacts, such as ringing or rippling, in the data if subjected to a filter. Temporal smearing of the artifact may contaminate CCEP components, particularly early components, even if they are not obscured by the artifact in the raw data. Thus, artifacts are often removed before any filters are applied. Many artifact removal and suppression techniques exist [19, 74, 182].

Channels and trials with excessive noise, putative inter-ictal spiking, and/or high amplitude electrical artifacts are often also removed from analysis to avoid biasing CCEP results.

Filtering

Filtering can be used to address the three categories of noise described above. DC noise can be reduced using high pass filters with cutoff frequencies $\leq$ 1Hz. Notch (or stopband) filters can mitigate line noise at specific frequencies and harmonics. Low pass filters are generally used to reduce the impact of non-neural white noise.

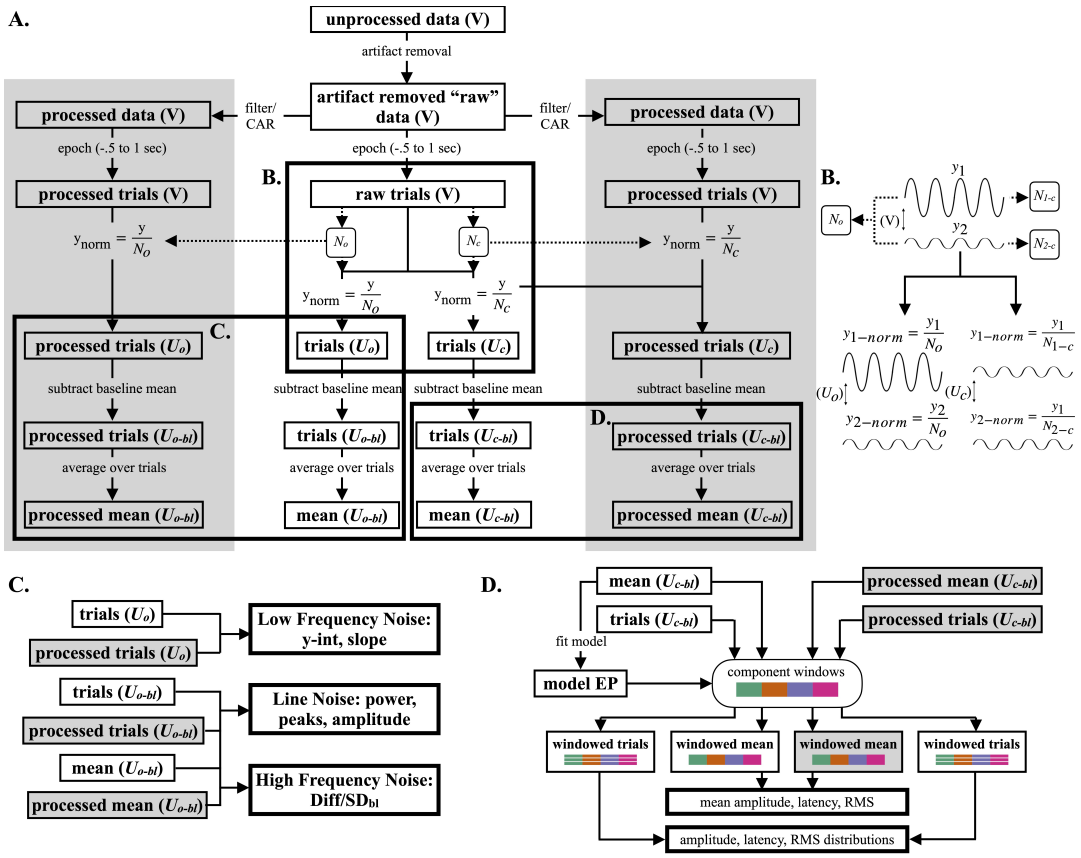

Figure 2.2: Schematic of data processing and quantification. (A) Data processing steps taken and units at each stage (in parentheses). Shaded areas represent filtered or re-referenced data – each processing strategy was applied separately but all processed data was treated equally. First, artifacts were removed from the data, then data were processed or left raw. The processed and raw data were epoched, and the raw data was used to compute normalization factors N_o and N_c. These values were used to normalize raw and processed trials, then local baselines were subtracted. A mean was taken over all trials. (B) Schematic explanation of the two normalization protocols, as applied to two "channels" of sinusoid data, in which y_1 has a larger amplitude than y_2. One N_o value is computed for all channels (the mean of all baseline standard deviations over all trials and channels), while N_c values are computed separately for each channel (the mean of all baseline standard deviations over all trials for a single channel). When divided by N_o, channels maintain their relative amplitude, but units become U_o rather than volts. When divided by N_c, each channel is scaled separately and units are U_c. (C) Noise quantification. Low frequency noise was quantified using the overall normalized trials without baseline subtraction; line noise and high frequency noise were quantified using the overall normalized data with baseline subtraction. (D) CCEP quantification. First, each channel's mean CCEP (the mean of the channel-wise normalized and baseline corrected, but unprocessed, data) was fit to a multi-component model to identify components and extract windows. Then, both mean and trial data and processed and unprocessed data were split using these windows and component amplitude, latency, and RMS were calculated from each. U_o: overall normalized units; U_{o-bl}: overall normalized units with baseline correction; U_c: channel-wise normalized units; U_{c-bl}: channel-wise normalized units with baseline correction; N_o: overall normalization factor; N_c: channel-wise normalization factor; V: volts.

Re-referencing

Commonly, the signal for each individual electrode is re-referenced to the mean or median of all electrodes on a grid or strip (ECoG) or probe (sEEG). This subtracts the signal shared between all channels, which could reflect common noise, neural signal introduced by the recording reference, and/or volume conduction. This common average re-referencing (CAR) is more commonly used in ECoG than in sEEG. Alternatively, and more commonly in sEEG, adjacent electrode pairs may be subtracted in a bipolar re-referencing scheme.

Normalization

CCEP data is often normalized with respect to baseline activity to (typically) compare response characteristics across subjects. Often, when only the averaged CCEP is quantified and no statistical distribution of measurements exists, a threshold is set for these normalized units and any components that exceed this value are considered significant [16, 99, 97]. Most commonly, the standard deviation of a pre-stimulation baseline is used as a normalization factor.

Baseline correction

For CCEP magnitude metrics to be meaningful, CCEPs must always be centered around zero. DC noise and other factors may shift the baseline of each trial and each recording channel in different ways. High pass filtering is one way of mitigating this offset, but transient, trial-by-trial baseline shifts may still be present even after filtering is applied. Baseline correction is a temporally localized way of reducing residual offset. A baseline period prior to stimulation is identified, and the average of this period is taken for each trial. This average is then subtracted from the corresponding trial, ensuring that the pre-stimulation signal is centered around zero.

2.1.5 Literature review

To assess the use of preprocessing in the field of CCEP analysis, we examined the methods sections of 36 CCEP papers published since 2010. A full table of the methods identified in each study is available in Appendix A, but we briefly describe findings here. Note that this review was not exhaustive. As studies from individual research groups are more likely to use similar methodologies, the number of papers using a certain processing strategy should not necessarily be accepted as representative of the field. Furthermore, studies may not always report every processing step taken. The findings of the review do not, therefore,

necessarily reflect how common or uncommon a given processing strategy may be. Instead, they highlight the lack of standard methods in CCEP processing.

Removal of stimulation artifacts and bad trials/channels

Most studies reported some form of stimulation artifact mitigation. The most common and simplest method was to exclude the first 5-20ms after stimulation onset from analysis. In other papers, the experimenters visually distinguished between CCEP and stimulation artifact [90, 95, 124, 119]. More complex, automatic or semi-automatic methods included interpolation-based methods [36, 106]; kurtosis-based methods [45, 105]; replacing the artifactual period with a reversed, tapered copy of a segment of clean, pre- or post-stimulation data [76, 75, 77, 86]; and Tukey filtering [146, 148, 150, 193].

Several studies also reported removing bad channels and/or bad trials using visual examination, thresholding, or anatomical metrics (i.e., excluding channels in white matter or within a certain distance from the stimulation electrodes). This included removal of artifacts related to epilepsy or excessive noise.

Filtering

The majority of studies reported use of a hardware high pass filter during recording or a subsequent digital high pass filter, with cutoffs ranging from 0.01Hz [81] to 10Hz [4].

Fewer studies reported an explicit line noise mitigation strategy using a notch filter [45, 86, 99, 97, 105, 110, 153, 176] or a line noise subtraction technique [10, 158](. Some studies essentially mitigated line noise using a low pass filter with a cutoff below 50 or 60Hz [30, 36, 76, 75, 77, 98, 106, 165].

Most studies reported use of a low pass, again either during recording or during digital processing, with cutoffs ranging from 30Hz [98] to 7500Hz [76, 75, 77].

Re-referencing

19 studies reported a bipolar re-referencing montage and five (all of which included ECoG data) reported a common average re-referencing montage. Two studies compared re-referencing schemes [30, 161]. Two studies explicitly stated that their data remained in a referential montage [79, 153]. 35 papers did not state whether or not they re-referenced the data.

Normalization and baseline correction

Approximately one third of papers normalized data relative to a baseline period. The most common method of normalization was z-scoring data relative to baseline, which also incorpo-

rates baseline correction by subtracting the mean. 11 studies reported an alternate method of baseline correction.

2.1.6 Goals

This paper aims to address gaps in the field regarding processing of CCEP and other evoked potential data recorded intracranially. We do not offer succinct recommendations for all CCEP studies, as processing needs will vary depending on study goals and noise of individual recording environments and/or rigs. Nor do we exhaustively test the nuances of filter design. Rather, we quantitatively demonstrate the importance of carefully choosing and thoroughly reporting processing of CCEP data. We examine the effects of filtering and common average re-referencing on CCEP quantification and observe that processing may introduce significant variability in CCEP magnitude and morphology. These differences in quantification may, in turn, alter interpretations of CCEP data. We conclude that minimal filtering (i.e., cutting out as few frequencies as is possible) can successfully address common noise issues while minimally affecting CCEPs. Common average re-referencing and averaging over multiple trials were both less effective at reducing noise than filtering, and re-referencing altered CCEP morphology and amplitude much more dramatically than filtering. Because it is difficult to conclusively establish the true, neurally-driven evoked morphology of a CCEP, which is the dynamic product of a multitude of overlapping influences (e.g., local/long-distance connectivity profiles, brain state, chemical milieu) at any given contact and juncture in time, we cannot say for certain that our recommendations are removing solely artifact. Rather, we urge caution when re-referencing and emphasize the importance of reporting and justifying re-referencing steps taken. Finally, we summarize a framework for choosing appropriate processing methods for CCEP data.

2.2 Methods

2.2.1 Subjects

Five patients (3 male, ages 23-44) undergoing clinical monitoring for intractable epilepsy gave informed consent for participation in research, in accordance with a protocol approved by the University of Washington Institutional Review Board. All subjects were implanted unilaterally or bilaterally with stereo-electroencephalography (sEEG) probes (Ad-Tech Medical Instrument Corporation, USA), yielding 126-164 electrode contacts per subject, up to 128 of which could be recorded by our system. Of these subjects, 2 had bilateral coverage, 2

had coverage of only the left hemisphere, and 1 had coverage of only the right hemisphere. Implant location was clinically determined. See Table 1 for subject demographics.

2.2.2 Electrode localization

Pre-operative MRI and post-operative CT scans were acquired for all epilepsy patients as standard clinical practice. Image registration, electrode visualization, normalization and contact anatomical labeling were achieved through published software (Localization of electrodes with a GUI, LeGUI) [37]. Briefly, the CT data was registered to the MRI data via a rigid-body alignment (6 parameters: 3 translations and 3 rotations) and a normalized mutual information cost function. The registered CT image was then transformed and resliced to match the MRI voxel by voxel using a fourth-degree b-spline interpolation. sEEG contacts were identified on the CT image using a maximum contrast algorithm and normalized into the MNI152 template brain. Contact labels were derived from applying and querying the Harvard-Oxford Cortical and Sub-cortical atlases and tissue type (grey matter, white matter, or cerebrospinal fluid) via parcellated of T1 image as previously described [37]. See Table 2.1 for labeled anatomical locations of recording contacts, including stimulation pair(s).

2.2.3 Data acquisition, channel selection, and stimulation

Data were recorded using a Tucker Davis Technologies (TDT, Alachua, Florida, United States) acquisition system, consisting of the RZ5D and PZ5 neurodigitizer. A maximum of 128 channels of data were acquired with a sampling rate $\geq$ 12kHz. Data were recorded with a scalp electrode as the reference. Simultaneous recording and stimulation were mediated using the TDT Subject Interface (SIM). Stimulation consisted of single bipolar (between pairs of sEEG contacts), biphasic pulses delivered at 6mA with a pulse width of 200μs/phase.

A sweep of consecutive electrode pairs in 32 of the 128 electrodes was initially performed. These 32 electrodes were chosen based on anatomical location of interest (varied between subjects; priorities often included the insula, parahippocampal cortex, and areas of the superior and medial temporal gyri, with priority often given to grey matter electrodes) and distance from the putative seizure onset zone. Each electrode pair was stimulated 5x with one of the contacts as the cathode, and 5x with the opposite polarity to mitigate artifact in the averaged signal [183]. One channel pair that elicited CCEPs at one or more sites, as determined by visual examination of stimulation-aligned averages of test pulses, was chosen for further testing. Only waveforms with no qualitative reversal (i.e., peaks turned to troughs and vice versa) between the two stimulation polarities were considered valid, because only artifacts, not consistent neural responses, are expected to reverse with stimulation polarity.

	Age	Sex	# Electrodes	Handedness	# Stim Sessions	Trials per Session	Jitter per Session	Polarity Reversal per Session	Electrode Coverage	Stim Site(s)
Subj. 1	44	M	126	R	2	200/ 100	no/no	blocked/ none	L: AG, CGp, HES, INS, MRG, MTGp, OFC, PHGp, PP, PT, SMGp, STGa R: ITGp, MFG, MTGa, MTGp, PHGa, PHGp, TFp, STGa, SubCC	STGa/ HES
Subj. 2	37	F	146	L	3**	100/ 100/ 100	yes/yes/ yes	interleaved/ interleaved/ interleaved	L: AG, CGp, HES, INS, IntraCAL, ITGa, ITGp, LING, LOCi, LOCs, MTGa, MTGp, OP, PHGa, PHGp, PreCC, PT, SMGp, STGp, TFus-p	PT
Subj. 3	23	M	164	R	1*	200	no	blocked	R: AG, CGa, CGp, FO, IFGtriang, INS, ITGa, ITGp, MTGa, MTGp, MTGto, PHGa, PHGp, PreCC, SMGp, TFus-p, TP	INS, FO
Subj. 4	23	M	160	R	3**	230/ 100/ 300	yes/yes/ no	interleaved/ interleaved/ interleaved	L: CGp, CO, FO, FP, INS, ITGto, MFG, MTGa, MTGp, MTGto, OFC, PHGa, PHGp, PP, PreCG, SMGp, STGa, STGp, TFus-p, TP	MFG
Subj. 5	44	F	146	R	1	200	no	blocked	L: CGp, INS, ITGp, ITGto, LOCi, LING, MFG, MTGa, MTGp, MTGto, OFus, PHGa, PHGp, PostCG, PP, PreCG, SMGa, STGa, TFus-p R: INS, MTGa, MTGp, PHGa, PHGp, PP, STGp	CGp

Table 2.1: Subject demographics, stimulation sessions, and electrode coverage. Abbreviations: AG: angular gyrus; CG: cingulate gyrus; CO: central opercular cortex; FO: frontal opercular cortex; FP: frontal pole; HES: Heschl's gyrus; IFGtriang: inferior frontal gyrus pars triangularis; INS: insular cortex; IntraCAL: intracalcarine cortex; ITG: inferior temporal gyrus; LING: lingual gyrus; LOC: lateral occipital cortex; MFG: middle frontal gyrus; MTG: middle temporal gyrus; OFC: orbitofrontal cortex; OFus: occipital fusiform cortex; OP: occipital pole; PHG: parahippocampal gyrus; PostCG: postcentral gyrus; PP: planum polare; PreCC: precuneous cortex; PreCG: precentral gyrus; PT: planum temporale; SMG: supramarginal gyrus; STG: superior temporal gyrus; SubCC: subcallosal cortex; TFus: temporal fusiform cortex; TP: temporal pole. *Session performed after high frequency stimulation [170]. **Sessions performed before high frequency stimulation, after high-frequency stimulation, and after 5 minute washout.

No data from the stimulation sweep is included in the analyses for this article.

Following the stimulation sweep, we commenced the stimulation session using the chosen stimulation pair. Each stimulation session consisted of 100-300 stimulation pulses, split between polarities (either in blocks or interleaved, see Table 2.1) [183], and delivered with an inter-pulse interval of 1.5-5.5s. For some stimulation sessions (all sessions for subject 2; sessions 1 and 2 for subject 4; see Table 2.1), 10-15% nonuniform random jitter was included in the stimulation interval.

For subject 1, separate stimulation sessions were performed with two different electrode pairs. For subjects 2 and 4, two stimulation sessions on the same electrode pairs were performed immediately before and after a period of high frequency stimulation [170], and session three was performed after a 5-minute washout period. The same protocol was performed for subject 3, but poor data quality precluded use of all but the post-stimulation session. Only

one stimulation session was performed with subject 5. The number of sessions and trials were determined based on time constraints on a per subject basis. Because the high-frequency stimulation may have conditioned changes in CCEPs between sessions [97], and due to differences between stimulation sites between sessions, trial- and mean-level quantifications and comparisons were performed only within, not across, stimulation sessions.

2.2.4 Data processing pipeline

Figure 2.2 shows, in detail, the steps taken between unprocessed data and quantification for noise or CCEP analysis. As outlined in Section 2.1.4, we follow five basic steps for processing — artifact removal, filtering, re-referencing, baseline correction, and normalization. However, due to the nature of our analyses (see below), we do not perform these steps sequentially, nor does all data go through all steps prior to analysis. Further information on each step is provided below, but an overview of the analysis pipeline is presented here and in Figure 2.2A.

All data were first run through artifact removal (Section 2.2.4). We then implemented one filtering strategy or re-referencing strategy on each of 10 copies of the data (Sections 2.2.4-2.2.4). We refer to each of these unique conditions as "processed" data, which are represented in grey shaded areas of Figure 2.2, in contrast to the "raw" data, which was unfiltered and not re-referenced. Both raw and processed data were split into trials. Then, from the raw data only, two normalization factors were computed (Section 2.2.4). Copies of raw and processed data were then divided by each of these normalization factors. Finally, a baseline period was subtracted from each trial (Section 2.2.4) and trials were averaged to form a mean CCEP.

Artifact removal

First, we excluded channels contaminated by large inter-ictal events and other artifacts. All channels were visually inspected for excessive noise or potential epileptic activity. A total of 17.77% of channels (225 out of 1266) were removed at this stage. This included channels that were disconnected or outside the brain.

Stimulation artifacts were removed from the time series data using a dictionary-based, unsupervised clustering, as previously described [19]. Minor modifications to the algorithm allowed for artifact removal prior to data epoching, and algorithm parameters, including length of the artifact period, were manually adjusted for each subject to avoid including the CCEP in the template. This process reduced the magnitude of artifacts but did not eliminate them. We quantified the residual artifact in each trial. Based on our analysis of artifact

smear after filtering, we excluded trials for which the residual artifact's amplitude exceeded 5x the standard deviation of a pre-stimulus period (5.83%, or 9559 of 164020 trials), which caused minimal amplitude changes in the non-artifact period (i.e., smearing) after filtering. This additional data control step was highly conservative.

Finally, we excluded noisy trials, including trials with potential inter-ictal spiking. For each channel, we took the median absolute deviation (MAD) over all trials. Any individual trial that deviated from the median by more than 5x the MAD. Any trial that was removed from 10 or more channels was visually inspected. If there was a clear artifact or inter-ictal event synchronized across multiple channels, that trial was removed from analysis for all channels. 7.55% of trials (123 out of 1630) were removed across all channels, and an additional 0.28% of trials for individual channels (430 out of 153461) were removed. This left a total of 153031 trial-channel pairs for our analysis.

Filtering

All filters used in this paper were 8th order Butterworth filters, built using MATLAB's butter function ([z, p, k] syntax). High pass filters were implemented at 0.1, 0.5, and 1 Hz and low pass filters were implemented at 100, 200, and 500Hz. Notch filters had a width of $\pm$3Hz around center frequencies. Either a single 60Hz notch filter or three filters at 60, 120, and 180Hz was used. Data were filtered with zero phase distortion (using MATLAB's filtfilt function) in continuous form, prior to epoching.

Common average re-referencing

For each sEEG probe, a mean or median was computed over all channels for each time point, then subtracted from the raw signals for this probe. When channels on a single probe were divided over multiple signal splitters (TDT S-BOXes), electrodes on each splitter were considered to be separate probes.

Normalization

After processing steps were applied, the signals were normalized. The normalized signal was defined as the signal, y, divided by a normalization factor, N. For our two primary analyses branches, we defined N in two different ways. For noise quantification, we used an overall normalization factor (N_o), while for CCEP quantification, we used a channel-wise normalization factor (N_c). Both N_o and N_c were computed using the raw, unprocessed signals and were held consistent across all processing conditions. In this way, both noise and CCEP metrics could be directly compared between the different conditions. Throughout

this paper, U_o and U_c are used as units to describe signal amplitude in each normalization scheme.

Justification. Signals from different channels in a single recording have different baseline levels of noise due to their placement relative to noise sources and variability in hardware or components, among other factors. In analyzing noise metrics, we wanted to capture this variability in relative noise among channels. To preserve this, we scaled all channels to a common, overall normalization factor (N_o). After normalizing to N_o, signals could be compared in a common unit space (U_o) across stimulation sessions and subjects, but the amplitudes of signals in one channel relative to another stayed constant (Fig. 2.2B, left).

However, a CCEP on a given channel is most effectively quantified relative to that channel's baseline fluctuations, addressing how much the CCEP stands out from the background signal. As a simple example, imagine two channels recording pure 60Hz noise at different amplitudes (Fig. 2.2B). Comparing the amplitudes of a 60Hz peak in U_o would indicate that one channel had a higher amplitude than the other (Fig. 2.2B, left). In contrast, after dividing by a channel-wise normalization factor (N_c), these peaks would have comparable amplitudes in N_c (Fig. 2.2B, right). This would allow us to identify that neither channel's peak amplitude is notably different from its noise level.

Overall normalization factor. To compute the overall normalization factor, N_o, we took the average standard deviation of the baseline period (0.4 to 0.1s prior to stimulation onset) over all trials and channels in a stimulation session. All signals from this session were divided by N_o. Computation of the overall normalization factor is summarized by Equation 2.1

$$N_o = \frac{1}{C}\frac{1}{T}\sum_c \sum_t \sqrt{\frac{\sum_x y_x - \mu}{X}} \tag{2.1}$$

where y is the amplitude of a channel's (c) baseline period (time points x) for a given trial (t) and μ is the mean of this baseline. No is the mean baseline standard deviation over all channels (C) and trials (T). Signals from all channels and trials in this stimulation session were divided by N_o to normalize.

Channel-wise normalization factor. Prior to CCEP quantification, we calculated a normalization factor for each channel individually by taking the mean standard deviation over all trials for that channel. This is summarized by Equation 2.2:

$$N_c = \frac{1}{T}\sum_t \sqrt{\frac{\sum_x y_x - \mu}{X}} \tag{2.2}$$

with all variables as in Equation 2.1. All trials from this channel were then divided by N_c.

Baseline correction

The final processing step was to subtract a local baseline for each trial, ensuring that all trials were centered around zero. The baseline period was defined as 0.4 to 0.1s prior to stimulation onset. The mean of all points in this range was subtracted from each trial. Unlike normalization factors, baselines were computed individually for each processing type, channel, and trial combination.

Baseline subtracted data were used in all analyses except the analysis of low-frequency noise (for which baseline offsets were of interest). Units are specified as U_{o-bl} or U_{c-bl} when the data were baseline corrected.

2.2.5 Quantifying CCEPs

The amplitude, latency, and RMS of the first four components of each CCEP were calculated both in individual trials and in the mean over all trials. The CCEP quantification process is shown schematically in Figure 2.2D.

Model fitting for component identification

To ensure that the same components were being consistently measured across trials and processing techniques, we identified each channel's CCEP component windows using the unprocessed average CCEP (units U_{c-bl}). We excluded the first 10 ms after stimulation onset to account for residual stimulation artifact and artifactually fast components. To identify windows in the presence of noise, we fit a single- or multi-component model to the remaining 990 ms of signal for each channel. Each component was modeled as follows:

$$f(x) = \frac{A}{t} \tan^{-1} \frac{t \sin(2\pi(\frac{1}{w/2})x}{1 - t \sin(2\pi(\frac{1}{w/2})x} \tag{2.3}$$

This is essentially a half-cycle of a sinusoid with amplitude A and frequency $\frac{1}{w/2}$, so that w represents the length of the component in samples. The factor t was introduced to allow for asymmetry — values near t = 0 corresponded to a peak directly in the center of the component (note that t could not equal zero, as this would leave the coefficient $\frac{A}{t}$ undefined), while negative t values shifted the peak left and positive t values shifted the peak right. A was constrained to be either between 0 and the signal maximum (peak) or between 0 and the signal minimum (trough) and t was constrained between -0.9 and 0.9. While w was never allowed to be negative, the exact upper and lower bounds were manipulated manually to achieve good fit depending on the relative width of each component for a given signal.

The full signal was modeled as a sequential sum of components:

$$\hat{y} = f(y_{1:w1}) + f(y_{w1+1:w2}) \dots \tag{2.4}$$

with forced alternation between negative and positive amplitudes (peaks and troughs).

Eight versions of the model were fit to each signal – models with 1-4 components in which the first component was either a peak or a trough. The model with the highest r^2 value was selected. Models were then manually inspected to ensure a good match to the overall signal. An experimenter (LHL) manually modified maximum and minimum values for w for each component if no good fit was found. A maximum of 4 components was chosen to reflect canonical CCEP morphology as described in early papers by Matsumoto et al. However, CCEP morphology is variable and more than 4 components may be present [127]. In this case, the first four components were chosen. The number of components and the polarity of the first component fit over all channels is shown in Table 2.2.

	1 component	2 components	3 components	4 components
first component trough	1	21	70	318
first component peak	8	24	150	423

Table 2.2: Model fitting component breakdown. A breakdown of the polarity of the first component and the total number of components in the fit models.

Typically, one metric is extracted from a CCEP rather than separate metrics for each component using a fixed time window [29, 120, 164]. It is not unusual for CCEP quantification to include visual identification of a particular component based on experimenter judgment, rather than quantitative metrics [120]. As we were interested in multiple CCEP components over many channels, we chose not to use a manual method of component identification. Of the supervised automatic methods that we tried, model fitting most accurately matched manual peak and trough identification, even with a low signal-to-noise ratio. The fit w values for a model defined the CCEP window for each channel's signal.

Peak amplitude and latency

Peak amplitude and latency were calculated within each identified component window. Local peaks and troughs for each window were identified using MATLAB's findpeaks function, and the peak with the highest prominence (i.e., stood out most from the surrounding samples; see MATLAB documentation) was recorded as the component peak. The amplitude of this peak (in units U_c), as well as its latency from stimulation onset was computed. Because findpeaks only identifies positive peaks, components with negative amplitudes were first multiplied by

-1 to ensure a trough was identified, then the amplitude value was again multiplied by -1 to find the true trough amplitude. This process was performed on mean CCEPs and on individual trials using the same windows. The number of peak amplitudes and latencies was the same as the number of components in the best-fitting (highest r^2) model, with a maximum of 4 components.

Component RMS

The RMS of the signal within each component window was computed in the mean CCEP and individual trials.

2.2.6 Quantifying noise

We developed strategies for quantifying each of the three noise categories of interest, with particular focus on developing metrics that meaningfully indicated the potential impact of noise on CCEP quantification. These metrics are thoroughly described and validated in Appendix B. We describe them briefly here, and they are schematized in Figure 2.2C.

To quantify low-frequency noise, we fit a linear model to the baseline averages over the course of an entire recording session. Nonzero y-intercept was used as a measure of DC offset and nonzero slope was used as a measure of signal drift over the session. To quantify line noise, we calculated normalized spectral power (using welch power spectral density) and oscillatory amplitude (using fast Fourier transform, FFT) at 60Hz and harmonics. The presence or absence of a peak in the power spectrum at these values was interpreted as consistent with bandlimited power increases caused by line noise. Finally, the sum and geometrical mean (RMS) of the FFT-derived amplitude values of high frequencies (250-2000Hz) were taken as an estimate of the contribution of non-neural, high-frequency noise.

2.2.7 Mixed effects linear model

To determine if filtering altered CCEP quantification in a statistically significant way, we fit three mixed effects linear models — one each for CCEP component amplitude, latency, and RMS. The model had crossed fixed effects for component and filtering method, to reveal if filtering had different effects on different components. It also included mixed effects to control for recording channel, stimulation session, and subject. For the amplitude model, trough amplitudes were multiplied by -1 to ensure consistent comparisons across channels.

2.2.8 Stimulation artifact modeling

Finally, we examine the effect of filtering on stimulation artifacts. Using the artifact removal method described in Section 2.2.4, we isolated 50 individual artifacts from one arbitrarily chosen channel per subject to use for our models. These artifacts were inserted into a long period of resting (i.e. no stimulation) data from the same channel. To vary artifact size, we scaled the absolute maximum of each artifact to the standard deviation of the 500ms of resting data immediately preceding it and multiplied the scaled artifact by several factors (1, 2, 5, 25, 50, 100, and 500). For comparison, the unscaled artifact was also examined. We compared filtered versions of the artifactual data to equivalently filtered versions of the artifact-free resting data to examine the impact of the filtered artifact on nearby data points.

2.3 Results

2.3.1 Processing strategy significantly affects CCEP quantification

Visual assessment of the impact of processing

Figure 2.3 shows the post-processing mean over trials for one example CCEP per subject, demonstrating how each processing step qualitatively alters CCEP signal.

High pass filtering tended to impact the earlier and later stages of the trials more, and a 1Hz cutoff (light blue) introduced a larger shift than a 0.1Hz cutoff (dark blue; Fig. 2.3A). With a high cutoff, a dip was introduced in the trial baseline before stimulation onset and the amplitude of the third and/or fourth components were decreased.

Both notch filtering (Fig. 2.3B) and low pass filtering (Fig. 2.3C) introduced the largest changes immediately prior to stimulation onset. Notch filtering introduced approximately 60Hz artifact into the ∼0.1s before stimulation, with amplitude increasing with proximity to stimulation. This was comparable whether one (orange) or three (red) notch filters were used. Low pass filtering sometimes introduced high frequency artifact immediately before stimulation. This was most pronounced when a short latency component or artifact was present in the 10ms following stimulation (e.g., subject 4). A cutoff of 500Hz (light green) introduced artifacts that were lower and amplitude and more temporally confined than for a 100Hz cutoff (dark green).

The impacts of common average re-referencing differed per subject (Fig. 2.3D). In subjects 3 and 4, for instance, the re-referenced signal had lower-amplitude CCEP components than the unprocessed data. In subject 1, re-referencing to a common median (light pur-

ple) slightly increased component amplitude while re-referencing to a common mean (dark purple) slightly lowered component amplitude.

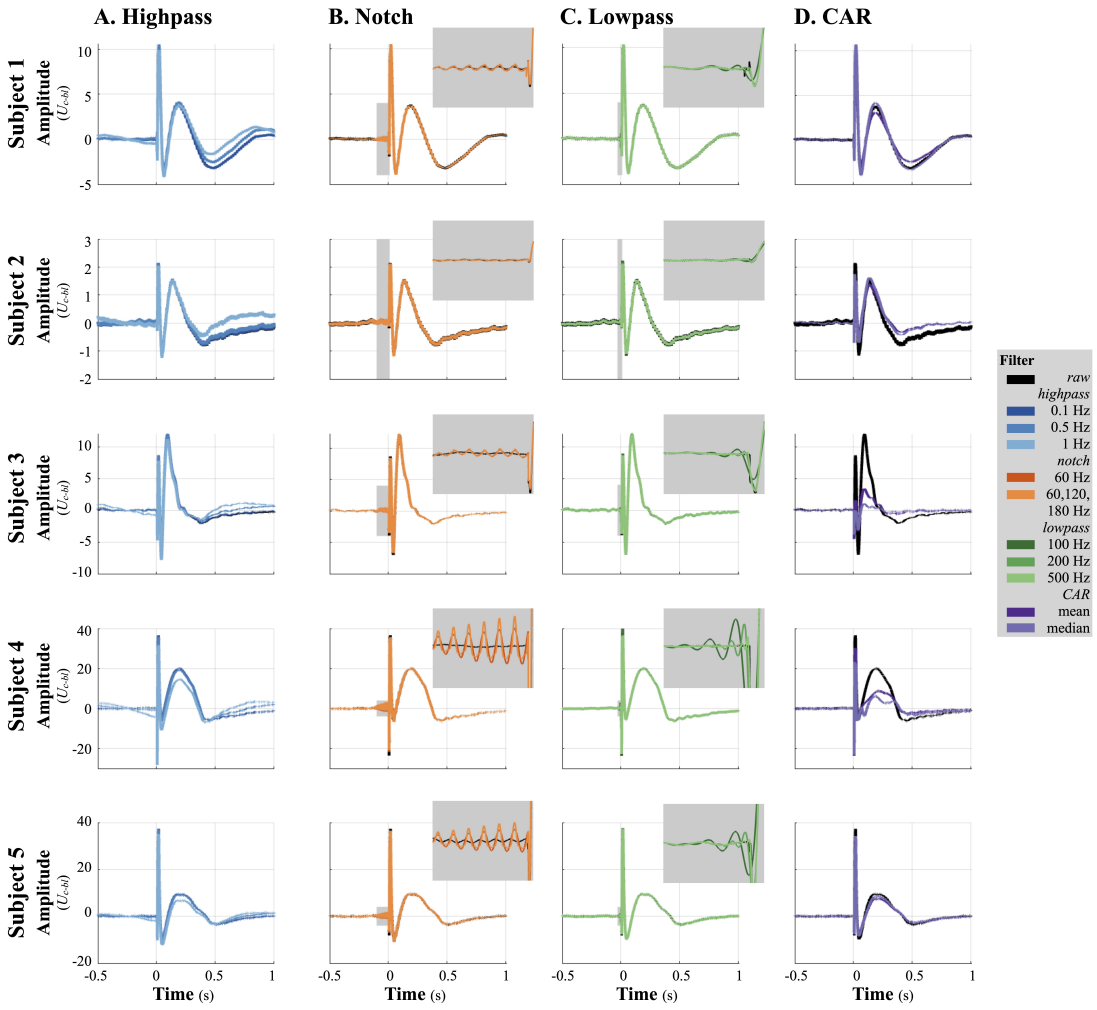

Figure 2.3: Examples of Mean of Filtered Data for all Subjects. For each subject (rows), one example CCEP was chosen. After stimulation artifact removal, high pass filters (A), notch filters (B), and low pass filters (C), as well as common average re-referencing (D) was applied to the continuous, unnormalized data. Data were then normalized on a per-channel basis (using the mean standard deviation of the raw signal's baseline periods as the normalization factor) and baseline corrected (local baseline mean subtracted). A comparison of the unprocessed (black) and processed (blue, orange, green, or purple) data is shown here.

Changes in CCEP quantification introduced by processing

The trends noted in the examples shown in Figure 2.3 are borne out by quantification of all CCEPs in each dataset. After quantifying the amplitude, latency, and RMS of CCEPs

Component	Amplitude				Latency				RMS			
	1	2	3	4	1	2	3	4	1	2	3	4
Unfiltered	17.584	-6.624	24.012	31.034	**38.043**	**54.731**	**177.637**	**377.688**	**1.671**	**-0.084**	**0.613**	**0.947**
HP 0.1 Hz	0.002	**-0.022**	**0.008**	-0.099	-0.010	0.023	0.027	0.022	-0.001	-0.002	-0.000	-0.006
HP 0.5 Hz	**-0.436**	**-0.012**	**-2.634**	**-6.651**	-0.060	0.046	-0.150	-0.643	**0.043**	**-0.034**	**-0.076**	**-0.281**
HP 1 Hz	-1.098	**3.018**	**-11.253**	-22.419	-0.128	0.032	-0.242	**-1.897**	**0.325**	-0.012	**-0.414**	**-1.017**
Notch (60 Hz)	-3.198	**0.300**	**-1.471**	-1.743	-0.567	0.349	0.167	0.210	**-0.256**	-0.007	0.005	0.006
Notch (60/ 120/180 Hz)	**-3.343**	**0.200**	**-1.708**	**-2.054**	-0.684	0.434	0.148	0.498	**-0.263**	-0.006	0.006	0.007
LP 100 Hz	-1.031	**-1.690**	**-3.946**	-4.146	-0.600	0.387	0.192	0.401	**-0.026**	0.018	0.002	0.003
LP 200 Hz	-2.322	**-0.219**	**-1.981**	-2.113	-0.143	-0.017	-0.123	-0.015	**-0.024**	0.009	0.004	0.005
LP 500 Hz	**-2.069**	**-0.197**	**-1.609**	**-1.723**	0.055	-0.146	-0.325	0.026	-0.018	0.000	0.002	0.003
CAR mean	**-8.812**	**-2.753**	**-25.563**	**-34.649**	**-0.985**	**4.137**	**9.381**	**12.182**	**-0.574**	**-0.161**	**-0.535**	**-0.801**
CAR median	-3.245	-4.868	-26.397	-34.908	**-1.116**	**4.285**	**9.101**	**13.089**	**-0.304**	**-0.157**	**-0.616**	**-0.750**

Table 2.3: Mixed-effects linear model of the effect of processing on component amplitude, latency, and RMS. We fit a mixed-effects linear model with crossed fixed effects for component and processing method and mixed effects for CCEP channel, stimulation session, and subject. All values are relative to the baseline (intercepts) of unprocessed data and component 1. Statistically significant effects (FDR corrected over all three models to $p = 0.05$) are bolded.

in processed and unprocessed data, we plotted the distribution of differences over all trials, channels, and stimulation sessions (Fig. 2.4). Table 2.3 statistically summarizes these results with three mixed-effects linear models assessing the impact of processing method on amplitude, latency, and RMS of each CCEP component after controlling for subject, channel, and stimulation session (all negative components were multiplied by -1 to always be comparing peak amplitudes, rather than combining peaks and troughs). Note that a given component may not be directly morphologically comparable in any two CCEPs, within or across subjects. Results are grouped by component to elucidate general trends in the effects of filtering on early versus late components, but this grouping should be interpreted with caution. Model values are interpreted as the average quantification differences in the processed data relative to the first component of the unprocessed data. Because all processing was a direct intervention in the data, we interpret these results causally.

High pass filtering. High pass filtering at 0.1Hz rarely introduced significant changes in amplitude, latency, or RMS of any component. High pass filtering at 0.5 or 1Hz significantly affected most RMS values, though the changes introduced again did not exceed ∼1AU (RMS). Contrastingly, these higher cutoff filters introduced larger significant effects in amplitude, shifting peaks by up to $11U_{c-bl}$ relative to the unfiltered signal (high pass filter at 1Hz, component 3). The effects on latency were rarely significant.

Notch filtering. Notch filtering at 60Hz or 60, 120, and 180Hz also significantly affected amplitude and RMS, but not latency. Changes in RMS tended to be smaller in magnitude than changes in amplitude.

Low pass filtering. In general, low pass filtering at lower cutoffs had more substantial effects on CCEP quantification than gentler filters with higher cutoffs, although the highest cutoff tested (500Hz) did introduce significant effects on amplitude exceeding $1U_{c-bl}$. No

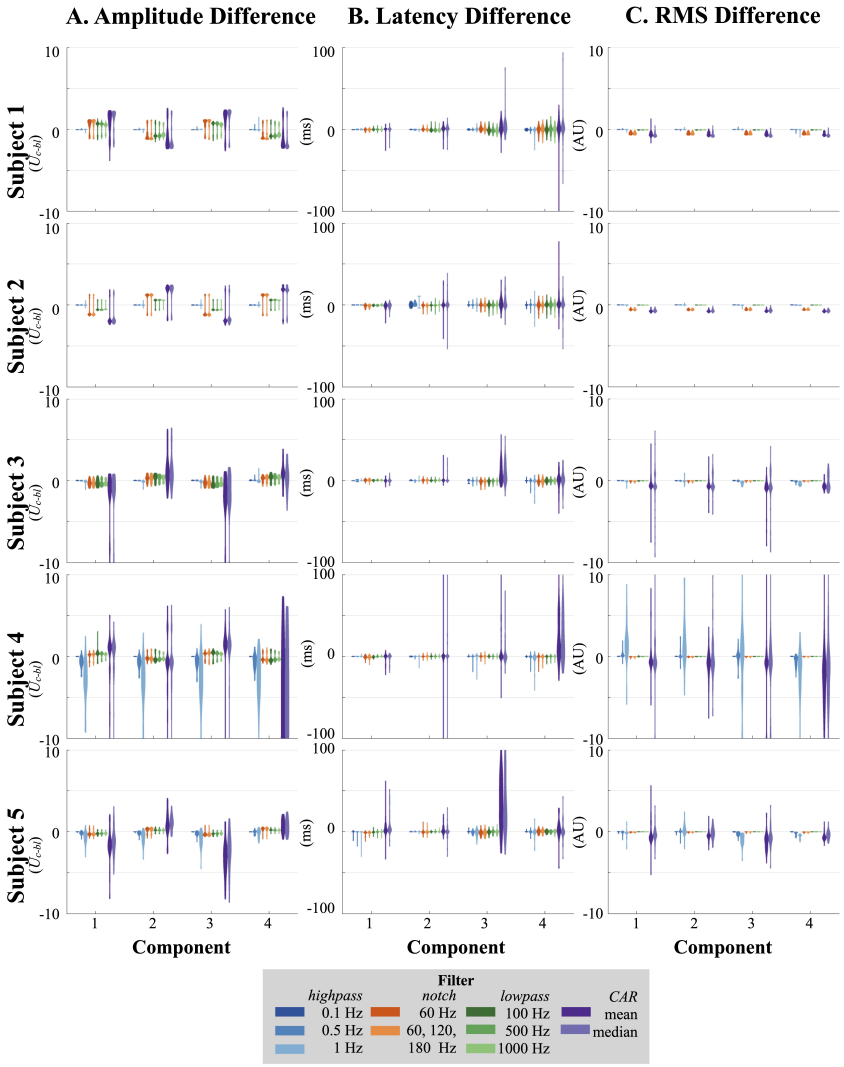

Figure 2.4: Filtering impacts CCEP quantification. For each subject (rows), collapsing over channels and trials, the distributions of differences between amplitude (A), latency (B), and RMS (C) values of the processed vs. unprocessed data is shown.

significant effects were seen on latency, and even significant effects on RMS were quite small. Amplitude differences were almost always seen as decreases in the magnitude of component amplitude and significant effects ranged as high as -3.9U_{c-bl} (low pass filter at 100Hz, component 3).

CAR. Unlike filtering, common average re-referencing introduced significant changes in all components' amplitudes, latencies, and RMS values. Component magnitude metrics were decreased, with amplitude of all components decreasing by 2.7 to 34.6U_{c-bl}. RMS magnitude was also decreased significantly for all components, but by <1AU. Re-referencing tended to move component 1 earlier and delay components 2-4, with later components seeing larger shifts (e.g., >12ms for component 4). An example of a large latency shift in a late component can be seen in Subject 4 (Fig. 2.3). In Figure 2.4, both CAR conditions have broad distributions, suggesting inconsistent changes in CCEP quantification.

Changes in variability of CCEP quantification introduced by processing

In addition to computing the differences in CCEP quantification estimates before and after processing (Fig. 2.4), we also computed differences in the stability of these estimates (as measured by the standard deviation over trials) before and after processing (Fig. 2.5). As with the metrics themselves, CAR processing introduced the greatest and most variable differences in standard deviation over trials. On average, it tended to decrease the variability in magnitude metrics (Fig. 2.5A and C), while increasing variability in latency (Fig. 2.5B). In subjects 3-5, high cutoff low pass filters (light blue) also had notably heterogenous effects on estimate variability, especially as compared to low pass filters with lower cutoffs (dark blue). Difference distributions for notch (orange/red) and low pass (green) filtering tended to be compact and approximately symmetrical around 0, although these distributions were broader for latency than for magnitude metrics.

2.3.2 Noise is present in CCEP recordings

We confirmed the presence of low frequency drift and DC offset (Fig. 2.6A), 60Hz and harmonic line noise (Fig. 2.6B), and high frequency noise (Fig. 2.6C) in CCEP data. Quantification strategies were designed and tested for each category of noise to capture the overall noise level of the raw signals (Section 2.2.6; Appendix B).

Low frequency noise

4/5 subjects (excluding Subject 1) had prominent and variable low frequency noise (DC offset and low frequency drift) in the recordings (Fig 2.6Aiv, upper). For these subjects,

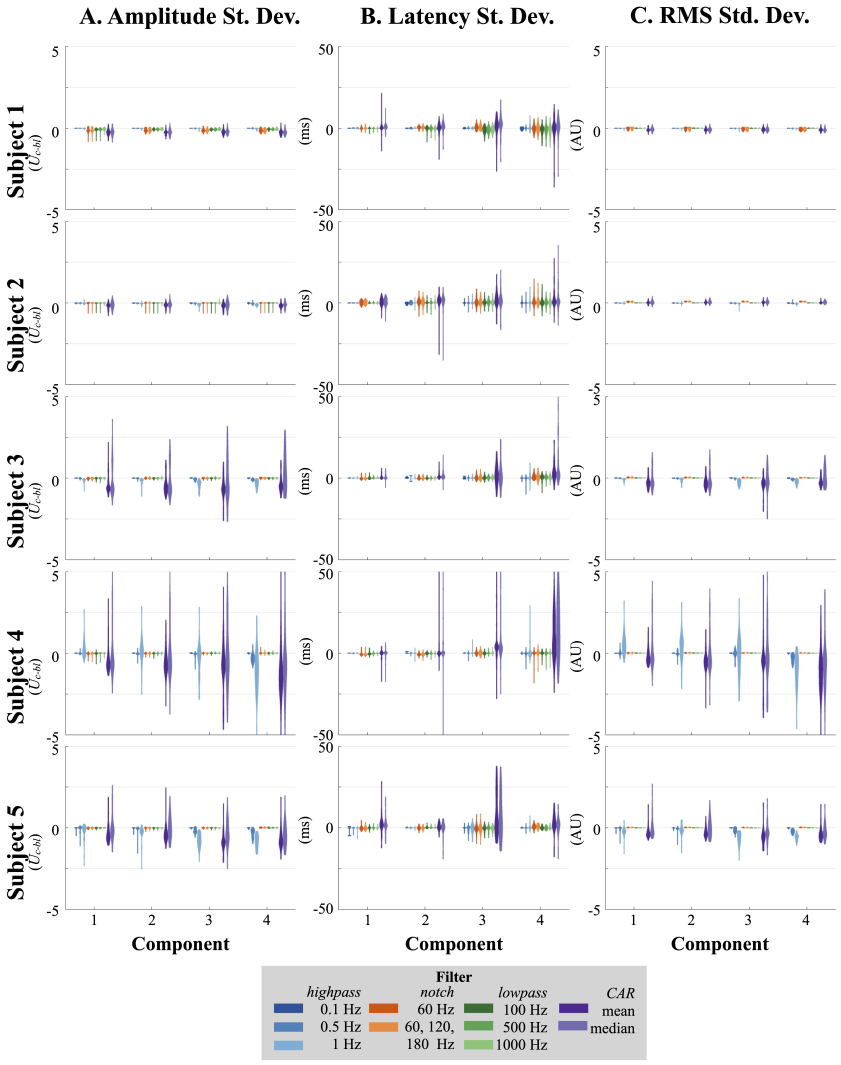

Figure 2.5: Filtering impacts variability in CCEP quantification. For each subject (rows), collapsing over channels and trials, we examine how the standard deviation of amplitude (A), latency (B), and RMS (C) distributions over trials changes between unprocessed and processed data.

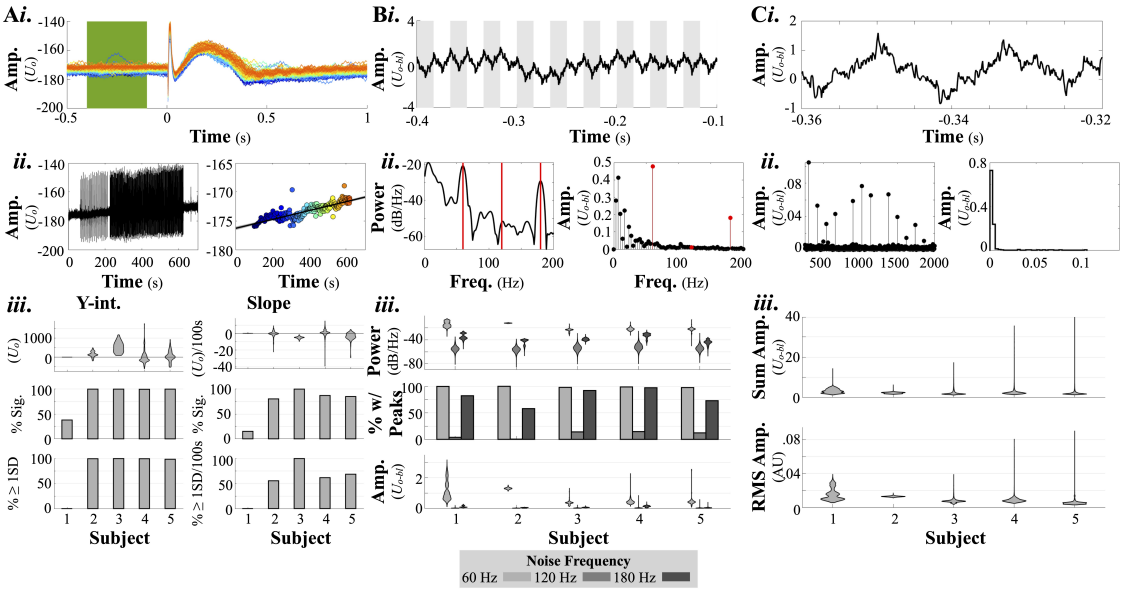

Figure 2.6: Low frequency, line, and high frequency noise are present in data. (A) Low frequency noise manifests as DC offset (nonzero intercept) and slow drift of data. (i) When trials are plotted in temporal order (blue = earlier trials, red = later trials), the slow drift is easily seen. Baseline period is highlighted in green. (ii) An entire stimulation session for one channel (left) and the extracted baseline mean of every trial, plotted against trial time (right). Note that stimulation initially began at a lower frequency, resulting in a visual difference in stimulation artifact density. A linear model is fitted to the baseline mean data (right; black line, shading represents 95% confidence intervals). (iii) Results of y-intercept (left) and slope (right) for all fitted models for each subject. Note that slope values are displayed as amplitude change per 100s to better capture the magnitude of the change over the course of the stimulation session. The distribution of values (top), percent of models with y-intercept and slope that are statistically nonzero (center; FDR corrected to $p < 0.05$), and the percent of models with values exceeding 1 normalization unit (lower). (B) Line noise is 60 Hz in the US. (i) 60 Hz oscillations can be easily seen in the baseline period of one trial (vertical grating represents 1/60s for comparison). (ii) The power spectrum (left) and Fourier transform (right) of the same trial show noise peaks at 60 and 180 Hz, but not 120 Hz. (iii) 60 Hz and harmonic noise summarized for all subjects as the power distribution (top), percent of trials with spectral peaks at each frequency (center), and amplitude distribution (lower). (C)(i) High frequency noise can be seen as fast fluctuations in the raw data. (ii) To quantify this, we divided the differential of the baseline period by the standard deviation of the same period, with higher ratios indicating more high frequency noise. (iii) Distributions of average differential to standard deviation ratios for all baselines are shown for each subject. U_o: overall normalized units; U_{o-bl}: overall normalized units with baseline correction; CAR: common average re-reference.

>75% of channels over all stimulation sessions had significantly nonzero y-intercepts and slopes (Fig 2.6Aiv, center; FDR corrected to p <0.05). Nearly every y-intercept in these subjects exceeded $1U_o$ (Fig. 2.6Aiv, lower), indicating that the baseline offset alone could induce a difference in CCEP amplitude estimates that exceeded the expected fluctuations in resting data. Between 44% and 100% of channels in these subjects had slopes that exceeded $1U_o$/100s (Fig. 2.6Aiv, lower). Thus, two identical CCEP measures taken 100s apart, which is well within the bounds of a typical stimulation session, could vary by more than $1U_o$ based only on their baseline drift.

Line noise

60Hz noise was easily visible in raw recordings (Fig 2.6Bi), power spectral density estimates (Fig 2.6Bii, left), and Fourier transforms (Fig 2.6Bii, right). Noise at harmonics of 60Hz (120 and 180Hz) could also be seen in frequency decomposition, though at a relatively lower power and amplitude than 60Hz noise (Fig 2.6Bii).

All subjects exhibited relatively higher power (Fig 2.6Biv, top) and amplitude (Fig 2.6Biv, lower) at 60 and 180Hz than at 120Hz. While nearly 100% of power spectral density estimates for trials had peaks at 60 and 180Hz, closer to 25% had peaks at 120Hz (Fig 2.6Biv, center). The estimated amplitude of oscillations at 60Hz and harmonics varied from subject to subject, but was consistently highest for 60Hz noise, with all subjects' recordings containing channels and trials where the 60Hz amplitude exceeded $1U_{o-bl}$ (i.e., was greater than the estimated average baseline fluctuations of the data; Fig. 2.6Biv, lower).

High frequency noise

High-frequency noise can be seen as point-to-point instability (i.e., not smoothness) in the data (Fig. 2.6Ci). Measured as either the cumulative amplitude contributions of frequencies 250-2000Hz or the normalized area under the curve (RMS) of the Fourier transform (FT) for these frequencies (Fig. 2.6Cii), a degree of high-frequency noise was seen in all subjects (Fig. 2.6Civ). For the most part, all frequencies in the specified noise range, combined, contributed an amplitude $<5U_{o-bl}$. However, in all subjects, there were trials and channels for which the effect was larger, up to $40U_{o-bl}$ (Fig. 2.6Civ). The RMS of the FT was generally quite small, well under 0.04AU for the majority of trials and channels in all subjects (Fig. 2.6Civ).

2.3.3 Preprocessing digital filters more effectively address low-frequency and line noise than common average re-referencing or averaging over trials

Filtering was the most effective way of reducing all three categories of noise, surpassing common average re-referencing to the mean or the median of the data or taking the mean over trials.

Low frequency noise

In 4/5 subjects, high pass filtering at 0.1, 0.5, or 1 Hz outperformed common average re-referencing for reducing DC offset and low frequency drift, as seen in an example stimulation session (Fig. 2.7Ai). High pass filtered signals (blue) had baselines closer to 0 than re-referenced signals (purple), although both processing techniques reduced $>150U_o$ of DC offset. Linear models of baseline values captured this difference, with lower y-intercept and slope values for the high pass filtered signals than the CAR processed signals (Fig. 2.7Aii).

These trends were consistent across Subjects 2-5 in all metrics used. Of all the methods, the high pass filtered signals had the tightest distributions of y-intercept and slope centered around 0 (Fig. 2.7Aiii, upper), the fewest channels with statistically nonzero y-intercept and slope values (Fig 2.7Aiii, middle), and the fewest y-intercepts exceeding $1U_o$ and slopes exceeding $1U_o$/100s (Fig. 2.7Aiii, lower). Filter parameters differed in efficacy across these subjects, with some subjects showing greatest noise reduction with a 0.1Hz cutoff and some with a 1Hz cutoff. In all subjects, high pass filtering at any of the tested cutoff frequencies reduced the number of channels with slopes exceeding $1U_o$ over the course of 100s to zero. In 3/5 subjects, y-intercepts exceeding $1U_o$ were also cut to zero by all high pass filtering.

Subject 1 had the lowest levels of both DC offset and low frequency drift (Fig. 2.6A, Fig. 2.7Aiii). Although models identified significantly nonzero y-intercepts and slopes in both raw and processed data (Fig. 2.7Aiii, middle), no y-intercept values exceeded $1U_o$ and no slope values exceeded $1U_o$ per 100s (Fig. 2.7Aiii, lower).

Line noise

In all subjects and on average, line noise removal was most effectively done using notch filters. This surpassed common average re-referencing or averaging over trials, even when jitter was introduced (i.e., when trials were not phase-synchronized with 60Hz noise).

In our example (subject 4, trials include jitter), visually discernible 60Hz noise in the raw data was noticeably reduced after notch filtering, common average re-referencing, and

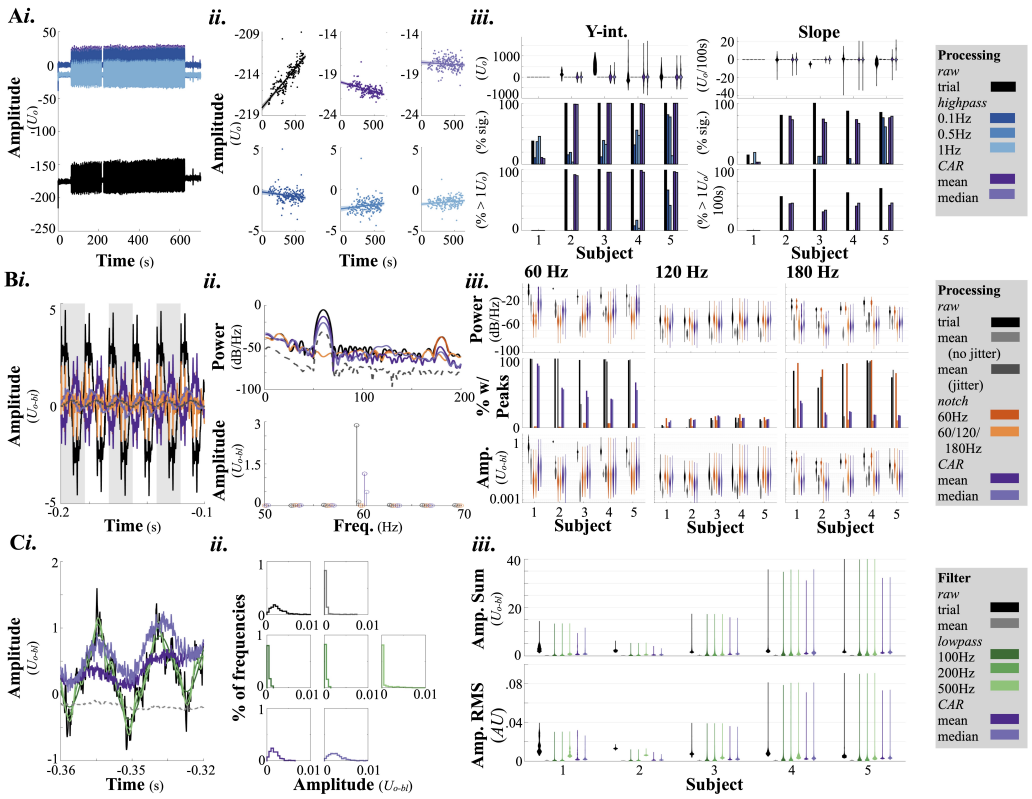

Figure 2.7: Efficacy of noise removal methods. (A)(i) Comparison of one stimulation session (session 1, subject 4) with and without preprocessing. (ii) Linear models fit to baseline means of each signal in Ai. Note that y-axis differs but an equal range is represented in each subplot. (iii) Upper: Distribution of y-intercepts (left) and slope (right) over all channels and all stimulation sessions for each subject. The slope over 100s, rather than 1s, is displayed to better visualize the cumulative impact of low frequency drift over a stimulation session. Middle: Percentage of y-intercepts (left) and slopes (right) over all channels and stimulation sessions for each subject that are statistically significant (i.e., nonzero) in the linear model (FDR corrected, p <0.05). Lower: Percentage of y-intercepts (left) and slopes (right) that exceed $1U_o$ (i.e., are offset from zero by more than $1U_o$ or have a baseline shift exceeding $1U_o$ over the course of 100s). (B)(i) Comparison of line noise in one trial baseline, with and without preprocessing, as well as the mean over all trials. (ii) Upper and lower panels show, respectively, the Welch power spectrum and the Fourier transform of these baseline periods. (iii) The distributions of power spectral density estimates over trials and channels (upper), percentage of trials and channels with peaks (middle), and distributions of amplitude over trials and channels relative to baseline (as estimated using a FFT, lower) for 60 (left), 120 (center), and 180 (right) Hz over all trials on all channels for each subject. The power spectral density of the mean signal's baseline is also shown. Stimulation sessions with (dark grey) and without (light grey) jitter are grouped together for the averages. (C)(i) Comparison of signal in one trial baseline, with and without preprocessing, as well as the mean over all trials. (ii) Distribution of amplitude contributions of all frequencies 250-2000Hz, shown as a proportion of the whole. (iii) Distributions of the sum (upper) and RMS (lower) of amplitudes for frequencies 250-2000Hz over all trials, channels, and stimulation sessions. U_o: overall normalized units; U_{o-bl}: overall normalized units with baseline correction; CAR: common average re-reference; RMS: root mean square; AU: arbitrary units.

averaging over trials (Fig. 2.7Bi; vertical grating marks the period of one 60 Hz cycle for reference). This reduction in noise levels can also be seen in frequency space, in both the power spectral density estimates (Fig. 2.7Bii, upper) and the Fourier transformed data (Fig. 2.7Bii, lower). Re-referencing to either the mean or the median leaves a residual, though small, peak at 60Hz.

Over all subjects, notch filtering was most effective at reducing 60Hz power and including notch filters at harmonics also reduced power at these frequencies (Fig. 2.7Biii, upper). Averaging and re-referencing reduced noise to lesser degrees (Fig. 2.7Biii, upper). Only notch filtering had a consistent effect on the presence or absence of power spectral density peaks at 60Hz and harmonics, with averaging and common average re-referencing changing the percentage of trials with peaks very slightly, if at all (Fig. 2.7Biii, middle). This indicates residual narrowband spiking at line noise frequencies after averaging or common average re-referencing, although the power distributions did generally indicate a drop in power with these methods (Fig. 2.7Biii, lower).

Results of a Fourier analysis of 60Hz (and harmonics) power were very similar to the power spectral density results, but both filtering and common average re-referencing failed to decrease relative power in certain outliers, particularly in Subjects 4 and 5 (Fig. 2.7Biii, lower). The power of these outliers sometimes exceeded $1U_o$, indicating that 60Hz or harmonic oscillations could account for differences that exceeded the average standard deviation of signals.

High frequency noise

The most effective method of reducing high-frequency noise was averaging over trials (Fig. 2.7Ci-ii). Low pass filters of any cutoff performed about as well as CAR for reducing the outlier trials and channels where the high frequencies contributed with large amplitude (15-$40U_{o-bl}$). However, low pass filtering was more effective than CAR at ameliorating high-frequency noise amplitude in most cases, with lower cutoffs more effectively reducing noise than higher cutoffs (distributions closer to 0 in Fig. 2.7Ciii). Additionally, the low pass filtered signals are visually much smoother than the raw or the CAR signals when looking at trial data (Fig. 2.7Ci).

2.3.4 Failure to remove artifact results in temporal spread after filtering

Passing high amplitude artifacts through filters may temporally spread the artifactual period beyond the short (∼1ms) duration of the raw artifact. To quantify this, we extracted artifacts

from stimulation data and added them to artifact-free resting neural signals at different amplitudes (scaled relative to the standard deviation of the resting signal), then compared the artifactual and artifact-free data after filtering (Fig. 2.8). High pass filtering at 0.1Hz resulted in little spreading of the artifact (Fig. 2.8Bi), but notch filters at 60, 120, and 180Hz (Fig. 2.8Bii) and a low pass filter at 200Hz (Fig. 2.8Biii) caused visually discernible temporal smear. Fig. 2.8C shows the greatest difference in magnitude, outside of the duration of the raw artifact, observed between the artifact-free and artifactual data after each filter was. For all subjects, artifacts exceeding 500x the standard deviation of the raw neural signal introduced differences exceeding 1AU (the average standard deviation of the baseline period over all trials and channels in a recording session) after low pass filtering (Fig. 2.8Ciii).

2.4 Discussion

2.4.1 The impact of processing on CCEP quantification

Processing may change CCEP quantification results both by decreasing noise and by introducing artifact. The former is a desired outcome; the latter is not. We cannot disentangle these causes and we have no ground truth of quantification against which to compare filtered CCEPs. Our goal is therefore not to judge the impact of filtering on quantification as "good" or "bad," but to point out that this impact exists, highlighting the importance of consistency and thorough reporting of processing techniques in all CCEP studies. More aggressive high pass and low pass filters introduce larger changes in CCEP magnitude and morphology than their less aggressive counterparts, as demonstrated with the mixed-effects linear models summarized in Table 2.3 and the difference distributions in Figure 2.4. High pass filters with a cutoff of 0.1Hz and low pass filters with a cutoff of 500Hz are the least impactful on CCEP quantification in terms of the magnitude of changes. Using a high pass cutoff <0.3Hz has been recommended in event-related potential studies [172], and our results suggest that this is also good practice for CCEP studies. Using one versus three notch filters did not change the impacts to CCEP quantification, which were minimal. Filtering generally had little effect on the latency of CCEP components (Table 2.3).

Common average re-referencing had the most profound effect on CCEP quantification. Table 2.3 shows significant differences in amplitude, latency, and RMS for all components in the re-referenced data as compared to the unprocessed data. In Figure 2.4, we see broad and variable distributions of the effects of CAR processing, suggesting high variability in the effects both within and between subjects. Re-referencing is addressed in greater detail below.

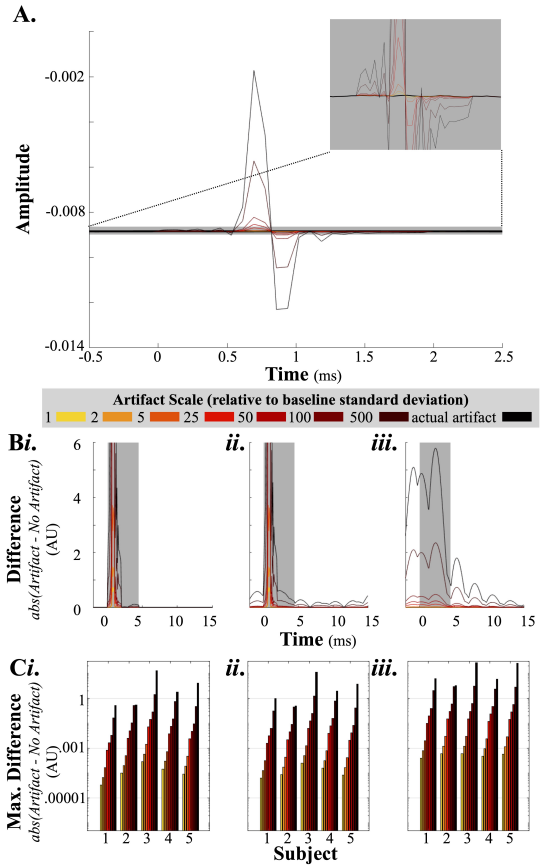

Figure 2.8: Artifacts are temporally spread by filtering. (A) We constructed artifact models for each subject (example: Subject 4) by extracting an artifact from an arbitrarily chosen channel with a visually distinguishable CCEP. We scaled the maximum amplitude of the artifact relative to the standard deviation of a resting period (yellow = relatively lower amplitude, dark red = relatively higher amplitude). Scaled artifacts were added to this resting period. The signal with the unscaled (raw) artifact is shown in black. (B) The artifactual signal, as well as the resting signal with no added artifact was then passed through a 0.1 Hz high pass filter (i), a 60/120/180 Hz notch filter (notch width $\pm$3 Hz; ii), and a 200 Hz low pass filter (iii). The absolute difference between the signals with and without artifacts, scaled to the appropriate stimulation session's normalization factor, is plotted as a function of time from artifact onset. The samples that contain the artifact in the unfiltered signal are shaded in grey. (C) For each subject and artifact size, the maximum differences, as shown in B, outside of the artifactual period of the raw signal (grey shaded areas in B), is shown for high pass (i), notch (ii), and low pass (iii) filtered conditions. Note logarithmic y-scale. AU: arbitrary units.

2.4.2 The issue of re-referencing

Re-referencing is meant to decrease the impacts of volume conduction and shared signal between electrodes. With a stereotyped signal like a CCEP, however, distinguishing between shared signal and similar but independent neurophysiological responses at two recording channels becomes very difficult. As discussed previously, we do not have the ground truth CCEP that we would need to assess this. Modelling studies have demonstrated that volume conduction occurs in sEEG stimulation data [153] . However, the canonical multi-component CCEP seen in many of our subjects (Fig. 2.3) and throughout the literature [99, 104] has been interpreted as a series of neurophysiological responses to stimulation [31, 99], which often have similar shapes across subjects and brain areas (although this multi-component structure is not always present in cortical responses to stimulation) [128]. If recording contacts along an sEEG probe or an ECoG array were all to exhibit CCEPs of similar shapes but different magnitudes, subtracting the average could reduce the component amplitude for larger CCEPs, eliminate components in CCEPs of similar magnitude to the average, and reverse component polarity for small CCEPs. Although we only analyzed sEEG data, we expect similar results when using CAR on an ECoG array or strip.

Regardless of whether this is a "true" correction eliminating a common signal or a "false" alteration of similar neural signals, the differences introduced by CAR processing were notable and variable. Although re-referencing is a standard method for processing sEEG [126], it is often eschewed in evoked potential studies [16, 55, 79, 122, 120].

Additionally, as discussed above, re-referencing alone is not sufficient to reduce low frequency, high frequency, or line noise. Therefore, when noise levels exceed tolerability for a CCEP study, CAR processing may address volume conduction, but does not sufficiently address other non-neural noise.

Re-referencing electrophysiological data has uses other than noise reduction as well. Re-referencing data can help more accurately localize the signal source [43, 108]. Recent work has shown that common average re-referencing is inadequate for localizing CCEP responses in sEEG and that bipolar and Laplacian re-referencing schemes may be more appropriate [43], and these are more common than CAR in sEEG.

Bipolar and Laplacian re-referencing schemes both result in montages that are distinct from the raw data. Because the present study relies heavily on direct comparisons between processed and raw data, assessment of these techniques is outside of the scope of this paper.

We urge caution in using CAR schemes when analyzing CCEP data and emphasize the vitality of reporting any re-referencing performed. In general, but especially when re-referencing is not performed, the original recording reference should be reported.

2.4.3 Tolerability of noise in CCEP data

The exact levels of noise present in any intracranial data, including CCEP data, varies greatly depending on recording equipment and environmental conditions at the research site. Not all noise can be removed, even with aggressive filtering, and, as discussed above, filtering can introduce tradeoffs for CCEP quantification. Therefore, it is important to define how much noise is tolerable in CCEP data and correspondingly the degree to which noise will need to be addressed using processing. This will vary depending on the signal-to-noise ratio required for a given project or experimental question.

As a general reference point for noise tolerability, we examine the degree to which noise can impact signal amplitude relative to the typical fluctuations in background activity averaged over all channels (described by units U_o and U_{o-bl}). Again, exact thresholds will vary, but we suggest that an amplitude difference in sEEG data exceeding $1U_o$ introduced solely by noise may become problematic. For example, if 60Hz oscillations in one channel were many times larger in amplitude than average baseline fluctuation, it would suggest that this noise alone could increase the amplitude of an identified peak by many units. Likewise, if low frequency drift can greatly shift the baseline amplitude from trial to trial over the course of a recording session, processing is likely necessary. While the actual quantification of CCEP amplitude may be ameliorated by using channel-wise normalization, we use the amplitude variation of $1U_o$ as a benchmark in our quantification of noise. When applicable, we also use intuitive, metric-specific benchmarks (e.g., percentage of channels with a significantly nonzero DC offset) to assess noise levels, tolerability, and the efficacy of processing.

2.4.4 The impact of processing on noise

We show in Figure 2.7 that filtering is most effective at reducing DC and line noise levels, more so than common average re-referencing or averaging across trials. Low cutoff high pass filters generally perform as well as or outperform more stringent filters. Averaging over trials is the most effective way of reducing high-frequency noise, but on the individual trial level, low pass filtering outperformed CAR (Fig. 2.7).

CAR tends to decrease DC offset but not bring the offset as close to zero as high pass filters (Fig. 2.7A). It has larger effects on low-frequency drift, but again is less effective by our metrics than filtering (Fig. 2.7A). As we were examining low frequency noise over a long time course, we did not assess the impact of averaging trials on low frequency noise.

Similarly, CAR processing is less effective than notch filtering at removing 60Hz noise and its harmonics, as measured by the power and the presence of a narrow peak in power (Fig. 2.7B). Interestingly, re-referencing had a greater impact on the power and the percentage

of channels and trials with significant peaks in power at higher harmonics (180Hz) than at lower harmonics (120Hz) or 60Hz itself (Fig. 2.7B). Re-referencing and notch filtering reduced 60Hz and harmonic frequency amplitudes to similar degrees (Fig. 2.7B). Averaging over trials, even when jitter was used in trial timing, did not reduce 60Hz noise. We would expect averaging with jitter to largely cancel out noise, while averaging with jitter would not, but saw similar levels of efficacy with both protocols, even when compared directly in a single subject (Subject 4).

Finally, low pass filtering outperformed re-referencing at reducing high frequency sampling noise in the data (Fig. 2.7C). Even low pass filtering with a relatively high cutoff (500Hz) decreased sampling noise substantially in most cases, although long upward tails in the distributions of cumulative and RMS power in subjects 3-5 suggest that there may be some cases when this high low pass is not effective (Fig. 2.7C). Averaging over trials has little impact on the power of high-frequency noise, likely because random white noise will not have consistent phase across trials, so it will not average out (Fig. 2.7C).

It is also worth noting that, in addition to decreasing noise measured during baseline periods, filtering CCEP data also introduced artifacts, as seen in Figure 2.3. High high pass filters (1Hz cutoff) introduced a low frequency decrease in the baseline value prior to the stimulation onsets, although this was not pronounced with lower cutoffs (Fig. 2.3A). Notch filtering increased 60Hz ringing or rippling artifact in the $\sim$0.1s prior to stimulation onset (Fig. 2.3B), and low pass filtering similarly introduced high frequency ringing or rippling artifact in this pre-stimulation period (Fig. 2.3C). The 60Hz artifact was not notably different when using 1 or 3 notch filters (Fig. 2.3B). High frequency artifact was more temporally restricted with higher cutoff low pass filters (Fig. 2.3C). These artifacts are directly counterproductive for the overall goal of reducing noise levels but, in the case of notch and high pass filters, most prominent in the pre-trial period rather than during the CCEP itself (although the CCEPs may obscure additional artifact).

Our stimulation artifact removal process included a quality control step based on the analysis shown in Figure 2.8. We implemented a threshold (5x the standard deviation of the pre-stimulus baseline) for acceptable residual stimulation artifact and excluded any trials for which the signal, after artifact removal, did not meet this standard. In our modeling, stimulation artifacts below this threshold did not introduce any high amplitude smearing after filtering (Fig. 2.8). Therefore, we do not expect the ringing or rippling artifact seen in Fig. 2.3 to be explainable by residual stimulation artifact. Rather, it may be early, high amplitude CCEP components – interpretable data that cannot easily be removed from the signal – that introduce this ringing when filtered.

2.4.5 A note on normalization and baseline correction

Normalization and baseline correction techniques are outside of the scope of this study. However, as they are important steps in processing, we will briefly address their use.

When using traditional CCEP quantification techniques, normalization and baseline correction are both vital for interpreting results across subjects. Because different subjects, and different channels within subjects, may have different baseline noise levels, directly comparing CCEP amplitude in units of volts, for instance, may not be valid. Additionally, when DC offset is present, comparing magnitude metrics is meaningless unless trials are recentered to zero, so baseline subtraction is also necessary.

For our analyses, we use two different normalization frameworks, both described in detail in Section 2.2.6. While we chose these as the most logical normalization frameworks to use in making direct comparisons between processed and unprocessed data, neither may be the most effective for most CCEP analyses. Specifically, in a fully-fledged processing pipeline, we would expect normalization to be one of the final processing steps. While a channel-wise normalization factor makes sense for CCEP analysis (see Section 2.2.6 for justification), it does not make sense to calculate this factor on the raw data and apply it to the processed data, as we did here. Rather, a channel-wise normalization factor can be computed from and immediately applied to the processed data. Previous work has suggested that using trial-wise normalization factors can bias event-related potential data [26, 69], which is why we take the average standard deviation over all trials' baseline periods for each channel and use this factor on all trials, rather than dividing each trial by the standard deviation of its baseline.

2.4.6 Framework for choosing an appropriate processing strategy

As previously stated, we do not intend to make any specific blanket recommendations for CCEP processing. However, here we present a framework for choosing an appropriate preprocessing strategy for CCEP data, using our data as an example.

The first step should be to assess noise and its tolerability. Of the 5 subjects in this study, 4 have DC offset and low-frequency drift that exceed our tolerability metrics in >50% of channels. While all subjects have some degree of 60Hz and harmonic line noise, we see notably lower levels of 120Hz noise across subjects than we do 60 and 180Hz noise. Although all or nearly all trials and channels have peaks in spectral power at 60 and 180Hz, the amplitude of 180Hz oscillations is generally quite low, not exceeding $1U_{o-bl}$ in any subjects. Finally, high-frequency noise has a relatively minimal effect on the data generally, but may have greater effect in outlier trials and channels.

In addition to examining noise levels, it is also important to assess the tradeoffs of all processing methods being considered. For example, high pass filtering with higher cutoffs was more effective than high pass filtering with lower cutoffs in some of our subjects. However, in all subjects, the high cutoff introduced low-frequency artifact that could be problematic. Using a 0.1Hz cutoff brought the slope within the range of tolerability for all subjects without introducing this artifact. Although it was less effective at reducing the offset (y-intercept) in Subjects 4 and 5, any residual offset would be addressed by baseline subtraction. Notch filtering introduced ringing or rippling artifacts prior to stimulation onset but was quite effective at reducing the 60Hz noise identified in the data. Low pass filtering also introduced some noise prior to stimulation onset, but this was relatively contained.

Bringing these pieces together, an appropriate processing pipeline can be developed. Based on the tolerability levels of our noise and the potential tradeoffs of our filters, we suggest that the following process would be appropriate for the data presented here:

1. Removal of stimulation artifact and rejection of channels and trials containing artifact and/or epileptic activity
2. Filtering (high pass filter with 0.1Hz cutoff, single notch filter at 60Hz, low pass filter with 500Hz cutoff)
3. Channel-wise normalization
4. Trial-wise baseline subtraction

This pipeline uses the gentlest filtering possible while still bringing noise within tolerability levels. It does not re-reference the data so as to maintain the morphology of CCEPs. The low pass filtering may not be strictly necessary from a noise perspective, but given its generally small impact on quantification, the minimal pre-stimulation artifacts introduced, and the benefits for visualization of a smoother signal, it may be included in the pipeline, particularly if latency and/or RMS were to be the primarily analysis metrics. Implementing a low pass filter would also allow us to downsample the data from 12kHz without introducing aliasing, making data storage easier.

2.4.7 Limitations and future directions

This study is far from an exhaustive examination of processing techniques used for CCEPs. Further work detailing the effect of processing on both noise and CCEP quantification will be needed, and each research group will need to consider the noise present in their own data. The parameter space of processing is infinite, so here we highlight a few variables

that could use further investigation. When filtering, filter design is important. We chose to use an 8th order Butterworth filter based on qualitative assessment and field standards [47, 139, 108]. However, many other options exist. Other filter types may be more effective at reducing noise, although the filters we use here are effective enough for our purposes. Filter parameters may also impact the amount of rippling and other artifact introduced. Notch filters that introduce less ringing or rippling artifact in CCEP data, for instance, would be useful to make the tradeoff between noise and filtering more favorable.

Further work is needed to assess how different processing strategies interact when performed together. This includes stimulation artifact removal — different artifact removal strategies may lead to different effects on CCEP quantification after filtering and re-referencing.

2.5 Conclusions

In this paper, we demonstrate that processing of any kind can introduce changes in CCEP quantification as compared to unprocessed data, but noise is present in intracranial CCEP recordings to a degree which may in and of itself impact quantification. We find that filtering is the most effective way to reduce this noise, although filtering can also introduce artifacts to CCEP data. With this in mind, we suggest a flexible, project-specific framework for identifying noise levels and assessing potential tradeoffs of processing techniques. Additionally, we identify filter cutoffs that effectively reduce noise while introducing minimal artifacts. We emphasize the importance of thorough reporting of any and all processing performed in CCEP studies, particularly re-referencing. We find that the re-referencing scheme used may have significant effects on the data, and suggest that any re-referencing, or lack thereof, should be thoroughly considered and its effects on data taken under consideration.

Chapter 3

CCEP trials and variability

3.1 Part I: CCEP Variability and Number of Trials

Cortico-cortical evoked potentials (CCEPs) are a well-established metric of effective connectivity measured in response to single pulses of electrical stimulation. The number of single pulse trials needed to yield reliable results while minimizing risk of stimulus habituation or temporal conditioning has not been previously characterized. We systematically approach the question of CCEP experimental power. We quantify variability of CCEP magnitude scalars (peak/trough amplitude; component root mean square, RMS) and temporal characteristics (peak/trough latency) as a function of the number of applied pulses. Methods: Using a subsampling approach, we examine the stability of CCEP amplitude, latency, and RMS quantification using subsets of 10 to 200 trials. We identify the statistical power of various trial numbers to detect changes in amplitude, latency, and RMS and test the null hypothesis that these metrics do not change over the course of a stimulation session. Additionally, we compare these results when quantifying the CCEP from a mean time series versus from individual trials. Analyses show that on average, CCEP quantification stabilizes and becomes more accurate using fewer trials when quantifying individual trials as opposed to quantifying the mean time series. Sufficient (>0.8) statistical power for changes in amplitude or RMS up to ±25% in magnitude and for changes in latency up to ±50ms can be achieved using ∼50 trials. Potential concerns about CCEP habituation/conditioning may arise in some subjects. We estimate that approximately 50 trials should be adequate for most CCEP analyses. Using standard stimulation parameters, collecting 50 trials should last less than 2 minutes per stimulation site, which should be tractable given clinical time constraints and ameliorates concerns about stimulation habituation/conditioning. We find that when fewer trials are used, quantifying individual CCEP trials may be preferable to quantifying the mean CCEP over all trials.

3.1.1 Introduction

Cortico-cortical evoked potentials (CCEPs) are a measure of effective connectivity obtained by applying single pulses of electrical stimulation to one area of the brain and recording responses elsewhere in the brain. The stereotyped, multiphasic CCEPs seen at a recording site are typically interpreted as the response of this site to activity at the stimulation site [62, 104, 99].

Physiological responses to electrical stimulation in the brain have been observed since the middle of the twentieth century [154, 155, 66]. Since being introduced as a metric of brain connectivity by Matsomuto et al. in 2004 [122], CCEPs have been broadly used in invasive human electrophysiology. CCEPs have been used to map networks [122, 79, 98], identify seizure onset zones in epileptic patients [75, 194, 94], and measure connectivity changes induced by interventions such as electrical stimulation conditioning [97].

Although the stimulation methods used to obtain CCEPs are relatively consistent across the field, the number of stimulation trials included in analysis vary widely. As few as 10 trials are used in some studies [79], while others include upwards of 1000 trials [97].

The number of CCEP trials often depends heavily on time constraints inherent to data collection in clinical populations. CCEP studies are typically performed using transiently implanted electrocorticography (ECoG) and/or stereo-electroencephalography (sEEG) electrodes. Frequently, as in this study, data is recorded in patients who have ECoG and/or sEEG electrodes implanted for approximately 1 week for clinical monitoring of intractable epilepsy. Data may also be recorded intra-operatively in patients undergoing craniotomy [89, 171].

In both intra-operative and post-operative spaces, factors outside of the experimenters' control can dictate the amount of time available to them for CCEP studies. For example, a patient's clinical schedule, visitor schedule, and sleep schedule can all contribute to their post-operative availability for research studies. As a result, using the fewest possible trials is often desirable. Additionally, using fewer trials limits any risk of introducing a habituation or conditioning effect on CCEPs as a result of repeated stimulation [97]. There are also reports of task- and state-dependent changes in CCEPs [119], and shorter data collection periods may be optimal for maintaining a consistent brain state. However, using fewer trials often means less reliable results. In this study, we analyze how the number of trials included in analysis can impact the consistency, accuracy, and sensitivity of CCEP quantification.

3.1.2 Methods

Subjects

CCEP measurements were taken with 14 patients (12 male, ages 22-45) while undergoing clinical monitoring for intractable epilepsy at Harborview Medical Center (Seattle, WA, USA). Patients gave informed consent in accordance with a University of Washington Institutional Review Board-approved protocol. Subjects were implanted unilaterally or bilaterally with stereo-electroencephalography (sEEG) probes (AdTech Medical Instrument Corporation, USA). Implant location was clinically determined to assess the origin of intractable seizures.

Electrode localization

As part of standard clinical practice, pre-operative MRI and post-operative CT were acquired from all subjects. Using published software (Localization of Electrodes with a GUI, LeGUI) [37], MRI and CT were co-registered and electrodes were visualized as previously described (cite preprocessing paper).

Data acquisition and stimulation

Data were recorded using a Tucker Davis Technologies (TDT, Alachua, FL, USA) acquisition system. The system consisted of the RZ5D, PZ5 neurodigitizer, and Subject Interface. Data were acquired from a maximum of 128 channels with a sampling rate >12kHz, using a scalp electrode as the reference. Single pulses of symmetric, biphasic stimulation were delivered in a bipolar fashion (between pairs of adjacent sEEG contacts) at 6mA with a pulse width of 200µs per phase.

CCEP protocol

For each subject, up to 32 contacts in anatomical areas of interest (areas of interest varied per subject) of suitable distance from the putative seizure onset zone were chosen for stimulation testing. CCEPs were elicited using single stimulation pulses at a frequency of 0.5Hz. In all but 3 subjects (Subjects 1, 13, and 14), random, nonuniform jitter up to +/- 200ms was introduced in stimulation onset. After stimulating all adjacent contact pairs in these 32 channels, one pair that elicited CCEPs was chosen for further testing. Subsequently, 200-500 stimulation pulses (depending on the amount of time available) were delivered in one continuous stimulation session. For the duration of testing, subjects were asked to rest in their rooms and we minimized distractions.

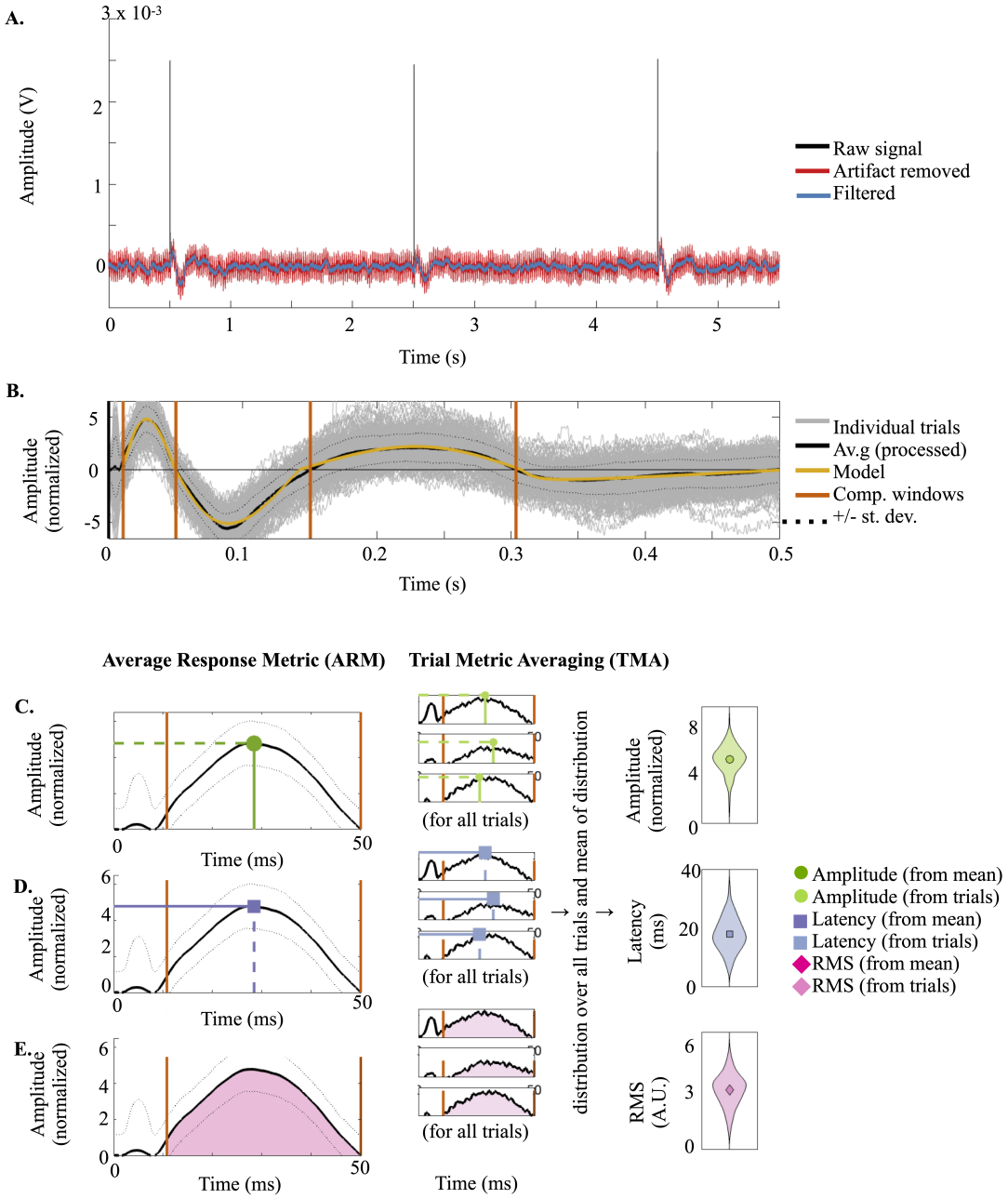

Figure 3.1: CCEP processing and quantification. (A) The stimulation artifact was removed from the data and the resulting time series was filtered (highpass filter at 0.1Hz; notch filters at 60Hz, 120Hz, 180Hz; lowpass filter at 500Hz). (B) We calculated the mean time series over all trials and z-scored the signal relative to a pre-stimulation baseline period. A multi-component model was then fit to the mean time series. From this model and the zero-crossings of the mean signal, component windows were identified. (C-E) Example quantification is shown using the first component of the CCEP pictured in (B). We quantified the amplitude (C) and latency (D) of component peaks/troughs as well as the RMS over the component window (E). We did this using the mean time series (left) and using individual trials (center). After performing trial-wise quantification, we had a distribution of amplitude, latency, and RMS values over all trials and took the mean of the distributions.

CCEP processing

First, data from all channels were visually examined. Channels that were unlikely to contain neural signals (e.g., electrodes that were outside of the brain) and channels with high-amplitude inter-ictal spiking or other artifacts were excluded. A modified version of the stimulation artifact removal method described by Crowther et al. was then used to eliminate stimulation artifact for each remaining channel (Fig. 3.1A) [35]. Rather than replacing a fixed stimulation artifact window with clean data, as in the original paper, we estimated the artifact window per each channel (extending a maximum of 10ms after stimulation onset) and replaced only this period.

The artifact-removed data was then filtered (Fig. 3.1A). Based on an examination of noise levels in the data, we performed highpass filtering at 0.1Hz; notch filtering at 60Hz, 120Hz, and 180Hz; and lowpass filtering at 500Hz. Data were then split into epochs spanning from 0.5s before stimulation onset to 1s after stimulation onset. Epochs contaminated by epileptic activity or other noise were removed from analysis. Remaining signals were z-scored relative to a baseline period from -400 to -100ms before stimulation and downsampled by a factor of 6 (Fig. 3.1B).

CCEP quantification

Average Response Metric (ARM) and Trial Metric Averaging (TMA). We compared two general approaches to CCEP quantification: (1) taking an average over all trials in the time domain and quantifying this average (Fig. 3.1C-E, left), and (2) quantifying each trial time series independently and subsequently averaging (Fig. 3.1C-E, center and right). For ease, we will refer to these strategies as the Average Response Metric (ARM) and Trial Metric Averaging (TMA).

Models to identify component windows. For both approaches, we first identified component (i.e., peak and trough) windows using the mean time series. Although the windows were fit using the mean signal and used in ARM, the same windows were also used as component boundaries for TMA. As previously described (cite preprocessing paper), we fit models to the mean time series to identify approximate component windows. Windows were adjusted slightly so that boundaries between components coincided with zero-crossings in the mean time series. If no zero-crossing was detected near the approximate boundary as identified by the model, the model's boundary was used (Fig. 3.1B).

Quantification. Using these windows, we then quantified each component in both the mean time series (ARM, Fig. 3.1C-E, left) and each individual trial time series (TMA, Fig. 1C-E, center and right). We used MATLAB's findpeaks function to identify the most prominent

peak (i.e., the peak that stood out the most from the rest of the time series) in each component window. The amplitude (Fig. 3.1C) and latency (Fig. 3.1D) of this peak were computed. The root mean square (RMS) over the component window was also taken (Fig. 3.1E).

Screening. CCEPs were then screened for inclusion in the analysis using the mean quantification. We discarded any CCEPs that (1) did not have at least one component where the amplitude exceeded 3 normalized units in either the TMA or ARM; (2) did not have a clear peak in the first component, which was usually indicative of poor separation between the stimulation artifact and the CCEP; and/or (3) had any components with more than one visually distinguishable peak or trough. The latter criterion was implemented to account for a weakness in the model fitting approach – if the signal does not cross zero between a peak and a trough, it is difficult for the model to distinguish these as separate components, so it tends to group them together. Any components with latency values exceeding 250ms in both the man and trial quantification were excluded.

Subsampling process

We used a subsampling approach to identify the effect of the number of trials on CCEP results. First, we randomly chose a subset of N trials from a stimulation session without replacement (i.e., no trial was included more than once in any subset; Fig. 3.2A and B, upper). Using only these trials, we performed both ARM (quantified the mean time series over subsampled trials; Fig. 3.2A, middle and lower) and TMA (quantified the subsampled trials independently and averaged these values; Fig. 3.2B, lower). We repeated this process with 1000 random subsamples to form a distribution of amplitude, latency, and RMS values using a sample of N trials (Fig. 3.2C and D). We used values of N ranging from 10 to 190 trials in increments of 10.

As the number of trials in a subset approached the total number of trials, any individual trial had a greater chance of being included in a subset, and thus subsets had greater chances of having many overlapping trials. This could make the standard deviation over the 1000 repetitions artificially low. To avoid this, we removed any bad trials for each CCEP channel, then calculated the total number of remaining trials. The maximum subset size for each CCEP channel was set to half of this total number.

While consecutive subsampling (i.e., using the first N trials of each stimulation session) may give an more accurate representation of a time-constrained experiment session, random subsampling enables us to perform more statistical tests.

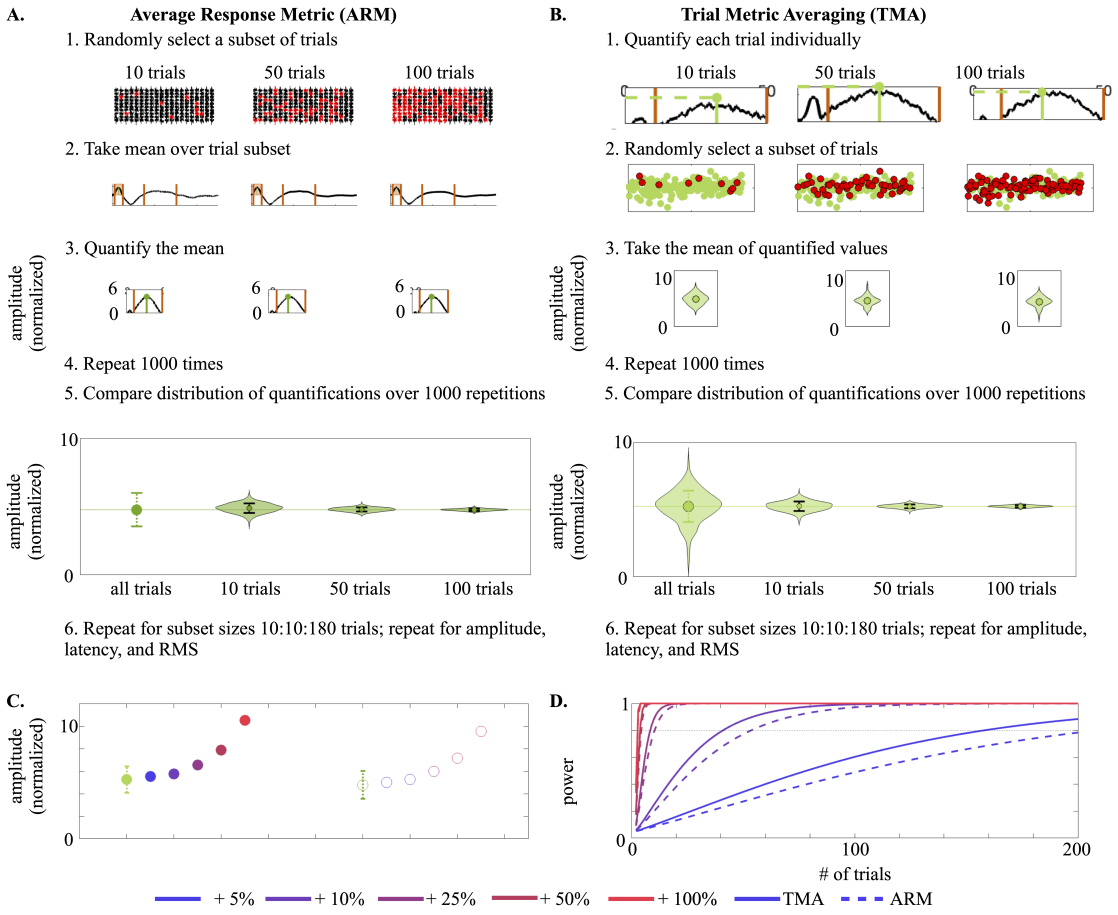

Figure 3.2: Subsampling and power analysis. (A) To quantify CCEPs using the mean of subsamples (ARM), we randomly selected a set number of trials (upper), took the average time series over these trials (middle), and quantified this average (lower; amplitude calculations shown but latency and RMS also quantified). We repeated this 1000 times for each number of trials. We compared the amplitude obtained from quantifying the mean over all trials (left) and to the distributions of values obtained over the 1000 repetitions of subsampling for each number of trials. (B) As in A, but with a TMA approach. We randomly selected a set number of trials (upper), averaged the values over these trials (lower, green dot; amplitude shown but latency and RMS also quantified). We repeated this 1000 times for each number of trials. As before, we compared the amplitude value when using all available trials in the TMA to the distributions of values computed over subsampling repetitions. (C) We calculated the mean and standard deviation obtained from mean quantification (right) and trial quantification (left) over the entire stimulation session. The mean was then adjusted by a factors (from 5% to 100%) for power analysis. We did not include mean quantification for latency or RMS due to the difficulty obtaining a standard deviation for those values. For latency, rather than adjusting the mean value by factors, we adjusted it by absolute differences in ms. (D) Statistical power obtained when distinguishing the actual mean from the adjusted means in (C) using different numbers of trials.

Subsampling analysis

Using the distributions obtained by the resampling process described above, we developed metrics for the consistency and accuracy of results for each number of trials. To measure consistency, we took the standard deviation of amplitude, latency, and RMS over the 1000 subsampling repetitions for each CCEP component over all subset sizes used for that component (black bars in Fig. 3.2A and B, lower). We fit an exponential decay model to the standard deviation as a function of number of trials used. We also calculated the difference between the quantification obtained for each of the 1000 repetitions and the quantification obtained using all available trials as a measure of accuracy. For amplitude and RMS, we expressed this difference as a proportional change. For latency, we expressed it in milliseconds.

Power analysis

We analyzed the statistical power to distinguish changes of different magnitudes in amplitude, latency, and RMS as a function of the number of trials included in the analysis. For each CCEP component, we used the mean and standard deviation of the amplitude, latency, and RMS over all individually quantified trials to define the null hypothesis. We then specified the mean of an alternate hypothesis by adjusting the actual mean by a factor (amplitude, RMS; Fig. 3.2C) or a set amount (latency). Using MATLAB's sampsizepwr function, we computed the statistical power to distinguish between the null and alternate hypotheses using sample sizes of 2 to 200 trials and a two-tailed test (Fig. 3.2D).

We also ran the same analysis defining the null hypothesis using the amplitude value from the mean quantification and the standard deviation over all trials at this latency (dotted lines in Fig. 3.2D). We did not perform this analysis using the mean quantification of latency and RMS, as it was more difficult to obtain approximate standard deviations for these values.

Changes in CCEPs over time

To examine if CCEP quantification changed over the course of a stimulation session, we fit linear models of the quantification of each trial versus the onset of stimulation for that trial in seconds for every CCEP component. We repeated this for amplitude, latency, and RMS and performed individual FDR corrections for each metric.

3.1.3 Results

Consistency and accuracy of CCEP metrics over different numbers of trials

To measure the consistency of CCEP metrics using different numbers of trials, we took the standard deviation over all 1000 repetitions of subsampling. As expected, the standard deviation decreased approximately exponentially with increasing number of trials used. Figure 3.3 shows the results of this analysis, pooled over all subjects, CCEPs, and components.

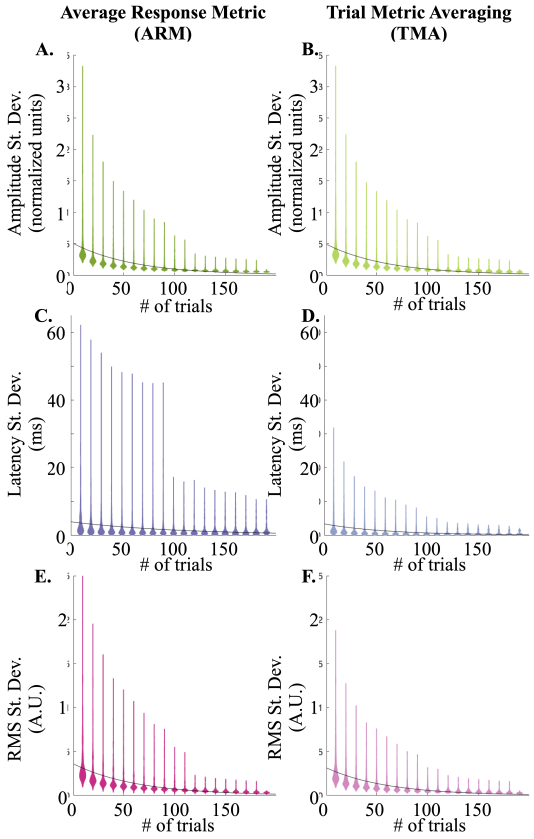

Figure 3.3: Consistency of CCEP quantification with different numbers of trials. We took the standard deviation of quantification over the 1000 subsampling repetitions for the amplitude (A and B), latency (C and D), and RMS (E and F), using both mean (A, C, and E) and trial-wise (B, D, and F) quantification approaches.

The standard deviation of amplitude over subsampling repetitions was similar whether the CCEPs were quantified using ARM (Fig. 3.3A) or TMA (Fig. 3.3B). This was largely true of latency and RMS as well, although long upper tails of the distributions when using the ARM (Fig. 3.3C and E) indicate high outlier standard deviation values as compared to the TMA quantification (Fig. 3.3D and F). This was particularly pronounced in the latency data.

We also measured the accuracy of each metric by computing the proportional difference between the mean over all 1000 repetitions and the values obtained when quantifying using all available trials. These results are shown in Figure 3.4.

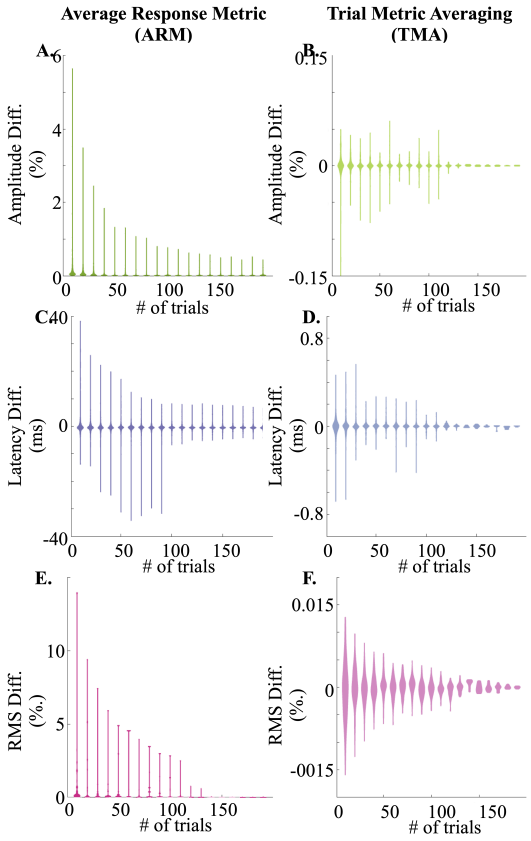

Figure 3.4: Accuracy of CCEP quantification with different numbers of trials. We took the difference between quantification over the 1000 subsampling repetitions and the quantification obtained using all trials for the amplitude (A and B), latency (C and D), and RMS (E and F), using both mean (A, C, and E) and trial-wise (B, D, and F) quantification approaches. For amplitude and RMS, the difference is shown as a proportional to the full trial quantification (0 is no change, positive numbers are increases, negative numbers are decreases). For latency, the difference is shown in ms. Note different y-axis scales.

Here, the long tails associated with RMA as opposed to TMA are even more pronounced (note differing y-limits for each axis). The amplitude (Fig. 3.4A) and RMS values (Fig. 3.4E) achieved when quantifying the mean time series of subset of trials was nearly always larger than the mean as quantified using the mean time series over all trials (see section 3.1.4). Other than this, distributions tended to cluster around zero. As in the standard deviation analysis, distributions clustered more tightly when a greater number of trials was used.

Preliminary results (not shown) may indicate that CCEPs may be more stable in some areas of the brain than in others. Particularly, CCEPs measured in certain temporal cortex structures seem to require more trials to reach the same consistency and accuracy as CCEPs measured in the frontal cortex. Because of the limited overlap between recording areas in CCEP subjects, statistics were not possible.

Power analysis

Figure 3.5 shows the results of power analysis. Very few trials were needed to achieve statistical power of >0.8 when looking for large effects, such as the doubling of CCEP magnitude (Fig. 3.5A and C, bright red) or a shift of 50ms in component latency (Fig. 3.5B, bright red). 50 trials were sufficient to reach 0.8 power when looking for changes in amplitude and RMS greater than +/-25% and latency shifts greater than +/-5ms.

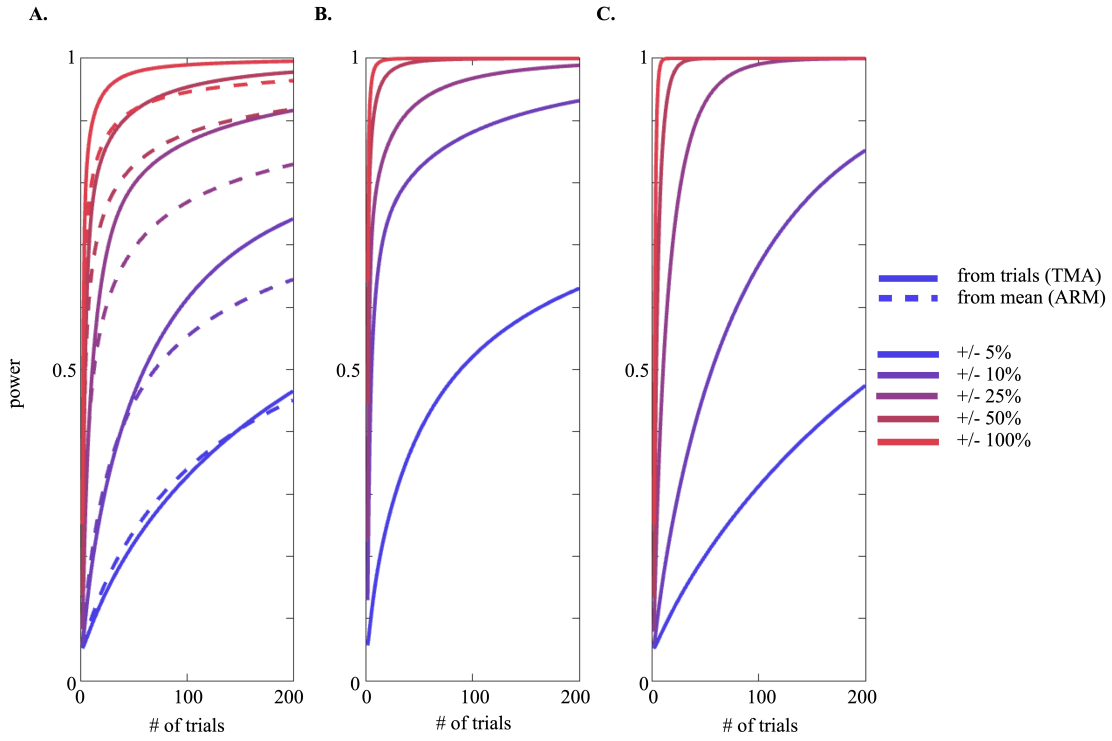

Figure 3.5: Power analysis. Using the mean and standard deviation of quantification over all trials, we calculated the power needed to see shifts of different sizes in amplitude (A), latency (B), and RMS (C). Note that amplitude and RMS were adjusted proportionally while latency was adjusted by a set number of ms.

Due to the nature of two-tailed power analysis, the power obtained when looking for a doubling in CCEP amplitude is equal to the power obtained when comparing the CCEP amplitude to 0 (i.e., detecting CCEP presence or absence using a t-test).

Power analysis was repeated using the amplitude of the mean time series over all trials and the standard deviation time series at that latency (Fig. 3.5A, dotted line) but was not repeated for latency and RMS due to difficulty identifying the standard deviation of these values using mean-based quantification. In general, more trials were needed to achieve the same statistical power as in trial-wise quantification, except for very small (+/- 5%) changes in amplitude, which had similar power in both analyses.

Changes in CCEP quantification over the stimulation session

For each component of each CCEP in each subject, we evaluated the linear relationship between the TMA amplitude, latency, and RMS of that component versus the onset time of the trial. There were significant linear (monotonic) trends in CCEP amplitude (Fig. 3.6A and B), latency (Fig. 3.6C and D), and RMS (Fig. 3.6E and F) over the course of the stimulation in some subjects and components. Six subjects (Subjects 1, 3, 7, 9, 13, and 14) tended to have greater proportions of CCEP components with significant trends over time. In general, slope magnitude increased with increasing amplitude, latency, or RMS – that is, changes tended to be roughly proportional to the quantified value of that component. Slopes tended to be either positive or negative within each subject over all metrics. If amplitude tended to decrease over time in a subject, RMS and latency decreased as well. No clear relationship was seen between the number of trials performed and the overall slope. All subjects for whom stimulation was delivered without jitter (at exactly 0.5Hz; Subjects 1, 13, and 14) were in the group with a greater proportion of CCEPs exhibiting significant trends over time. Across the board, subjects tended to have fewer components with significant changes in latency over the stimulation session than with significant changes in amplitude and RMS.

3.1.4 Discussion

Number of CCEP trials needed will vary depending on analytical goals

For each component of each CCEP in each subject, we evaluated the linear relationship between the TMA amplitude, latency, and RMS of that component versus the onset time of the trial. There were significant linear (monotonic) trends in CCEP amplitude (Fig. 3.6A and B), latency (Fig. 3.6C and D), and RMS (Fig. 3.6E and F) over the course of the stimulation in some subjects and components. Six subjects (Subjects 1, 3, 7, 9, 13, and 14) tended to have greater proportions of CCEP components with significant trends over time. In general, slope magnitude increased with increasing amplitude, latency, or RMS – that is, changes tended to be roughly proportional to the quantified value of that component. Slopes

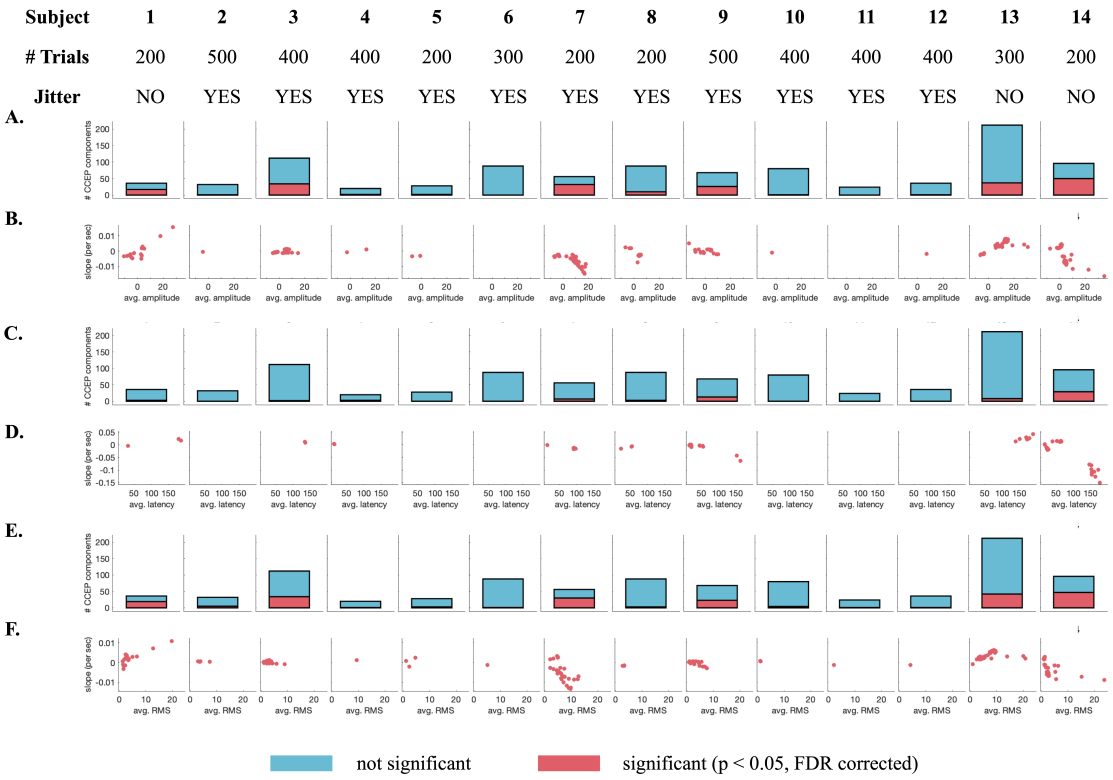

Figure 3.6: Changes in CCEP quantification over the course of a stimulation session. For each subject, we calculated the number of all CCEP components (including components over all channels) with a significantly nonzero slope (red) in a linear regression of stimulation onset time versus trial-wise quantification of amplitude (A), latency (C), and RMS (E), FDR corrected to p = 0.05 per each metric. The slope of the linear model is plotted versus the average value of the component amplitude (B), latency (D), and RMS (F) over all trials in significant components. The number of trials in the stimulation session as well as whether stimulation was delivered with jitter is shown for each subject.

tended to be either positive or negative within each subject over all metrics. If amplitude tended to decrease over time in a subject, RMS and latency decreased as well. No clear relationship was seen between the number of trials performed and the overall slope. All subjects for whom stimulation was delivered without jitter (at exactly 0.5Hz; Subjects 1, 13, and 14) were in the group with a greater proportion of CCEPs exhibiting significant trends over time. Across the board, subjects tended to have fewer components with significant changes in latency over the stimulation session than with significant changes in amplitude and RMS.

In the same resting, task-free, condition we found variability in the CCEP across trials within the same session. Our results suggest that 50 CCEP trials should provide consistency

and accuracy sufficient for most – but not all – CCEP analyses. The consistency (Fig. 3.3) and accuracy (Fig. 3.4) tend to begin to level out near 50 trials, particularly when quantifying trials individually (TMA) rather than quantifying the average time series over all trials (ARM). Approximately 50 trials is also sufficient for medium (∼25-50%) and large (>%50) changes in CCEP amplitude, latency, and RMS to be detected when comparing CCEPs at multiple time points, such as before and after a plasticity-inducing intervention. Long tails in consistency and accuracy measurements, indicating outlier data, tended to plateau around 100 trials, suggesting that using more than 100 trials may result in diminishing returns.

For example, Keller et al. (2018) found amplitude increases and decreases of ∼25-50% after plasticity-inducing stimulation using an ARM approach to quantification (averaging in the time domain prior to quantifying) and using t-tests to calculate significance [97]. With a TMA approach in which trials were quantified individually, 50 trials would likely have provided sufficient (e.g., >0.8) power for these tests (Fig. 3.5). With an ARM approach, our data suggest that ∼150 trials would have been sufficient. In either case, this would have decreased the amount of time needed to collect CCEPs compared to the up to 1273 trials they included in a stimulation session.

The exact number of CCEP trials needed will, of course, depend on quantification approach and metrics of interest. When looking for small changes (e.g., <25% difference from the original value) in CCEP amplitude, latency, or RMS, particularly if using an ARM approach to quantification, more trials will be needed (Fig. 3.5).

On the other hand, when testing for CCEP presence using a t-test against 0 (or a putative zero, such as the pre-stimulus baseline), as in [46], very few trials may be sufficient. A t-test versus zero would be equivalent to a t-test versus a 100% increase in CCEP amplitude, latency, or RMS (red lines in Fig. 3.5). Our data suggest that as few as 10 trials may be appropriate for this kind of analysis.

Our results suggest that looking for differences in amplitude may require more trials than looking for changes in latency or RMS (evidenced by the slower slope in Fig. 3.5A than in Fig. 3.5B-C). To achieve a similar power as in TMA-based amplitude metrics (solid lines, Fig. 3.5A) ARM-based amplitude metrics (dashed lines, Fig. 3.5A) required a higher number of trials. While our methodology limited us to only looking at ARM-based amplitude, similar trends may be present in latency and/or RMS.

TMA quantification poses advantages when fewer trials are available

In addition to the power analysis, other results also suggested that a trial-based quantification approach may be advantageous, particularly when data collection time is limited. On average, TMA quantification resulted in a slightly lower standard deviation over repetitions

in our permutation analysis (Fig. 3.3), suggesting more consistent results. Additionally, when comparing the results obtained with a small subset of trials to results when using all available trials (Fig. 3.5), TMA resulted in smaller differences than ARM, suggesting increased accuracy.

In Figure 3.4A and E, we saw that the amplitude and RMS results when calculated with ARM were nearly always higher when calculated with a small versus a large number of trials. This could be because the signal-to-noise ratio of a time domain mean will be higher when more trials are included in the average. Because CCEP analysis often focuses on peaks and troughs, the time point with the greatest magnitude of amplitude is important. Comparing a noisy to a less noisy time series, some amplitude points will be higher and others will be lower, but peak and trough quantification will always pick the values of the greatest magnitude, resulting in systematic overestimation of amplitude and RMS with fewer trials.

In general, we saw a high correlation between ARM- and TMA-based quantification, although this was less pronounced for smaller amplitude, latency, and RMS values. ARM and TMA quantifications are nearly always going to be slightly different, and one way isn't inherently more accurate than the other. However, our results suggest that TMA may give more consistent results when comparing stimulation sessions with different numbers of trials (e.g., across subjects), particularly if some sessions have <50 trials. Across CCEP literature, quantifying trials individually is less common than quantifying trials from the mean time series, but appropriate data pre-processing (see Chapter 2) may ameliorate concerns about noise in individual trials.

Risk of change in CCEP quantification increases with larger numbers of trials

We found that some components of some CCEPs exhibited significant linear change over the course of a stimulation session. This is consistent with the findings of Cornblath et al. (2023), who noted monotonic trends in CCEP amplitude over the course of 30 trials [30]. However, they show CCEPs that more than double (or more than halve) in amplitude over the course of 30s, whereas the changes in our data, particularly in CCEPs with large average amplitudes, were more modest (Fig. 6).

This change could be because Cornblath et al. delivered stimulation at exactly 1Hz for 30s, whereas our stimulation was at 0.5Hz, with or without jitter, for longer. It is possible that the 1Hz stimulation had a conditioning effect on CCEPs as seen in [97], or that the neural circuitry was habituating to stimulation over this time period. All subjects in our analysis that had stimulation delivered without jitter had a relatively high proportion of components with significant effects, which could indicate that jitter disrupts any conditioning effects. However, as only 3 subjects had stimulation without jitter, the relatively high change in

CCEP components could be due to inter-subject variability. Note that [30] also saw larger trends in electrodes in the seizure onset zone or with high interictal spiking rates, which were likely removed from our analysis.

The change in quantification of CCEPs over the course of trials is generally small compared to the values themselves. However, if these changes continue to be linear, they will add up over time. For example, a change in amplitude of 0.01 normalized units per second, as seen in Figure 3.6, would lead to an average difference of 1 normalized unit over the course of a 50 trial (100 second, at 0.5Hz) stimulation session. This could be an issue with small-amplitude CCEPs, particularly if using a standard deviation-based cutoff for significance testing as in [98]. As the slope of the linear models tended to be larger only when component amplitude, latency, or RMS was large to begin with and only a minority of components had significant linear effects (Fig. 6), we do not expect this to be a major issue for CCEP analysis. It does, however, provide additional impetus for minimizing the number of CCEP trials, and therefore the total time of the experiment.

Because of the high variability between subjects, it is difficult to tell if higher total number of trials is, in and of itself, related to greater slopes. Examining nonlinear trends in data with many stimulation trials could reveal changes in CCEPs that, for example, are only induced after longer periods of stimulation.

3.1.5 Conclusions

Our results suggest that the trial-to-trial variability of CCEPs requires approximately 50 stimulation trials to provide sufficiently consistent, stable, and statistically sensitive results when analyzing CCEP data. We also conclude that quantifying trials individually, rather than quantifying a CCEP as averaged over all trials, may pose advantages when comparing results over stimulation sessions of different lengths, particularly if few trials (<50) are available in one or more of those sessions. Collecting 50 stimulation trials at an average of 0.5Hz will take 100 seconds, making the protocol tractable in intra-operative and post-operative settings, even when repeating the process at multiple stimulation sites. We estimate that a 100s data collection period will also pose minimal risk of conditioning or habituation of CCEPs that can bias results.

3.2 Part II: Variabiltiy in CCEPs Recorded on Consecutive Days

Cortico-cortical evoked potentials (CCEPs) are a measure of effective connectivity that can be recorded in stereoencephalography (sEEG) in response to electrical stimulation. CCEPs may be a useful metric in long-term neuroplasticity studies. We aim to measure how consistent sEEG CCEPs are when they are recorded on separate days in the same patient. In four sEEG subjects, we statistically compared recorded CCEP signals and the amplitude and latency of CCEP components on two consecutive days of recording. Correlation between the signals over two days was high (r^2 >0.7). However, most CCEP components had a significant (Wilcoxon rank-sum test, p <0.05, FDR-corrected) change in amplitude (73.27%) or latency (77.88%). Conclusion: CCEP amplitude and latency may vary over multiple days of sEEG recordings, with subject-specific differences in the magnitude of the variability. We suggest possible mechanisms of this change. Long-term CCEP studies will need to be designed to account for this.

3.2.1 Introduction

Cortico-cortical evoked potentials (CCEPs) are a metric of effective connectivity between a stimulation site and a recording site. CCEPs can be measured using electrocorticography (ECoG) or stereo-electroencephalography (sEEG). They are interpreted as a proxy for the overall synaptic connections projecting from the stimulation site to the recording site.

Given this status as a proxy for connectivity, CCEPs have been used to probe human connectivity networks [122, 123] and measure the effects of stimulation hypothesized to induce neuroplasticity [97]. The latter case is of interest for improving existing stimulation therapies like deep brain stimulation and creating new therapies to promote recovery from other brain diseases and injuries, such as stroke [132]. For these therapies, CCEPs could be a useful tool for measuring long-term effects of plasticity-inducing interventions. For example, CCEPs have previously been used to measure plastic changes in effective connectivity resembling long-term potentiation, long-term depression, and spike-timing dependent plasticity after electrical stimulation conditioning in humans [97] and monkeys [192]. However, these experiments only examined plasticity effects for a relatively short period, and only compared CCEPs within experimental days, not across them.

Little work has been done to examine the consistency of CCEPs over longer periods of time (i.e., days rather than hours) in the absence of such interventions, although there have been reports that CCEPs change with changing brain states [119]. Many CCEP studies are

intra-operative, allowing for CCEP measurement only in the limited time available during a craniotomy or another surgical procedure. Most post-operative CCEP studies are performed in patients undergoing monitoring for intractable epilepsy. During monitoring, epileptic patients stop taking their prescribed anti-epileptic drugs (AEDs) to make it more likely for the clinical team to observe seizures. While these subjects are often available for a week or longer, many Institutional Review Boards (IRBs) require that no electrical stimulation is performed until the patient is back on AEDs, limiting the already-tight schedule for experimenters to measure CCEPs.

However, recent work has demonstrated that electrical stimulation at the amplitudes usually used for CCEPs and other research is unlikely to provoke seizures, even when patients are off AEDs [67]. This has opened the possibility of increasing the amount of time available for stimulation studies, including measuring CCEPs across multiple calendar days.

We examine CCEP data from epilepsy subjects recorded using an IRB-approved protocol that does not require restarting of AEDs prior to stimulation. In four subjects, we measured CCEPs over two consecutive days at the same stimulation site. We compare the CCEPs across these days. While we see high correlation (r^2 >0.74) between the average CCEPs recorded on separate days, we also see significant differences between amplitude and/or latency of CCEP components in nearly every recorded CCEP channel. This suggests that caution should be used when pooling or comparing CCEP data across multiple days of recording.

3.2.2 Methods

Four patients (all right-handed and male, ages 22-45) underwent clinical monitoring for intractable epilepsy at Harborview Medical Center in Seattle, WA. In accordance with a protocol approved by the University of Washington IRB, all subjects gave informed consent. Subjects were implanted bilaterally with stereo-encephalography (sEEG) probes (Ad-Tech Medical Instrument Corporation, USA). Pre-operative MRI and post-operative CT scans were co-registered and contacts were anatomically labeled using Localization of Electrodes with a GUI software [37] as previously described (Section 3.1.2).

Up to 128 channels were acquired for each subject with a sampling rate >12kHz using a Tucker Davis Technologies (TDT, Alachua, Florida, United States) acquisition and stimulation system consisting of an RZ5D, PZ5 neurodigitizer, and Subject Interface as previously described (Section 3.1.2). A scalp electrode was used as the reference. All stimulation consisted of single bipolar, biphasic pulses delivered between pairs of sEEG contacts at 6mA with a pulse width of 200μs/phase.

We chose 32 contacts based on areas of anatomical interest (varied per subject) and performed a stimulation sweep at all consecutive pairs in those 32 contacts to choose a site for the complete stimulation session (see Section 3.1.2). The stimulation session consisted of 200-500 stimulation pulses at 0.5Hz +/- 10% nonuniform random jitter, randomly interleaving the stimulation polarity (i.e., which of the stimulation electrodes was set as the cathode). This protocol was repeated at the same stimulation site the next day. Final analysis was performed agnostic to the anatomical locations of stimulation and recording electrodes.

Data were processed as previously described (Section 3.1.2). Briefly, we visually excluded channels with excessive noise or inter-ictal spiking (channel with excessive noise on either recording day was removed from both days). We then removed stimulation artifacts using a modified version of the method proposed by [10], and removed trials with other artifacts or coordinated inter-ictal activity. Then, we filtered the data (highpass at 0.1Hz, notch at 60/120/180Hz, lowpass at 500Hz) and z-scored relative to baseline. We did not re-reference the data.

We then identified channels with potential CCEPs using an amplitude threshold and visual examination. Any channel with a potential CCEP in either recording day was quantified for both days. We fit multi-component models to CCEPs as previously described (Section 3.1.2), ensuring that the same number of components and polarity pattern (i.e., peak first or trough first) for the models for both days. These models were used to define component windows.

For each individual stimulation trial, we identified the most prominent peak or trough for each component window using MATLAB's findpeaks function and recorded the amplitude and latency. Only components with an average latency less than 250ms after stimulation onset on one or more days were included in the analysis.

We performed a non-parametric Wilcoxon rank sum test for the amplitude and latency of each component comparing all trials on day 1 to all trials on day 2 and calculated the difference between the mean values for the two days. p-values from the rank sum test were corrected using a false discovery rate (FDR) to an alpha level of 0.05. We also calculated the nonparametric correlation between the average over stimulation trials on days 1 and 2.

3.2.3 Results

CCEP similarity across recording days varied between subjects. Figure 1 shows examples of a CCEP that was similar across the two recording days (Fig. 3.7A, left) and a CCEP where the morphology differed more notably (Fig. 3.7A, right). We quantified trials individually and compared the distributions of amplitude (Fig. 3.7B) and latency (Fig. 3.7C) values

between the two days.

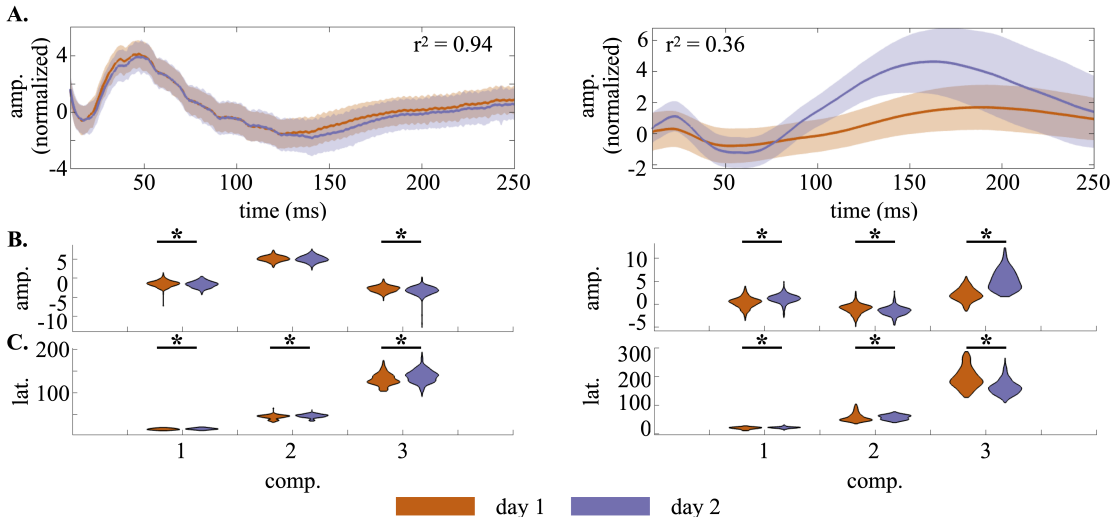

Figure 3.7: Example of CCEPs over multiple recording days. (A) Examples of CCEPs with little change between days 1 and 2 (left, subject 1) and with a larger amount of change between days 1 and 2 (right, subject 3). Shaded area is +/- standard deviation. (B) Distribution of amplitudes for three CCEP components over all trials on days 1 and 2. Stars indicate significant difference (Wilcoxon rank-sum test, p <0.05, FDR corrected). (C) As in B, but with component latency.

Even in the example with a high correlation coefficient between the CCEPs on the two days (Fig. 3.7A, left, $r^2 = 0.94$), there were significant, though small, differences between the amplitude and latency distributions of some components. The changes in CCEP quantification were larger, and significant, in the example with a low correlation coefficient (Fig. 3.7A, right, $r^2 = 0.36$).

Of all components pooled over all CCEPs, 73.27% had a significant (Wilcoxon rank-sum test, p <0.05, FDR corrected) shift in amplitude and 77.88% had a significant shift in latency between the two recording days. All subjects had components with significant differences and components with insignificant differences. There was no CCEP which had no significant difference in amplitude and no significant difference in latency for all components.

While all subjects exhibited some variability between the two days, the magnitude and direction of changes in amplitude and latency varied greatly from subject to subject (Fig. 3.8). In general, components with the largest starting amplitudes in each subject had amplitude changes of the greatest magnitude (Fig. 3.8A). In subject 1, the amplitude tended to decrease on the second day while in subjects 2 and 4, it tended to increase and subject 3 had more mixed results.

Components with longer latencies also tended to have the greatest change in latency,

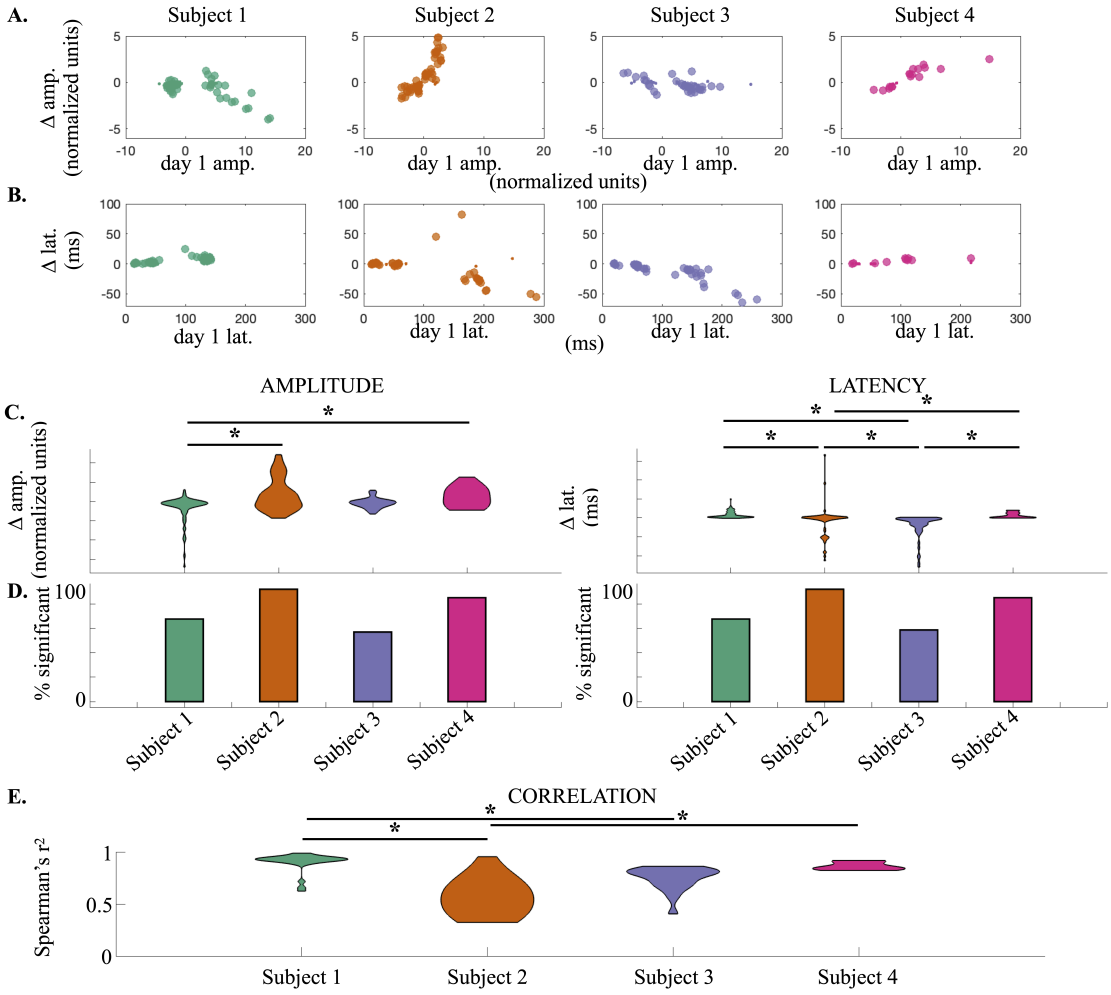

Figure 3.8: Inter-subject differences in multi-day CCEP stability. (A) The difference in amplitude between CCEP components on day 1 and day 2 plotted against the day 1 amplitude. Small dots represent differences that were not significant in a Wilcoxon rank-sum test. (B) As in A, but for component latency. (C) Distributions of differences in amplitude (left) and latency (right) over all CCEP components for each subject. (D) Percentage of CCEP components with a significant change in amplitude (left) and latency (right) over the two recording days. (E) Distributions of r^2 values for the nonparametric correlations of CCEPs recorded on the two days. Stars indicate a significant difference ($p < 0.05$, Sidak corrected) in a post-hoc Dunn's test on the results of Kruskal-Wallis tests for the effect of subject.

though this effect was most prominent in subjects 2 and 3 (Fig. 3.8B). In both subjects, late CCEP components tended to shift earlier on day 2.

In one-way Kruskal-Wallis tests, we saw a significant effect of subject on the magnitude of changes in both amplitude (Fig. 3.8C, left) and latency (Fig. 3.8C, right). Post-hoc comparisons using Dunn's test (with Sidak correction for multiple comparisons) showed that subjects differed the most from each other in latency. Examining the percentage of components with significant changes in amplitude (Fig. 3.8D, left) and latency (Fig. 3.8D, right) showed that subjects 2 and 4 tended to have more significant change in components than subjects 1 and 3.

Another Kruskal-Wallis test comparing the Spearman's r^2 value for average CCEPs on both days also found a significant effect of subject. While subject 2 had more CCEPs with low correlations, the other subject with more significant changes, subject 4, had very high correlations despite large differences in amplitude and latency on the two days.

Across subjects, the mean absolute change in amplitude between day 1 and day 2 was 0.85 normalized units (range in individual subjects: 0.41 to 1.34 normalized units). The mean absolute change in latency was 15.1ms (range: 6.3 to 22.3ms).

3.2.4 Discussion

In this brief report, we demonstrate that CCEP amplitude and latency may not be stable across multiple days of recording in sEEG. While these changes were larger in some subjects than in others, both were present across all subjects tested.

This finding indicates that CCEPs may alter over time, possibly with changes in brain state, which is consistent with previous reports that changes in effective connectivity may happen during sleep [119, 116]. Using extracortical methods (transcranial magnetic stimulation and high-density EEG), Massimini et al. found that the strength of effective connectivity varied during different stages of sleep, suggesting that evoked connectivity may change during different stages of consciousness.

The changes that we see in CCEPs over two recording could also be due to differences in the recording subjects' attention over the two recording days. Other factors could also contribute to this change, including differences in the subjects' activity levels, medications, and/or seizure frequency over the two days. Brain shift may also play a role [126].

Further study with a larger number of subjects and stimulation sites is needed to confirm these results. With more data, including data from multiple subjects with stimulation in a similar area, we could also investigate the relationship between CCEP changes and anatomical areas and explore potential mechanisms underlying this change.

While this difference in CCEPs over multiple days is interesting in and of itself, it may pose problems for longitudinal studies of engineered neuroplasticity if CCEPs change independently of any intervention. The degree to which these changes may be an issue will depend on the research questions at stake in long-term neuroplasticity experiments. Changes of +/-20ms in the latency of a component is unlikely to be meaningful in a longer-latency component, which we observed as changing the most.

However, a change of about 1 normalized unit in a CCEP may be more problematic. Many studies use a z-score threshold to make a binary determination of CCEP presence or absence, so this change could be the difference between a significant and an insignificant CCEP on two different days of recording. In subject 1, some CCEP components more than doubled between the two recording days (Fig. 3.8A), which could be a confound in studies where amplitude increases of 25-5% are of interest [97].

As we see significant changes in CCEP amplitude and latency in most cases across the four subjects presented here, we urge caution when designing experiments that compare CCEPs over the course of multiple days or longer.

This does not mean that long-term experiments tracking neuroplasticity using CCEPs are impossible. Appropriate controls could allow for correction of data collected over multiple days, or study design could avoid inter-day comparisons. Measuring baseline day-to-day changes in subjects at the start of long-term experiments could help minimize confounds. Alternatively, certain functional connectivity may be more stable across multiple recording days [23] and could be used to contextualize CCEPs in this kind of study.

Chapter 4

Intraoperative Characterization of Subthalamic Nucleus to Cortex Evoked Potentials in Parkinson's Disease Deep Brain Stimulation

Deep brain stimulation (DBS) of the subthalamic nucleus (STN) is a clinically effective tool for treating medically refractory Parkinson's disease (PD), but its neural mechanisms remain debated. Previous work has demonstrated that STN DBS results in evoked potentials (EPs) in the primary motor cortex (M1), suggesting that modulation of cortical physiology may be involved in its therapeutic effects. Due to technical challenges presented by high-amplitude DBS artifacts, these EPs are often measured in response to low-frequency stimulation, which is generally ineffective at PD symptom management. This study aims to characterize STN-to-cortex EPs seen during clinically relevant highfrequency STN DBS for PD. Intraoperatively, we applied STN DBS to 6 PD patients while recording electrocorticography (ECoG) from an electrode strip over the ipsilateral central sulcus. Using recently published techniques, we removed large stimulation artifacts to enable quantification of STN-to-cortex EPs. Two cortical EPs were observed one synchronized with DBS onset and persisting during ongoing stimulation, and one immediately following DBS offset, here termed the "start" and the "end" EPs respectively. The start EP is, to our knowledge, the first long-latency cortical EP reported during ongoing high-frequency DBS. The start and end EPs differ in magnitude ($p < 0.05$) and latency ($p < 0.001$), and the end, but not the start, EP magnitude has a significant relationship ($p < 0.001$, adjusted for random effects of subject) to ongoing high gamma (80–150 Hz) power during the EP. These contrasts may suggest mechanistic or circuit differences in EP production during the two time periods.

This represents a potential framework for relating DBS clinical efficacy to the effects of a variety of stimulation parameters on EPs.

4.1 Introduction

High frequency deep brain stimulation (DBS) in the subthalamic nucleus (STN) has been commonly used to treat symptoms of advanced Parkinson's disease (PD) since the late 1990s [185], but its basic mechanisms remain debated. Pathophysiology of PD at the cortical level, particularly the primary motor cortex (M1), is well-established from electroencephalography (EEG) and electrocorticography (ECoG) recordings of PD patients and includes high-amplitude beta oscillations [112, 34] and tight phase-amplitude coupling between beta and gamma frequencies [39]. Some studies have observed reduction of these pathological oscillations with clinically effective DBS [103, 40], suggesting that such abnormal activity is suppressed by STN stimulation. However, our understanding of basal ganglia-cortical interactions, their role in PD, and how they are altered by DBS is limited, and these observations have not yet contributed significantly to clinical treatment [reviewed by 42].

The structural and functional circuits connecting the basal ganglia and the cortex are classically grouped into three pathways – the direct, indirect, and hyperdirect pathways. Of these, STN DBS may directly modulate the latter two [185]. The indirect pathway is a cortico-basal ganglia-thalamo-cortical loop that connects the primary input structure of the basal ganglia, the striatum, to the primary output structure, the internal segment of the globus pallidus (GPi), via the external segment of the globus pallidus (GPe) and the STN. From the GPi, the pathway then projects through motor areas of the thalamus to feed back on the motor cortex [185]. The hyperdirect pathway consists of fibers descending from motor cortical areas directly to the STN [131, 130]. The ascending portions of these circuits are implicated in both the pathophysiology of PD and the therapeutic efficacy of DBS. Many hypotheses exist as to how high-frequency stimulation affects the output of the basal ganglia and how these changes improve PD symptoms [42]. The "informational lesion" hypothesis posits that DBS activates outgoing axons of the STN, thus preventing the transmission of pathological basal ganglia activity to the cortex without disrupting the structural connectivity [70]. The "selective filter" hypothesis suggests a more limited disruption that leaves some functional information transmission between STN and cortex intact while specifically blocking high amplitude, low frequency activity patterns from the basal ganglia [1, 197], leading to an overall enhancement of activity in cortico-basal gangliathalamo-cortical loops [64]. A third, increasingly popular hypothesis suggests that DBS disrupts pathological synchrony within the basal ganglia, thus disrupting abnormal cortical oscillations and phase-amplitude

	Age	Sex	Preoperative PD medication	Disease duration	Implant hemisphere	Recording hemisphere
Subject 1	77	M	Carbidopa-levodopa	11 years	Bilateral	L
Subject 2	76	M	Carbidopa-Levodopa; Entacapone	20 years	L	L
Subject 3	69	M	Pramipexole; Carbidopa-Levodopa; Rasagiline	5 years	R	R
Subject 4	71	M	Carbidopa-Levodopa; Rasagiline; Ropinirole	8 years	Bilateral	R
Subject 5	63	M	Carbidopa-Levodopa	35 years	Bilateral	L
Subject 6	78	M	Carbidopa-Levodopa	5 years	Bilateral	L

Table 4.1: Subject demographics.

coupling entrained and propagated through cortico-basal ganglia-thalamo-cortical loops [40, 187]. Further exploration of the functional impacts of STN stimulation on cortical physiology could help elucidate subtle differences between these theories.

An extensive literature has explored evoked cortical activity (e.g., EEG, ECoG) in response to single stimulation pulses in the STN [42]. Both short- and long-latency evoked potentials (EPs) are observed at the cortex after single stimulation pulses in the STN and GPi [42]. The short-latency ($\sim$2–10 ms) EPs elicited by STN stimulation are temporally consistent with antidromic activation of the hyperdirect pathway, implying this circuit may be activated and/or modulated by DBS [130]. Longer latency (18–25 ms or longer) EPs are thought to reflect multisynaptic, orthodromic transmission through the indirect pathway [5, 42]. While the exact significance of these EPs remains debated, it is thought that they reflect changes in cortical excitability in response to STN stimulation [5].

One limitation of these subcortical-to-cortical EP studies is that they typically look at responses to single DBS pulses, delivered at a low frequency (typically 5–30Hz) to allow for long-latency responses uninterrupted by further stimulation pulses, which would also introduce stimulation artifacts that could obscure cortical signals [42]. However, low frequency stimulation of STN is typically ineffective at treating symptoms of PD [185]. To better understand how therapeutic DBS impacts cortical activity, a characterization of cortical evoked activity in response to high-frequency (>100 Hz) stimulation is necessary.

This study begins to address this gap in our understanding of the functional subcortical-cortical interactions at play in highfrequency STN DBS. We combine ECoG in an intraoperative setting and a recently published artifact removal method that post hoc subtracts artifacts from recordings [19] to reveal physiological signals during ongoing DBS. We then examine cortical EPs during and immediately after trains of high-frequency stimulation that resemble clinical DBS protocols.

4.2 Methods

Subjects

Six subjects (6 M, ages 63–77) undergoing clinical STN implantations for DBS underwent additional, temporary placement of unilateral or bilateral subdural ECoG strips and intraoperative DBS for research purposes. All research methods were conducted in accordance with a University of Washington Institutional Review Board-approved protocol with informed consent obtained from participants. Of the 6 patients, 4 received bilateral DBS implants, 1 received only a right implant, and 1 received only a left implant. The ECoG strip was placed ipsilaterally to the electrode used for stimulation (4 left, 2 right). One patient (Subject 4) was bilaterally implanted with ECoG strips, but only the strip ipsilateral to stimulation (right) was analyzed. Subject demographics, implant information, and medications are summarized in Table 4.1.

For several reasons, we did not seek to directly examine data in relation to the therapeutic effects of DBS for individual subjects due to limited and/or inconsistent clinical follow-up data: (1) Not all patients underwent DBS programming at the University of Washington, making it difficult to obtain accurate records with extensive mapping of clinical response, (2) Patients that we do have records for were often assessed using monopolar or novel stimulation configurations, rather than the bipolar configuration used here, and (3) In at least one subject, the clinical team re-positioned the DBS electrodes after the research team collected data.

4.2.1 Clinical Procedures for DBS and ECoG Placement

All patients were under total intravenous anesthesia as well as PD medication (see Table 4.1) for the duration of the implantation and research protocols. Once in the operating room and deeply anesthetized, patients' heads were fixed at three points using a skull clamp and long DORO Transitional Member Radiolucent headrest system (Pro Med Instruments GmbH). After affixing bone fiducials (Medtronic Inc.) to the skull, a pre-implant CT scan was obtained (see below) and registered to a pre-operative MRI using FrameLink (Medtronic Inc.). The co-registered imaging was used to form a surgical approach plan to the STN (unilaterally or bilaterally, as described above). A Stimloc burr hole cover (Medtronic Inc.) was secured to the skull and the dura mater was opened widely in a cruciate fashion over the hemisphere(s) where the ECoG strip(s) was to be placed. An eight contact macro-scale ECoG strip (2.3 mm diameter exposed surface per electrode, 1 cm inter-electrode spacing, Ad-Tec Medical Instruments Corp.) was slipped underneath the dura posteriorly, parallel to

the midline, so as to approximately cross the hand/upper extremity region of primary motor cortex. A NexFrame frameless stereotactic system (Medtronic Inc.) was then positioned and DBS lead (1.5 mm inter-contact spacing, Medronic Inc., model 3387) placement continued as previously described [82]. A second, post-implant CT was then acquired in order to confirm the position of the DBS lead. This CT was subsequently used to localize surface ECoG electrodes. For one subject (Subject 2), the clinical team repositioned the DBS lead three times in response to imaging examination, but only recordings obtained with the original implant position were analyzed. See Figure 4.1 for positions of ECoG (Fig. 4.1A) and DBS (Fig. 4.1B) electrodes for all subjects.

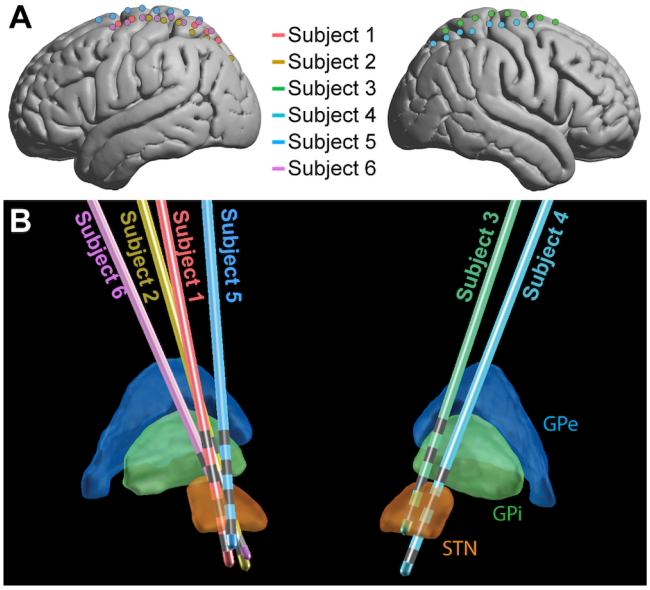

Figure 4.1: Electrode placement. ECoG (A) and DBS (B) electrode locations shown for the 6 subjects in MNI space. For ECoG strips, electrode 1 was the most posterior and electrode 8 was the most anterior. The 4 gray bands on each DBS contact (B) represent the contacts, with electrode 0 the deepest and electrode 3 the most superficial (Medtronic naming conventions). GPe, globus pallidus external segment; GPi, globus pallidus internal segment; STN, subthalamic nucleus.

4.2.2 Intraoperative Stimulation and Recording

All stimulation and recording for research purposes was performed with a Tucker David Technologies (TDT, Alachua, Florida, United States) acquisition system. A TDT IZ2H-16 stimulator with LZ48-400 battery pack was used to stimulate through DBS electrodes, and both STN and cortical electrodes were recorded using a System 3 RZ5D and PZ5 Neurodigitizer. A scalp EEG electrode was used as a reference for all recordings. No stimulation

parameters used in this study exceeded a charge density of 60 $\mu C/cm^2$/phase to ensure patient safety and avoid tissue damage [27].

The stimulation protocol delivered a series of high-frequency stimulation trains, each of 180 (n = 4) or 185 (n = 2) Hz. Each train was 0.5 s in duration with an inter-train interval of 2.5 s (Fig. 4.2A).Stimulation pulses were monophasic and delivered in bipolar configurations between contacts on the DBS electrodes, with pulse widths of 60 (MU)s. 60 stimulation bursts were delivered in blocks to each consecutive bipolar configuration on the DBS lead (0–1, 1–2, 2–3), with trains divided evenly among 4 voltage levels (determined individually for each subject based on the trained clinical team's [AK] recommendations). Each DBS electrode pair was tested in both possible bipolar configurations (i.e., anodic first and cathodic first), for a total of 360 bursts per subject. Only the 90 of these bursts delivered at 3 V (the highest stimulation voltage that all subjects had in common) were considered for analysis, yielding 30 bursts per DBS electrode pair. While DBS stimulation was delivered, recordings were obtained from the 8 cortical strip electrodes at 48 kHz.

4.2.3 Imaging and Electrode Localization

Preoperative clinical Magnetic Resonance Imaging (MRI) and intraoperative Computerized Tomography (CT) were used for electrode localization and anatomical computations. A Philips 3T Achieva scanner with a standard 8 channel SENSE head coil was used to acquire high-resolution 3D T1 magnetization prepared rapid gradient echo (MRPAGE) sequence (repetition time (TR)/echo time (TE)/flip angle: 4.17/51/8°). Slice thickness was 0.750 mm, and the scan included 640 × 640 FOV matrix with 214 overlapping slices, resulting in in-plane resolution of 0.4 × 0.4 mm3. Intraoperative CT scans were acquired on a CereTom scanner (NeuroLogica Inc.), resulting in a 512 × 512 × 88 matrix and an in-plane resolution of 0.5 × 0.5 mm with 1.25 mm slice thickness.

The MRI and CT were co-registered using a standard affine transform in Freesurfer (http://surfer.nmr.mgh.harvard. edu/) and surface electrodes were manually identified. The electrode coordinates were then transformed into 152MNI space (1 × 1 mm). Brodmann areas were determined manually using an MNI-based atlas.

LEAD-DBS [84] was used to localize DBS electrodes on co-registered MRI and CT scans and project them into MNI space. The DISTAL atlas [56] was used in LEAD-DBS to visualize the location of electrodes relative to the thalamus and STN (Fig. 4.1).

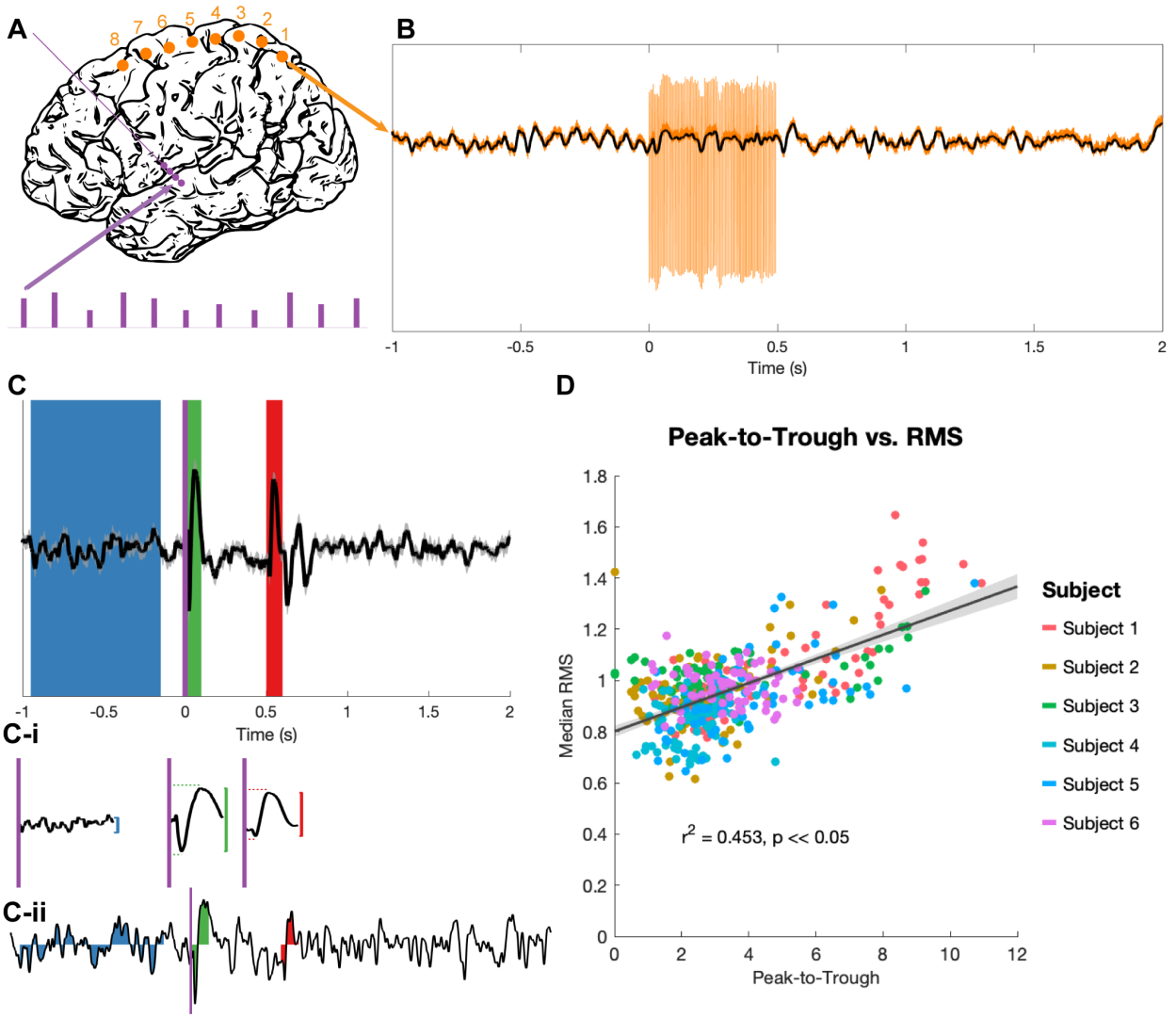

Figure 4.2: Stimulation and evoked potential measurement. (A) Monophasic stimulation was delivered in a bipolar configuration to DBS electrodes (purple dots). Stimulation occurred in 5 s bursts at 4 amplitudes (purple bars), though only EPs evoked by 3 V stimuli were analyzed. Signals were recorded at cortical electrodes (orange dots). (B) Raw trial (orange) shows stimulation artifacts, which were removed by an unsupervised dictionary-based learning algorithm (black). (C) The average of 30 trials (top trace, ±SEM, z-scored) was used to identify EPs. A long baseline period (blue) prior to stimulation onset (purple vertical line) and the 100 ms windows immediately after stimulation onset (t = 0 s, green) and offset (t = 0.5 s, red) were the regions of interest. The peak-to-trough amplitude was computed for each period (vertical red and green lines), as well as the latency to peak and trough components for the two EPs (horizontal red and green dashed lines, C-i). The RMS amplitude was extracted for these time periods for each z-scored individual trial (example trial shown in C-ii). (D) The peak-to-trough of the average trace and the median RMS of all trials (separate medians for the start and end EPs) were highly correlated across subjects in a non-parametric test (generalized linear model in black with confidence intervals in gray, r^2 and p from Spearman correlation).

4.2.4 Data Pre-processing

For EP analysis, minimal pre-processing was used in an attempt to preserve the shape and latency of the complex, multiphasic responses. No re-referencing was performed, as many (if not all) cortical electrodes in each subject exhibited simultaneous EPs of different sizes but similar shapes, so bipolar or common average referencing would have reversed the polarities of some of these EPs. EPs were averaged over trials during the periods of interest.

The collected time-series data were first segmented into 2.5 s epochs, each containing 1 s of rest, 0.5 s of stimulation, and another 1.5 s of rest. Epochs were then run through an unsupervised, dictionary-based artifact rejection pipeline as previously described [19] (Fig. 4.2B). Briefly, this clusters each ECoG channel's artifacts based on shape to create a dictionary, matches each individual artifact to its closest dictionary entry, and subtracts a scaled version of this template from the trace to flatten the artifact and approximate the underlying signal. Residual artifact (which was minimal) and additional high-amplitude spike-like noise (not uncommon in the intra-operative setting) lasting less than 0.5 ms were removed and the resulting gaps were linearly interpolated. Each trial was then visually examined, and trials with remaining highamplitude noise were removed. An average of 1.67/90 trials were removed per subject.

After artifact removal, time-series epochs were lowpass filtered at 200 Hz using a fourth order Butterworth filter and downsampled by a factor of 8, for an ultimate sampling rate of approximately 6 kHz. 60 Hz line noise and harmonics were removed with fourth order Butterworth notch filters. Finally, the data were baseline corrected by subtracting the mean voltage of a 0.5 s period before the start of each stimulation burst.

4.2.5 Evoked Potential Analysis

90 stimulation trains delivered at 3 V were processed for each subject, then grouped by bipolar stimulation pair. Average EPs from the 30 traces for each recording pair and stimulation condition were calculated (for example, see Fig. 4.2C). The 100 ms period immediately following stimulation onset (t = 0 to 0.1 s) and the 100 ms period immediately following stimulation offset (t = 0.5 to 0.6 s) were extracted as the "start" and "end" EP windows respectively. For statistical contrast, an 800 ms period prior to burst onset (t = -0.95 to -0.15s) was defined as a baseline. A z-transform over the entire EP period was used to standardize amplitudes across subjects, then the largest amplitude difference between a consecutive peakto-trough or trough-to-peak pair was taken ("peak-to-trough measure," Fig. 4.2C-i). The latencies between the start of the EP period (stimulation onset or offset) and the positive and negative peaks were also noted.

Individual trials were too variable to get a reliable peak-to-trough measure, so the root mean square (RMS) of the EP was used to quantify deflection from the zero for individual trials [152, 164]. RMS values of the z-scored trials were computed for the three time windows identified above (Fig. 4.2C-ii). Because RMS is an average-based measure, having a longer baseline period did not inflate the values as compared to the EP periods, and a longer baseline allowed for a more stable estimate of "baseline" activity despite high trial-to-trial variability.

4.2.6 Spectral Analysis

Low gamma (30–80 Hz) and high gamma (80–150 Hz) power series were also constructed for each artifact-free trial, following the pre-processing steps described above. Fourth order Butterworth bandpass filters for the low and high gamma frequencies were applied to individual trials, then the square of the analytical amplitude from the Hilbert transform was taken as power time series. These were then baseline normalized to a period 0.5 to 0.1 s prior to stimulation onset using a z-transform (the median rather than the mean was used for the average because of the unstable baseline) to correct 1/f scaling. Using this baseline rather than the 800 ms baseline used in EP analysis allowed us to better avoid edge artifacts, leaving a 500 ms buffer on the front end of each trial. The median of the gamma-filtered series was taken over each set of trials to construct a single power series for each stimulation-recording electrode pair.

4.2.7 Statistics

To identify non-zero EPs, the distributions of RMS measures for each trial of the EP period were compared to the RMS distribution of the corresponding trial's baseline using a non-parametric, paired (signed rank) test. EPs that differed significantly ($p < 0.05$, FDR-corrected) from the baseline period were counted as "significant EPs" The median RMS of all trials for each significant EP, along with the latency values recorded from the average trace, was contrasted between the two EP periods using a non-parametric, unpaired (Wilcoxon rank-sum) test (significance cutoff of $p < 0.05$, FDR corrected).

RMS and latency values were then split by the Brodmann area (BA) of the corresponding cortical electrode. Only BAs with consistent coverage among subjects (1/2/3, 4, 6, and 7) were included in these analyses, although values for all other BAs (19, 39, 40) were pooled together and shown for transparency. Evoked activity for all recording electrodes and stimulation conditions, not just significant EPs, were included in this analysis. The start and end EP values for each metric were compared within each BA using Wilcoxon

rank-sum test, and then the effect of BA on each metric within the start and end EPs was determined using a non-parametric, one-way analysis of variance (Kruskal-Wallis test). For metrics and EPs for which a significant ($p < 0.05$, FDRcorrected) effect was detected, post hoc testing (using MATLAB's multcompare command) was performed to reveal significant differences between individual BAs.

A mixed linear model was used to assess the relationships between high and low gamma and EP magnitude (RMS), adjusting the intercept and slope for random effects of subject on EP and spectral data. From the high and low gamma power series for each stimulation-recording electrode pair (3 stimulation electrodes and 8 recording electrodes for 24 pairs per subject, see Section 4.2.7), the median power during the start (0–0.1 s after stimulation onset) and end (0.5–0.6 s after stimulation onset) EP periods was extracted. This was regressed against the median RMS over all trials for each stimulation-recording electrode pair. We adjusted our model to control for random effects of subject on EP RMS and gamma power.

4.3 Results

After removing stimulation artifacts from cortical recordings obtained during DBS, we quantified EPs during ongoing stimulation and compared them to EPs following stimulation offset.

4.3.1 Measures of EPs

The peak-to-trough measurement of the average EP (computed from the average of 30 trials) and the RMS measurement of the same EP (the median of the RMS measures over the same 30 trials) correlated tightly ($r^2 = 0.453$, $p < 0.05$; Fig. 4.2D). Because the RMS provides a magnitude distribution rather than a single magnitude value for each EP, it was used as the primary measure of EP size for all statistics.

4.3.2 Characterizing Start and End EPs

23/90 and 21/90 stimulation conditions produced EPs during the first 100 ms of stimulation and immediately following stimulation offset, respectively, that differed significantly from baseline (Fig. 4.3A and B). Start EPs were observed in only two subjects, with the majority ($\sim$75%) seen in Subject 1. Conversely, at least one significant end EP was observed in 5/6 subjects. Most EPs (start and end) had a characteristic biphasic shape with a narrow negative deflection followed by a longer positive deflection (Fig. 4.3E). We noted similar features in other stimulus-triggered averages during the start and end windows that did not meet the statistical criteria. For example, Subject 3, channel 7, stimulation condition

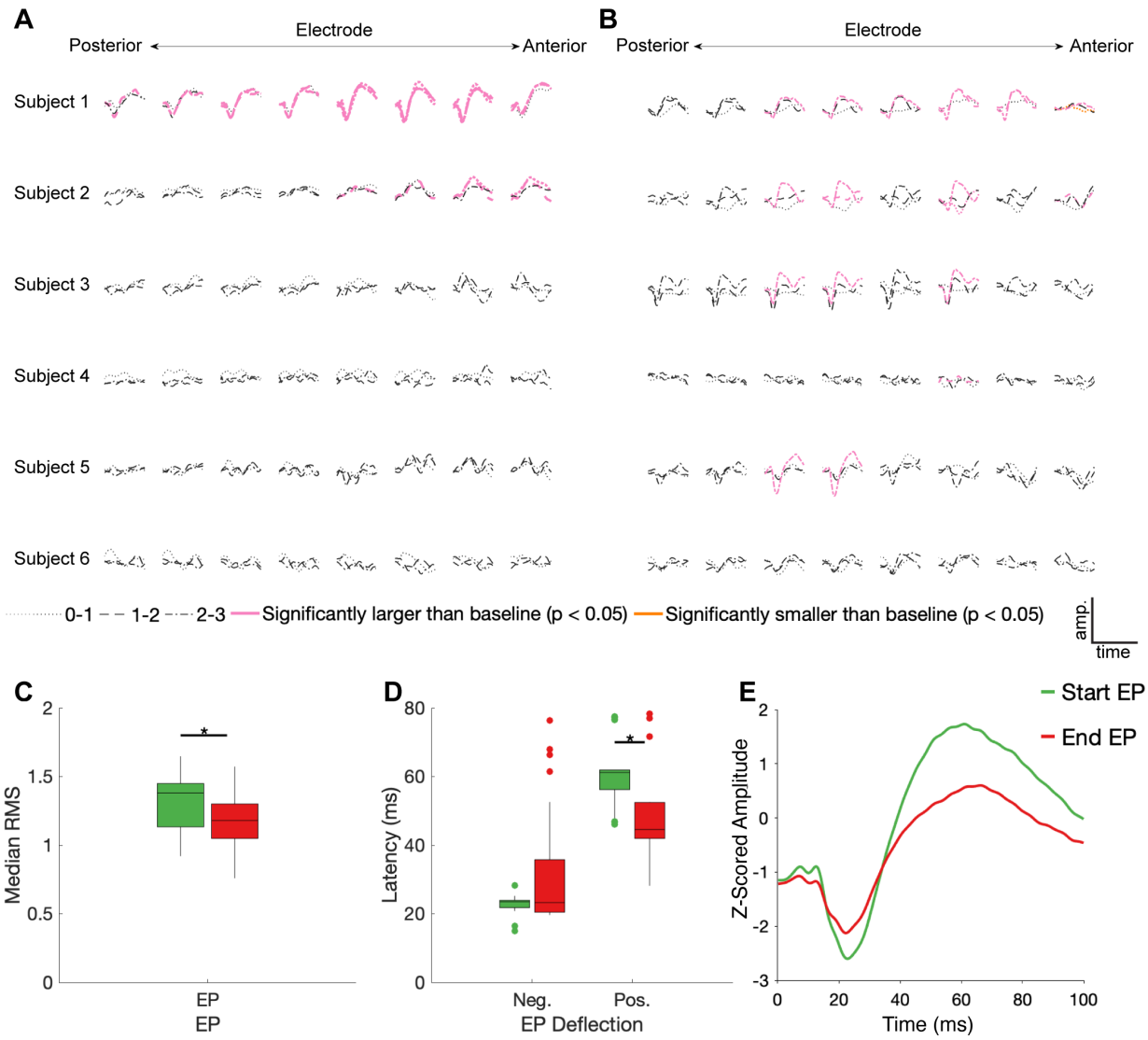

Figure 4.3: STN DBS evokes start and end EPs. Z-scored start (A) and end (B) EPs (average of 30 trials) are shown for each electrode (columns, contacts were in different BAs for each subject – see Fig. 4.1), subject (rows), and DBS stimulation electrode pair (line type). EPs in pink had a statistically significantly larger magnitude than baseline deviations ($p < 0.05$, FDR corrected by subject). The one trace in yellow was also statistically different than baseline, but it had a lower magnitude. Median RMS (C) and latencies to negative and positive deflections on the average traces (D) were compared between the start and end EPs; significant ($p < 0.05$, FDR corrected) differences indicated by stars. (E) The average of all significant start (green) and end (red) EPs.

2-3 and Subject 5, channel 6, stimulation condition 1-2 may have small start and end EPs respectively.

No discernable pattern was seen connecting the location of the stimulated electrodes to any features of the EPs. Of the 12 cortical electrodes with significant start EPs, 8 had significant EPs in more than one stimulation configuration, while 11/16 cortical electrodes had significant end EPs in multiple conditions. 9 cortical electrode-STN stimulation site pairs had significant start and end EPs.

Among the significant EPs, the magnitude (as measured with RMS) of start EPs were significantly larger than that of end EPs (median start RMS = 1.38, median end RMS = 1.18, p = 0.018; Fig. 4.3C). Additionally, relative to stimulus onset and offset respectively, the positive deflection of start EPs occurred significantly later than that of end EPs (median start latency = 61.19 ms, median end latency = 44.56 ms, p = 2.32e-4; Fig. 4.3D). No significant difference in negative deflection latency was observed between EPs, although there was a trend toward the start EP having a shorter latency to the negative deflection (median start latency = 23.51 ms, median end latency = 23.27 ms, p = 0.055 Fig. 4.3D). This was likely driven by the much greater degree of variability in this latency for the end EP.

4.3.3 EPs by Brodmann Area

BA1/2/3 (primary sensory cortex, S1), BA4 (primary motor cortex, M1), and BA6 (premotor and supplementary motor areas, PMA/SMA) all had a >10% chance of producing a significant start and/or an end EP in response to STN stimulation (Fig. 4.4A). All subjects had one or more electrodes on each of these BAs. BA7 (visuo-motor coordination area) also had a relatively high likelihood of producing a start EP and a non-zero likelihood of producing an end EP. In other BAs represented (BA19, associative visual area; BA 39, angular gyrus; and BA40, supramarginal gyrus – areas not primarily associated with sensorimotor function), no start EPs and few end EPs were elicited that differed significantly from baseline. The averages of significant EPs (Fig. 4.4E) was generally similar between BAs, following the overall patterns seen in Figure 4.3E. The exception was in BA6, where the characteristic biphasic EP shape was less clear.

Within individual BAs, RMS and deflection latencies of start and end EP periods were not statistically distinct, despite the overall differences seen in the pooled EPs, except in one case – in BA 7, the positive deflection of the start EP occurred significantly later than that of the end EP (median start latency = 42.02 ms, median end latency = 38.01 ms, p = 0.0034; Fig. 4.4B–D). Across BAs, there was a significant effect on both the positive (p =

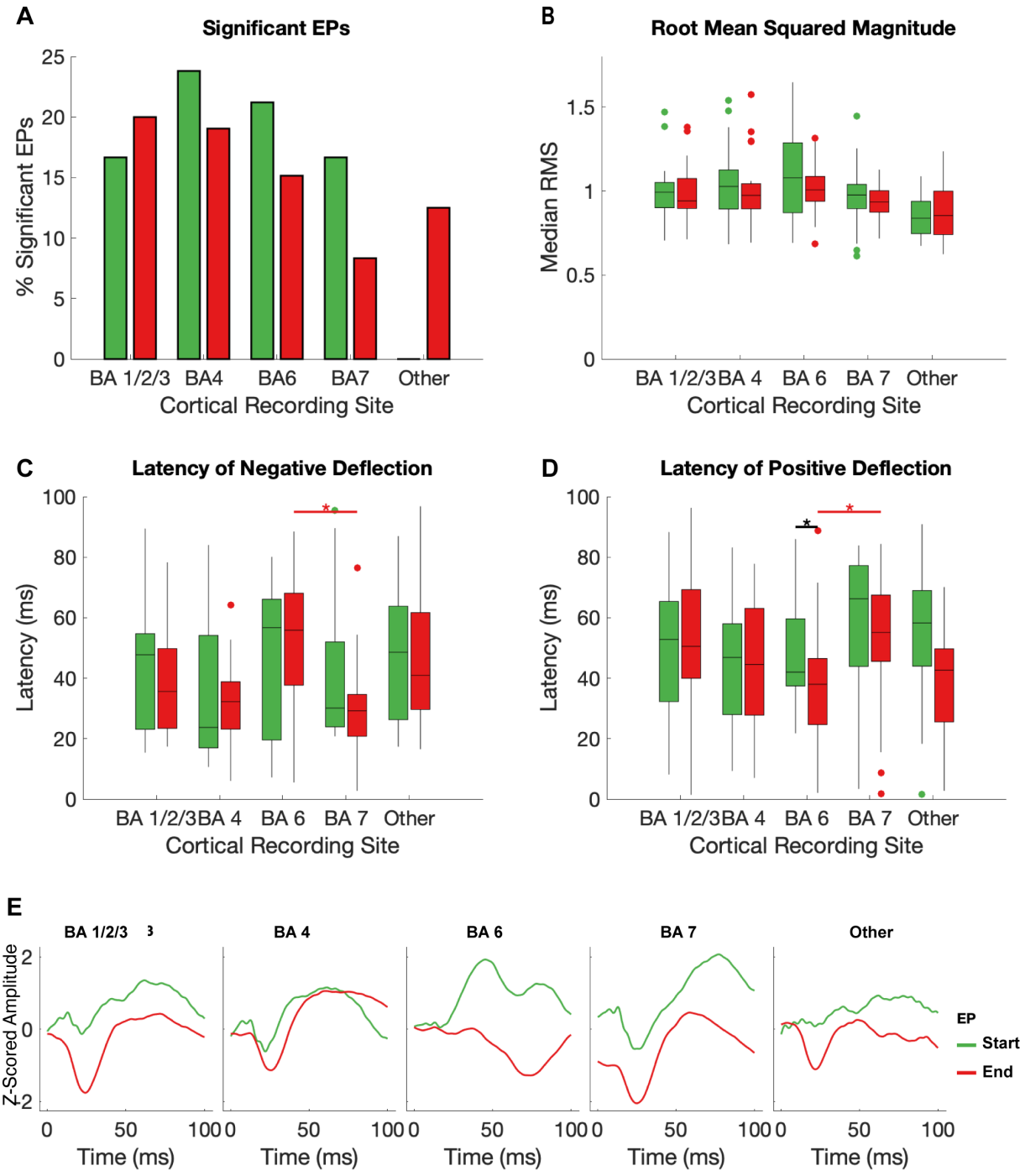

Figure 4.4: Effects of Brodman Area on EPs. The median RMS (A), percent of EPs that differed significantly from baseline amplitudes (B), latency to negative deflection (C), and latency to positive deflection (D) were compared between start and end EPs with recording electrodes grouped by Brodman area across subjects. Brodmann areas with inconsistent coverage across subjects were pooled and shown for comparison but not included in statistical analysis. Black stars indicate significant ($p \leq 0.05$, FDR corrected) differences between start and end EP measures within each BA. Red stars indicate significant ($p \leq 0.05$, FDR corrected) post hoc comparisons between end EPs in different regions after a Kruskal-Wallis test revealed dependence of both latency measures on BA. The mean of all start (green) and end (red) EPs for each electrode in each BA are shown in (E).

6.4204e-5) and negative (p = 0.0043) latency of the end EP only. Post hoc testing revealed that this was driven by statistical differences between BAs 6 (median negative deflection latency = 55.87 ms, median positive deflection latency = 38.01 ms) and 7 (median negative deflection latency = 29.25 ms, median positive deflection latency = 55.13 ms) in the case of both the negative (p = 0.0026) and positive (p = 2.3087e-5) deflections. These data are summarized in Table 4.2.

4.3.4 High and Low Gamma Power During EPs

Using a linear mixed effects model with subject as a random variable, we tested the relationship between low and high gamma power with RMS during the start and end EP windows. Statistically significant relationships were observed between low gamma power during the 100 ms EP windows and magnitude of both the start (slope = 2.56, $p = 2.56 \times 10^{-4}$) and end (slope = 6.875, p = 0.00217) EPs (Fig. 4.5A,B). High gamma power during the same windows correlated significantly with the magnitude of the end (slope = 3.199, $p = 5.88 \times 10^{-9}$), but not the start (slope = 1.405, p = 0.0547) EP (Fig. 4.5C,D).

4.4 Discussion

With acute, intraoperative subdural ECoG implants, we measured evoked potentials and power spectra at a number of cortical sites in response to high-frequency stimulation of the STN in PD patients. After reliable removal of the stimulation artifact [19], we observe two distinct responses that resemble canonical subcortico-cortical EPs – one during the first 100ms of a high-frequency, 500 ms stimulation train ("start EP") and one during the 100ms immediately following the offset of these trains ("end EP"). This provides additional characterization of EPs in cortex during ongoing, continuous and clinically relevant DBS. Within the framework of classic informational lesioning or transmitter depletion theories of STN DBS, the novel end EP may be indicative of a "rebound" in cortical activity after high-frequency DBS is turned off.

Responses at the cortex in response to high frequency STN DBS have previously been reported in EEG [6], but have not been quantified due to lack of sufficient artifact removal techniques. Although Baker and colleagues noted slow wave oscillations during stimulation artifact of 100ms of stimulation, their primary focus was on slower EPs that occurred after termination of the stimulation artifact [6]. Our observed deflections during ongoing stimulation are more pronounced than previously reported. This discrepancy potentially may be due to a closer proximity to the dipole source and resulting higher fidelity of ECoG record-

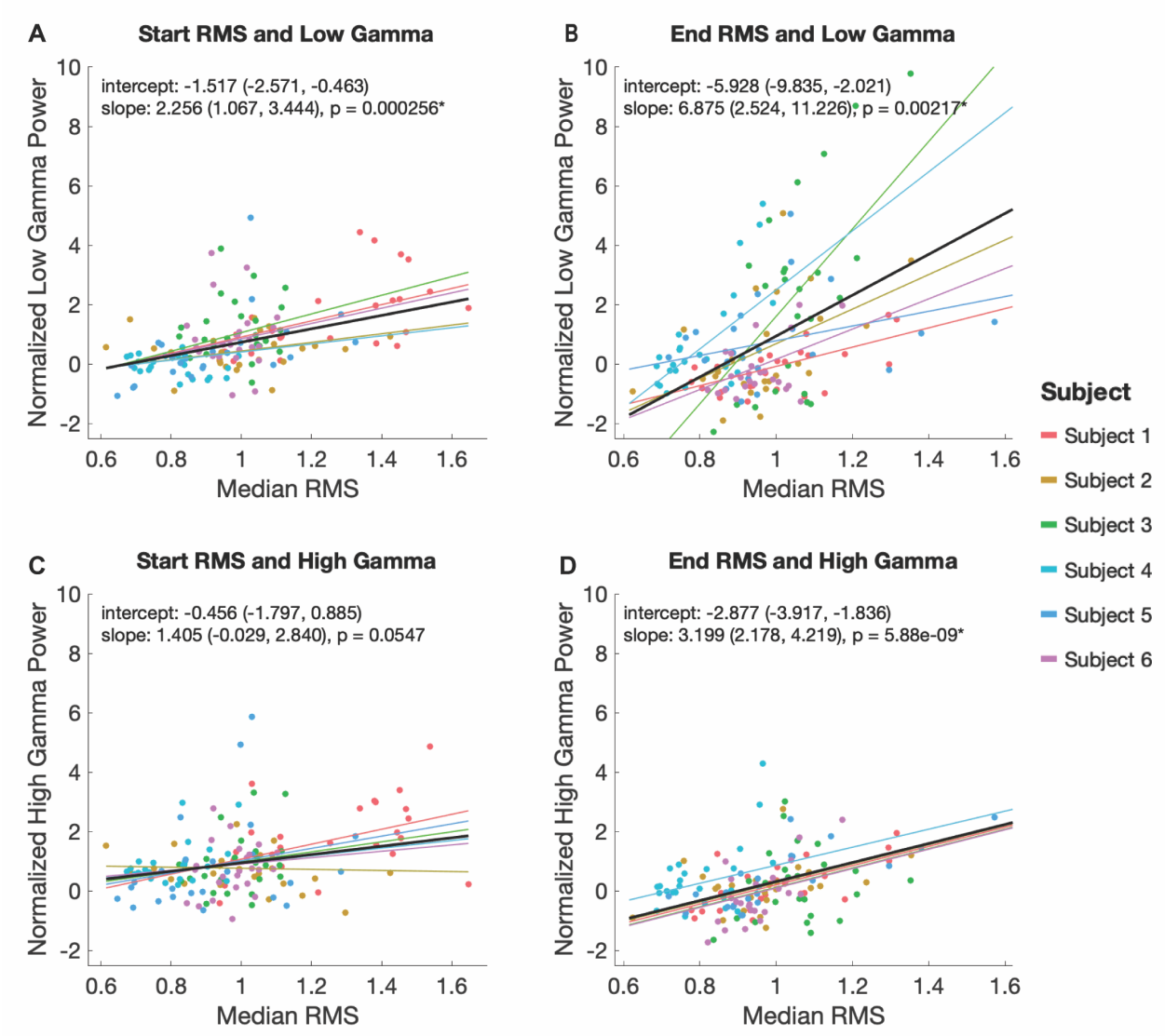

Figure 4.5: Relationship between EP magnitude and gamma power. A mixed linear model was used to assess the relationship between EP magnitude low (30–80 Hz; A,B) and high (80–130 Hz; C,D) gamma power during the start (A,C) and end (B,D) EP intervals. The model controlled for random effects of subject, adjusting for intercept and slope. Each plot shows the model's predicted fits for each subject as well as the overall model in black. Overall model and slope are reported along with 95% confidence intervals.

ings with respect to EEG. It is unclear whether the slow oscillations (140–230 ms after stimulation onset, or 40–130 ms after stimulation offset) in the EEG is similar to the end EPs described here. Although there is some overlap in the time window, the first component of the observed end EP is still faster than the earliest component reported by Baker et al. More work is necessary, including varying the length of stimulation period, to elucidate these discrepancies.

The start and end EPs are grossly similar in shape (i.e., wave morphology) and are consistent with previously reported subcortico-cortico EPs [73, 130]. We do, however, note some quantitative differences between the two EPs. The start EPs tend to be larger and longer than the end EPs. Additionally, start EP magnitude correlates with both high and low gamma power, while end EP magnitude correlates only with low gamma power. These differences may be attributed to several unique and/or overlapping possibilities, including, (1) residual DBS artifacts surviving our artifact removal process, (2) evoked responses within distinct pathways and mechanisms, or (3) modulation of EP elements from ongoing high-frequency DBS.

We further note that, consistent with previous DBS studies, medium- to long-latency EPs are seen primarily in cortical areas corresponding to sensorimotor function and integration, consistent with the signals traveling through known cortico-basal ganglia-thalamo-cortical loops of the indirect pathway. The site of stimulation in relation to the STN did not have a significant effect on EP magnitude or on the likelihood of producing a statistically significant (larger than baseline) EP, which may indicate that current spread within any given bipolar electrode configuration may play a role in the transmission of these signals from the STN to the relevant tracts.

4.4.1 Start vs. End EPs

The EPs we observe immediately following stimulation onset and offset resemble previously described STN-to-cortex EPs in shape and latency – a negative deflection around 20–30 ms and a positive deflection around 40–60 ms following stimulation onset or offset [73, 130]. These canonical EPs are observed in ECoG [130], magnetoencephalography [73], and electroencephalography [183]. Their timing is consistent with orthodromic, multisynaptic transmission [183, 73]. The circuits through with this occurs are, as of yet, not fully understood, but modeling and experimental evidence have suggested that high-frequency stimulation activates STN efferents to the GPi and/or directly activates pallido-thalamic fibers [129, 125], indicating propagation through the indirect pathway.

Our ability to generalize the findings about start EPs is limited because the majority of

Table 4.2: Start and End EPs by BA.

		BA 1/2/3	BA 4	BA 6	BA 7	Other	p-value (effect of BA)
RMS	Start EP	0.993	1.027	1.054	0.976	0.838	0.348
	End EP	0.941	0.974	0.978	0.934	0.854	0.327
	p-value (start vs end)	0.309	0.715	0.159	0.414	–	–
Negative Deflection Latency	Start EP (ms)	47.759	23.757	56.689	30.147	48.579	0.047
	End EP (ms)	35.635	32.276	55.951	29.245	40.960	
	p-value (start vs end)	0.805	0.903	0.016	0.096	–	–
Positive Deflection Latency	Start EP (ms)	52.838	46.858	42.844	66.273	58.245	0.312
	End EP (ms)	50.545	44.564	38.093	55.132	42.680	6.42x10-6
	p-value (start vs end)	0.159	0.715	0.411	0.003*	–	–

Median RMS (Fig. 4B) and median latency to negative (Fig. 4C) and positive (Fig. 4D) deflections by Brodmann area (BA). For each measure and BA, the p-value from a sign rank test for difference between start and end EP is shown. Additionally, the results of a Kruskal-Wallis test for effects of BA on EPs are given for all measures and for both the start and end EPs. Both negative and positive deflection end EP latency showed a significant (p ¡ 0.05, FDR corrected) effect of BA. Post-hoc testing indicated that the only significant difference between groups was for BAs 6 and 7 (negative deflection end EP latency p-value comparing BAs 6 and 7 = 2.31e-5; negative deflection end EP latency p-value comparing BAs 6 and 7 = 0.0026).

start EPs (75%) were seen in a single subject (Subject 1). Classic EP-like waveforms that did not achieve statistical differences in magnitude over baseline periods were, however, seen in other subjects during both EP periods. Larger sample sizes and ranges of stimulation amplitude and quantification of EP thresholds are clearly needed to determine the relative prevalence of start and end EPs and determine if large, consistent start EPs like those seen in Subject 1 are associated with electrode position, disease process, or any other factors.

Interestingly, we do not see any evidence for short-latency EPs, like those previously reported [130], after individual stimulation pulses within a stimulation train. These are generally attributed to antidromic activation of the hyperdirect pathway and have expected latencies of 2–10 ms. With the high frequency (180–185 Hz) stimulation used in this study, responses longer than 5 ms would be obscured by the next stimulation pulse in the train, so responses of the expected length may not be visible in our data. More work will need to be done to see if the long-latency start and end EPs have an impact on short-latency EPs following individual stimulation pulses.

4.4.2 Effect of Broadmann Area on EPs

Overall, we observed a greater likelihood of seeing an EP with a significantly larger magnitude than baseline in Brodmann Areas (BAs) associated with sensorimotor function than in any other BAs. This is consistent with the hypothesis that EPs are propagated through motor cortico-basal ganglia-thalamocortical loops, of which the STN is a part [125, 129, 42].

Magnitude of EPs did not vary significantly with the BAs from which the EPs were recorded, nor did latency to either peak of the start EP. There was a significant effect of BA on end EP peak latencies, which was revealed by post hoc testing to be a result of differences between BA6 and BA7. The EPs observed in BA6 are less like the consistent biphasic EPs seen in S1, M1, and BA7, and the start and end EPs have approximately opposite polarities – the positive deflection comes before the negative deflection in the end EP of BA6, whereas negative comes before positive in all other EPs over sensorimotor areas. This polarity shift is responsible for the significant differences seen between start and end latencies within BA6, and likely also contributes to the overall effect of BA on EP latency without greatly impacting EP magnitude.

4.4.3 Relationship Between EP Magnitude and High and Low Gamma Power

In addition to measuring time-locked evoked potentials during the periods immediately following stimulation onset and offset, we also extracted high-frequency power responses. Average low gamma (30–80 Hz) power during both time windows correlated significantly with the magnitude of EPs seen in the same windows, but a similar correlation with high gamma (80–150 Hz) power was only seen for the end EP. The functional distinction of low gamma activity in the cortex is debated. Some reports have associated low gamma power with cognitive function and stimulus dependence [8], while others have found that the lower end of this frequency range more closely resembles canonical beta oscillations in movement-related amplitude modulation [178]. High gamma power is known to correlate tightly to firing rates of local neural populations and is therefore often interpreted as a measure of local activity [156]. The findings here suggest that the impact of high-frequency electrical stimulation of STN may be associated not only with EP production, but also with higher stimulus-dependent activity in this case, some variant of motor processing. However, a higher rate of cortical neuronal activity seems unique (with respect to the selected windows used in our analysis) to the period at the end of ongoing high-frequency stimulation. The mechanisms giving rise to observed distinctions in RMS-high gamma power associations between analysis windows are unclear. Among other possibilities, it is conceivable that this association is an effect of

DBS entrainment or evoked processing within local circuitry. Additionally, there is a trend in the data toward a relationship between start EP RMS and high gamma power that might reach statistical significance if we had additional trials.

4.4.4 Study Limitations

Many aspects of this study limit our ability to firmly draw conclusions. One limitation is that all subjects were anesthetized for the duration of this study, which has been found to change cortical oscillation patterns and lower evoked potential thresholds. Additionally, due to restricted time with each subject in the operating room, the number of trials we were able to run for each subject was highly limited. Our EPs are the average of only 30 trials, but we expect that we would see similar results but greater consistency if more trials were added, enhancing our statistical power. ECoG EPs are regularly characterized clinically with only 10s of trials, and studies have been published using as few as 20 trials per EP [e.g., 121, 96].

As noted previously, our inability to relate our data to clinical follow-up is a significant limitation. Further behavioral work must be performed before the clinical relevance of these findings is established. Our predictions of potential relevance to clinicians are outlined below but are entirely speculative. Potential Clinical Relevance of EPs in Response to High-Frequency DBS While DBS is often effective in treating PD, symptom relief varies from patient to patient. Personalizing a DBS treatment plan to fit an individual's needs and best treat their symptoms is a time-consuming process for both clinicians and patients during which multiple stimulation parameters are tuned via behavioral testing. Better understanding how high frequency stimulation affects patterns of transmission between the STN and upstream cortical areas may provide insight into more efficient ways of individualizing therapies. If measurable events at the cortex during ongoing high frequency STN stimulation correlate with therapeutic efficacy of the stimulation parameters, these events could serve as a biomarker to more rapidly test a series of stimulation parameters without exhaustive behavioral testing. Doing this intraoperatively or postoperatively would narrow the parameter space for behavioral testing.

Additionally, better understanding basal ganglia-to-cortex functional connections could contribute to engineering new DBS devices, such as devices that pair cortical recording and/or stimulation with traditional STN stimulation to try to maximize efficacy in all patients. In order to determine how cortical and subcortical devices could work synergistically, we need a quantitative metric of their functional connectivity to test how the neural circuits respond to different types of stimulation. Previous high-frequency STN DBS efforts for example has examined EMGs modulation [28]. The EPs we observe during high-frequency

DBS may represent the basis for this kind of metric.

4.5 Conclusion

We demonstrate the existence of two cortical evoked potentials in response to high-frequency stimulation of the STN similar to that used clinically for DBS to treat PD. One EP occurs immediately after stimulation starts and is, to our knowledge, the first longlatency cortical EP reported during ongoing stimulation. A lack of effective artifact removal methods has made measuring activity during continued stimulation difficult up until recently. The second EP occurs after the offset of high-frequency stimulation, and intriguingly suggests some sort of cortical "rebound" when DBS is turned off. Significant further work will be required to elucidate the mechanisms by which these EPs are produced and if and how they are related to the therapeutic efficacy of DBS. Here, we provide a foundation for that work by describing this cortical evoked activity.

Chapter 5

CCEPs and FC

Over the past two decades, cortico-cortical evoked potentials (CCEPs) have become a popular method of measuring neural connectivity in vivo in human populations. However, CCEPs are a difficult metric to interpret, either at the level of neural circuitry or in terms of their functional implications. Comparing brain networks derived from CCEPs to brain networks derived using resting state functional connectivity (rsFC) metrics, which have been linked more directly to neural circuitry and functional behavioral states, can help clarify these interpretations. In three pairs of subjects (six subjects total) who underwent CCEP measurement in three corresponding brain areas, we investigate the relationship between CCEPs and four metrics of rsFC in six canonical frequency bands, as well as phase-amplitude coupling across frequencies. We find no clear, consistent evidence of such a relationship. Certain rsFC measurements and frequency bands were stronger at recording sites with CCEPs and/or correlated with the magnitude of CCEPs, but these varied between subjects, including between subjects with anatomically similar stimulation sites. These negative findings may still have utility toward interpreting the circuit-level mechanisms of CCEPs. The anatomical and functional features associated with common metrics of functional connectivity likely do not give rise at a group level to CCEP phenomenon.

5.1 Introduction

Cortico-cortical evoked potentials (CCEPs) are characteristic, stereotyped neural responses that can be recorded intracranially in response to single pulses of direct electrical stimulation of the cortex [122, 99, 104, 180]. CCEPs are a measure of effective connectivity [55] and CCEPs of large magnitude are interpreted to mean close connections between the stimulation and recording sites.

However, many issues may arise when trying to interpret CCEPs. CCEPs are the are

the sum of many synapses, likely incorporating influences from many neural pathways [99, 104]. While different temporal components of CCEPs may reflect mono-synaptic versus multi-synaptic pathways [99, 104], CCEPs alone are insufficient for detailed tracing of the circuitry underlying effective connectivity. The relationship between CCEPs and functional output of neural circuitry is also unclear [99].

Understanding CCEPs in the context of the brain at rest could help clarify the mechanisms by which they occur and reveal a proxy of specific elements of functional and anatomic circuits. This would help to focus CCEP studies interpret their results. For example, one possible application of CCEPs is to quantify neuroplasticity by contrasting connectivity before and after a therapeutic intervention, such as electrical conditioning [97, 86], a proposed approach toward treating neurological insults such as stroke. Better understanding what exactly CCEPs measure could help generate hypotheses about interventions that will change effective connectivity, relate those changes to possible functional recovery, and understand the mechanisms underlying this neuroplasticity.

A handful of studies have compared CCEPs to various measures of resting state functional connectivity (rsFC) measured intracranially [86, 79, 174, 32, 96, 142] and in functional imaging [98, 118, 188, 175]. Functional and neurophysiological correlates are more clearly understood for rsFC than for CCEPs, so examining CCEPs in relation to rsFC can help build context. There are many existing metrics of rsFC, and most studies have examined CCEPs in comparison to a few chosen metrics in one or more canonical frequency bands of interest. rsFC metrics that have been compared to CCEPs include correlation [32, 96], cross-correlation [79, 32], Granger inference [79, 32], and phase coherence/magnitude squared coherence [86, 174, 32].

Collectively, previous studies have had mixed results when comparing CCEP networks to rsFC networks, with findings varying depending on the rsFC metric(s) of choice and the method of comparing networks. In general, these studies have noted broad similarities between CCEP and rsFC networks but differences in more granular network characteristics. For instance, Keller et al. noted overlap between the spatial distributions of electrocorticographic (ECoG) electrodes with CCEPs and electrodes with positive power correlations with the stimulation site, but differences in graph metrics (degree, indegree, outdegree) of these networks [96]. More complex graph-based metrics of rsFC tend to be more similar to CCEPs than traditional rsFC metrics like correlation, cross-correlation, and coherence [174, 142]. Network similarity using these traditional metrics have varied across studies — for instance, cross-correlation was strongly correlated to CCEPs in [79] but not in [32].

Crocker et al. compared CCEPs not only to functional networks, but to structural ones as well [32]. They found that DTI networks were more closely correlated with CCEP

networks than rsFC networks were in electrodes farther away from the stimulation site, whereas correlation was more closely related to CCEPs in nearby electrodes. High overlap between structural and effective metrics has also been noted elsewhere [29, 145].

Building on these studies, we systematically compared CCEP networks to rsFC networks using a variety of coupling metrics. These included correlation, cross-correlation, Granger inference, and coherence, which have been examined in relation to CCEPs previously, as well as phase-amplitude coupling, which (to our knowledge) has not. Additionally, we examined the effect of the anatomical location of CCEP stimulation areas on these rsFC-CCEP comparisons. We demonstrate high subject-to-subject variability in the comparison of rsFC and CCEP networks, including between subjects for whom stimulation was delivered in the same anatomical area.

5.2 Methods

5.2.1 Subjects, electrode localization, and data acquisition

Implantation, electrode localization, and data acquisition were performed as described in Chapter 3. Six of the 14 CCEP subjects used in Chapter 3 Part I were selected for FC analysis based on similarities in the location of the stimulating electrodes, with three pairs of subjects with at least one stimulation electrode in the same anatomical areas. Electrode location was identified with the Harvard-Oxford (H-O) cortical atlas [111, 60, 41, 68] the Neuromorphetrics, Inc. (NMM) atlas [169] and a probabilistic label in either atlas was accepted for the purposes of subject inclusion. Electrode locations are shown in Table 5.1 and Figure 5.1.

Group	Subject	Stim Hemisphere	H-O Atlas		NMM Atlas	
			Electrode 1	Electrode 2	Electrode 1	Electrode 2
A: AnG	1	R	AnG		WM	AnG
	2	L	AnG		WM	
B: PCC	3	R	PCC		WM	
	4	L	PCC		WM	
C: TrIFG	5	L	OFC	TrIFG	TrIFG	
	6	L	OFC		WM	TrIFG

Table 5.1: Atlas locations of stimulation electrodes. Abbreviations: angular gyrus (AnG), posterior cingulate cortex (PCC), triangular part of the inferior frontal gyrus (TrIFG), orbitofrontal cortex (OFC), white matter (WM).

5.2.2 CCEP data collection and processing

CCEP data was collected and processed as previously described (Ch. 3) with one exception – after filtering, epoching, and normalizing the CCEP data, they were then re-referenced to

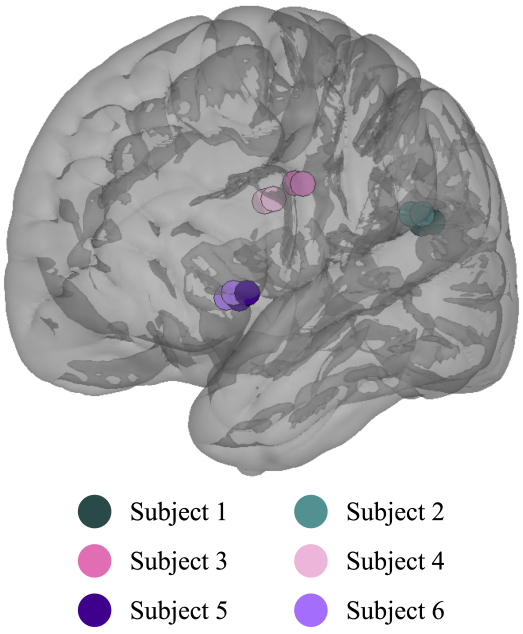

Figure 5.1: Stimulation electrode locations. The location of stimulation electrodes for each of the six subjects included in this analysis. Subjects were paired by anatomical location of the stimulation electrodes (Subjects 1 and 2 in the angular gyrus, Subjects 3 and 4 in the posterior cingulate cortex, and Subjects 5 and 6 in the triangular part of the inferior temporal gyrus). Subjects 1 and 3 were stimulated on the right side of the brain; electrode locations are mirrored to the left hemisphere for ease of visualization.

a bipolar montage. We made the decision to re-reference for two reasons. First, we intended to bipolar re-reference the resting state data to avoid spuriously high functional connectivity metrics [9], and it was easier to directly compare functional and effective connectivity when the data were on the same montage. Additionally, as opposed to previous chapters, anatomical patterns of CCEP responses were of interest, and recent work has shown that a bipolar montage improves accuracy in determining the source of CCEP signals [43]. Channels with CCEPs were identified as any channels in which the absolute z-score amplitude of the average exceeded 1 (in subject 6, a subject with relatively greater noise, the cutoff was set to 0.5) and in which visual examination confirmed a multi-component morphology. Models were then fit to CCEP means for component identification and each trial was quantified using the peak or trough amplitude for these windows. We took the peak or trough with the highest absolute value and used this as a quantification of the overall CCEP. Results from RMS analyses are not shown, as they closely mirror results from amplitude analyses.

5.2.3 Resting state data processing

Resting state connectivity was quantified by first extracting 50s of resting state data were extracted prior to the onset of CCEP testing. During this period subjects were instructed to remain still and rest without falling asleep. LFP data were examined and channels with excessive noise or with high inter-ictal spiking were removed from further analysis. The resting state data was then filtered in a similar way to the CCEP data – a highpass filter at 0.1Hz, notch filters at 60/120/180Hz, and a lowpass filter (8th order Butterworth filters). Resting state data was lowpass filtered at 250Hz, rather than 500Hz as with CCEP data, to allow for more aggressive downsampling. The data were then downsampled to approximately 500Hz (with the exception of data for Granger causality, which was downsampled to approximately 250Hz) and re-referenced using a bipolar montage.

5.2.4 Time-frequency decomposition

Time-frequency decomposition using complex Mortlet wavelets was then used to extract frequency data. The wavelets were set to a total length of 2s, with the Gaussian taper set to 5 cycles. These settings were chosen to ensure that the wavelet for the lowest frequency of interest (2Hz) tapered to zero. Complex time series data for 50 frequencies from 2 to 150Hz, logarithmically spaced, were extracted. Line frequencies from 57-63Hz and harmonic frequencies 117-123Hz were discarded. We squared the absolute value of the complex time-frequency data to obtain the power and extracted the imaginary portion to get the phase time series. The first and last 5s of data were discarded as a conservative measure to avoid edge artifact contamination, and the remaining 40s of stimulation were used for analysis.

5.2.5 Functional connectivity analysis

For all connectivity analysis, the bipolar re-referenced signal between the two consecutive stimulation channels was set as the seed. The bipoles immediately consecutive (i.e., including the stimulation channels but not between the stimulation channels), were excluded from analysis. All other bipoles between pairs of good channels were kept as test signals. Connectivity was computed between the seed site and each test site at each frequency. We then took the average of each metric over all frequencies within each canonical band (delta = 2-4Hz, theta = 4-7Hz, alpha = 7-13Hz, beta = 13-30Hz, gamma = 30-80Hz, high gamma >80Hz).

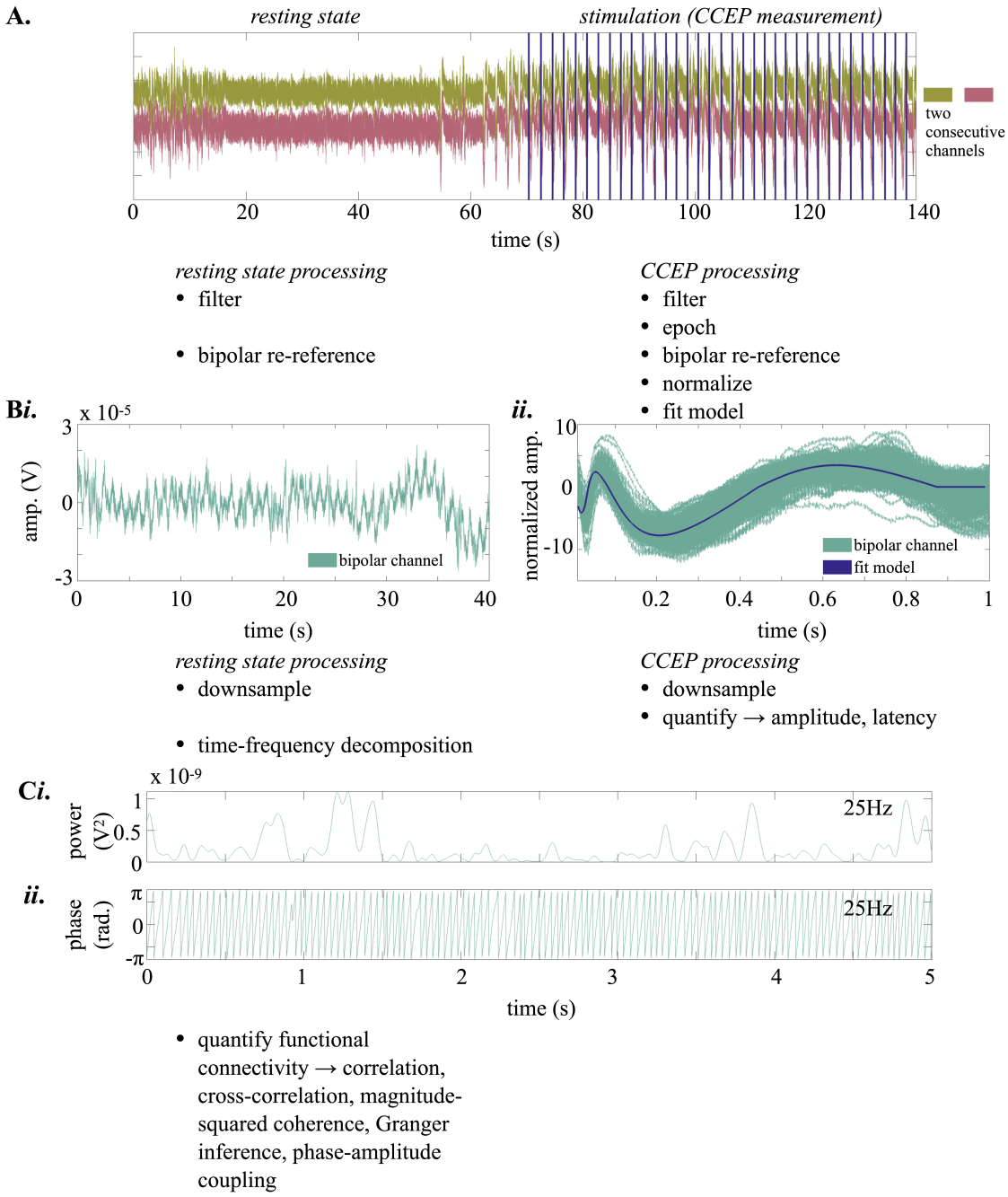

Figure 5.2: rsFC and CCEP methods. (A) Raw data during pre-stimulation resting state (left) and CCEP testing period (right, artifact removed). Two consecutive channels on the same sEEG probe are shown. After artifact removal, both signals are filtered. CCEPs are then epoched, then bipolar re-referencing is implemented (using the same montage for both rsFC and CCEPs). CCEPs are then normalized trial-wise to the pre-stimulation baseline and a multi-component model is fit to the average over all trials. (B) Post-processing resting state (i) and CCEP (ii) data. The fit model for the CCEP data is also shown. At this stage, the data are downsampled. CCEPs are quantified by the amplitude and latency of identified components. (C) Resting state data is transformed using Mortlet wavelets and power and phase data are extracted for functional connectivity analyses.

Phase-amplitude coupling (PAC)

We computed the using the traditional modulation index approach to estimate phase-amplitude coupling between low-frequency (2-30Hz) phase at the seed site and a normalized high-frequency (31-150Hz) amplitude at the test site, and for high-frequency amplitude at the seed site and low-frequency phase at the test site (Fig. 5.3A). For both analyses, we extracted the maximum PAC value and the corresponding phase and amplitude frequencies. Because of the intensive processing time, PAC was calculated using 5s time windows with 1s overlap, then results were averaged over windows.

Correlation

The nonparametric (Spearman) correlation was taken between the power series of the seed and each test site for each extracted frequency to obtain a Spearman's rho value for connectivity between the seed site and each test site in each frequency band. Correlation was calculated for 1s time windows with no overlap, which were then averaged.

Cross-correlation

The nonparametric cross-correlation was also obtained, using lags of up to 50ms. We took the mean cross-correlation vector over all windows and frequencies for each frequency band, then extracted the maximum value of rho and the lag of the maximum. Cross-correlation was calculated for 1s time windows with no overlap, and averaged across all windows.

Magnitude-squared coherence

We used the MATLAB function mscohere to calculate the magnitude-squared coherence between the time series at the seed site and test sites over sliding windows for the same 50 logarithmically spaced frequency values as were used for wavelet decomposition. Magnitude-squared coherence was calculated using 1s Hanning windows with no overlap. Mscohere computes the coherence based on time-series data.

Granger inference

We used the MVGC MATLAB toolbox [7] to calculate Granger inference from the seed site to each test site. To achieve the assumption of stationarity without overfitting the model, we anti-aliased the time series data again with a lowpass filter at 100Hz and downsampled by an additional factor of 4 for an ultimate sampling rate of 127Hz [79]. We also applied first-order differencing to the data to enhance stationarity [79, 18]. We set the model order

to 13 to capture 50ms of history, as in [79]. The MVGC package then computed the Granger inference for 50 linearly spaced frequencies from 0 to 63.5Hz (the Nyquist frequency) using the method described by [7]. Granger inference was calculated for 1s time windows with no overlap, which were then averaged.

5.2.6 Statistics

For each connectivity metric, we used permutation testing to calculate a z-score for the raw values. First, we shuffled the continuous (i.e., unwindowed) time series, power, and phase data as in [86]. Briefly, we split the 30s resting state window into 20 segments of random lengths and randomly shuffled these segments, then quantified the windowed data as described above. Permutation testing was repeated 1000 times with 1000 random segmentations, and each rsFC metric was calculated using the shuffled version of the appropriate time series, power, and/or phase data. Only one channel (typically the stimulation site channel) was shuffled for each comparison. We used the mean and standard deviation of the distribution of shuffled results to z-transform each rsFC metric.

Two statistical tests were performed on the z-transformed data. Examples of these tests are shown with the PAC data from Subject 1 in Figure 5.3. First, we compared the z-transformed value of each rsFC metric in the channels with and without CCEPs (Fig. 5.3B) using a rank-sum nonparametric test and correcting for multiple comparisons. In the subset of channels with CCEPs, we also calculated the Spearman correlation coefficient between the CCEP amplitude and each rsFC metric (Fig. 5.3C). These results were compared across subjects (Fig. 5.3D, rank-sum test results not shown as no significant p-values were found in any subject).

5.3 Results

5.3.1 CCEPs and PAC

Results of PAC analyses revealed mixed results. Across subjects, there was no clear relationship between the magnitude of peak PAC (Fig. 5.33Ci) or the associated phase (Fig. 5.3Cii) and amplitude (Fig. 5.3Ciii) frequencies and the magnitude of the CCEP. Although some subjects had very high correlation coefficients with one or more of the aspects of PAC tested, the strength and direction of correlation varied across subjects (Fig. 5.3D). No correlation values were significant ($p < 0.05$, FDR corrected). Additionally, no significant ($p < 0.05$, FDR corrected) differences between PAC magnitude or frequency was seen between CCEP and non-CCEP channels in any subject (A representative example (subject 1) shown

in Fig. 5.3B). Results did not differ greatly depending on if the stimulation site was used as the phase or the amplitude signal.

5.3.2 CCEPs and other rsFC metrics

Similarly mixed results were seen when comparing CCEPs to other metrics of rsFC. Figure 5.4 shows the results of rank-sum tests for unequal rsFC medians across channels with and without CCEPs in five rsFC metrics (correlation, coherence, maximum cross-correlation, lag of maximum cross-correlation, and Granger inference) across canonical frequency bands. In Subjects 3-5, no significant ($p < 0.05$, FDR corrected) differences were seen between CCEP and non-CCEP channels in any rsFC metric or frequency band. While there were significant effects in some rsFC bands in the remaining subjects, the metrics and frequencies in which significant results were found varied from subject to subject. Out of 25 significant comparisons, 15 were in Subject 2. No significant comparisons occurred in the maximum lag of the cross-correlation metric. In all cases where a significant difference was present in CCEP and non-CCEP channels, the median rsFC value in the CCEP channels was higher than that in the non-CCEP channels.

We also analyzed the Spearman correlation coefficient between CCEP amplitude and rsFC metrics in the subset of channels with CCEPs (Fig. 5.5). As with PAC, we saw some positive and some negative correlations. However, all significant correlations were positive (i.e., greater CCEP magnitude was associated with greater rsFC magnitude). Again, no significant tests were observed when comparing cross-correlation lag. All subjects except Subject 6 had at least one significant correlation value. Across all subjects, about 7% of rsFC metrics and bands had both significant difference in the rank-sum test described above and significant correlation (Table 5.2). 14% had significant difference or significant correlation but not both, and the remaining 79% had no significant tests.

We also calculated correlations between rsFC metrics and CCEP latency and saw no significant correlations (results not shown).

	Significant Correlation	No Significant Correlation
Significant Difference	12	10
No Significant Difference	14	138

Table 5.2: Overlap between significant CCEP/non-CCEP difference in rsFC and significant CCEP-rsFC correlation. Pooled over analyses in Figures 5.4 (difference) and 5.5 (correlation).

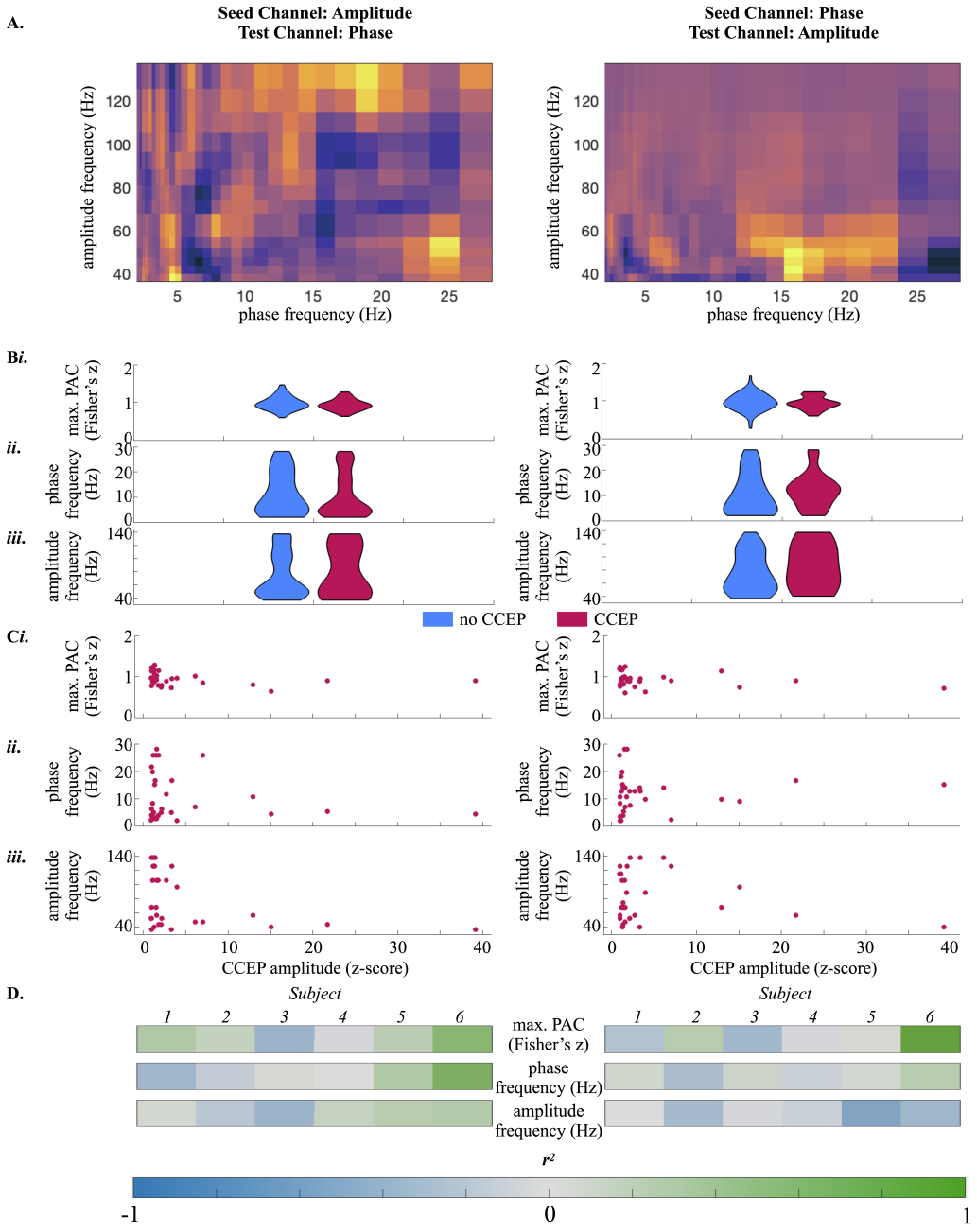

Figure 5.3: Phase-amplitude coupling results. (A) PAC was computed for phase frequencies from 2-30Hz and amplitude frequencies from 35-145Hz. This was done using the amplitude from the seed (stimulation) channel and the phase from the test (recording) channel (left) and vice versa (right). (B) A comparison of the distributions of CCEP versus non-CCEP channels for the maximum PAC value (i) and the corresponding phase (ii) and amplitude (iii). (C) Scatter plots of CCEP amplitude versus maximum PAC value (i) and the corresponding phase (ii) and amplitude (iii). (D) Pooled correlation coefficient values (as obtained from analysis in C) over all subjects.

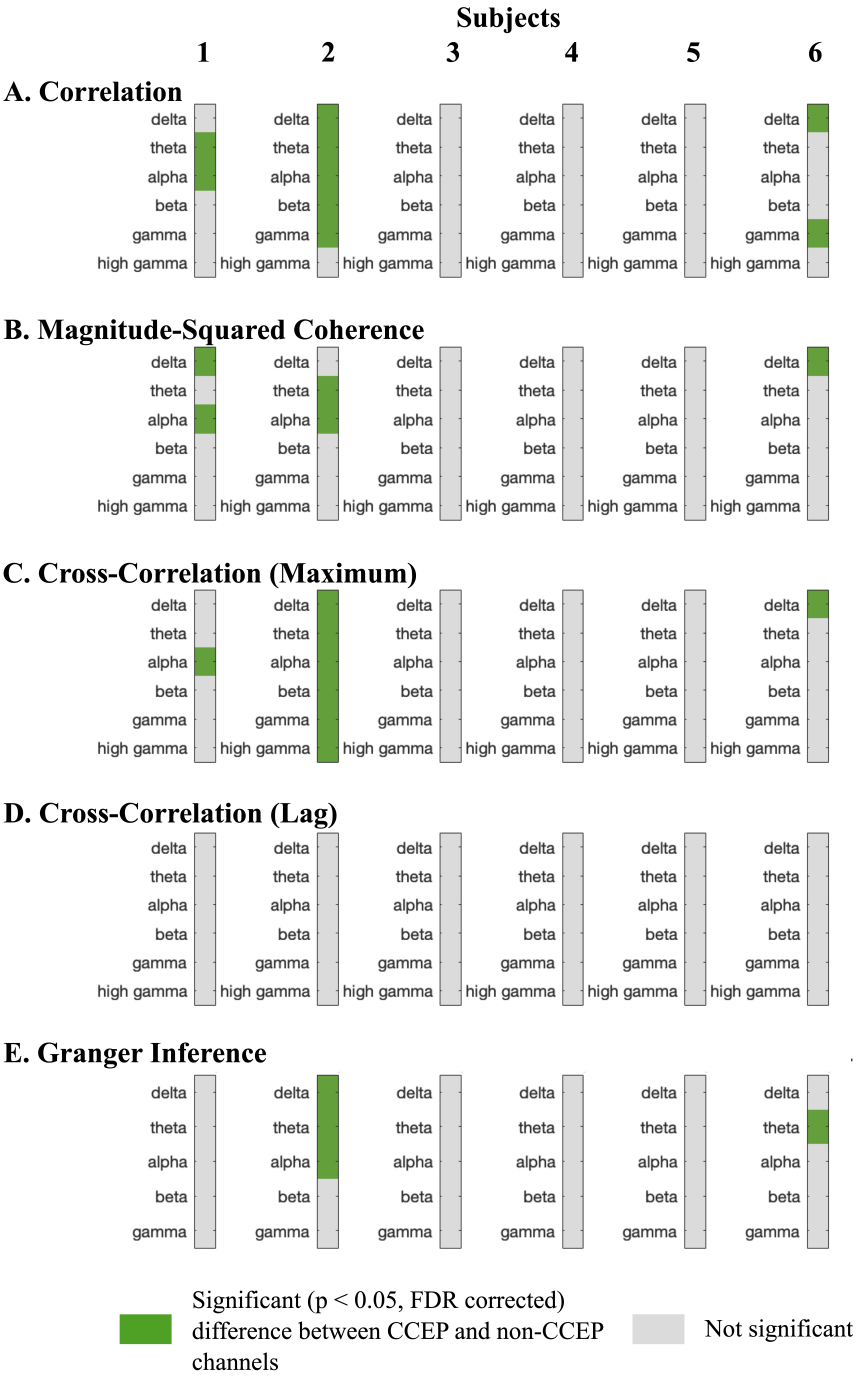

Figure 5.4: Significant differences between rsFC metrics in CCEP and non-CCEP channels. Plots, which show whether the rsFC of channels with CCEPs differed significantly from the channels without CCEPs (in a ranksum test, p <0.05, FDR corrected) in each canonical frequency band, are organized by rsFC metric (rows) and subject (columns).

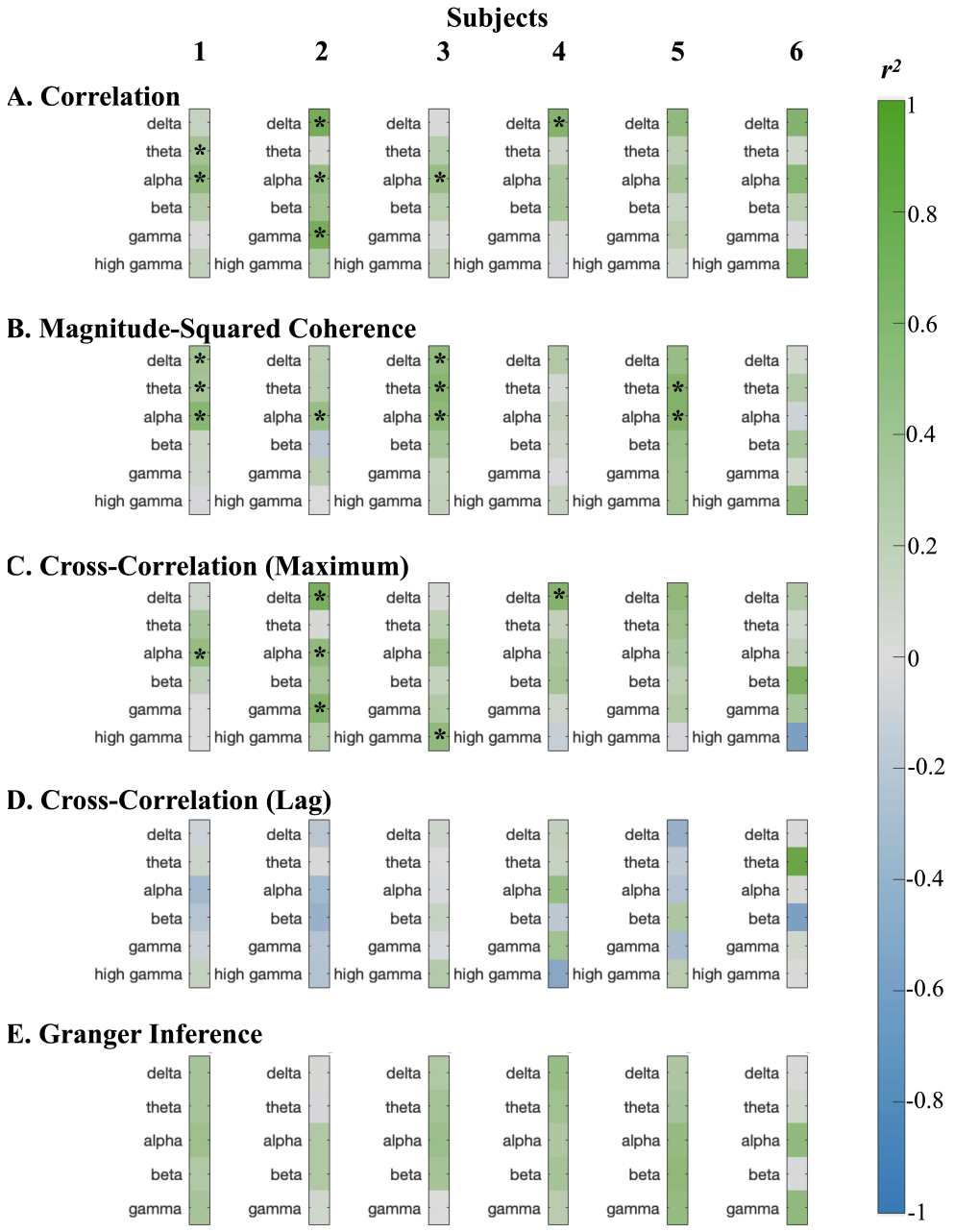

Figure 5.5: Spearman's correlation coefficient between CCEP amplitude and rsFC metrics. Plots, which show r^2values for canonical frequency bands, are organized by rsFC metric (rows) and subject (columns). * indicates a significant correlation ($p < 0.05$, FDR corrected).

5.3.3 Effect of stimulation site on CCEP-rsFC relationship

We hoped to be able to assess if the anatomical location of CCEP stimulation was related to the relationship between CCEPs and rsFC. However, due to the high degree of variability between subjects, this analysis proved difficult. Both significant difference in rsFC value and significant correlation between rsFC value and CCEP magnitude had similar variability between subjects with stimulation in the same anatomical area as between subjects with stimulation in different anatomical areas.

5.4 Discussion

5.4.1 No clear, consistent relationship between CCEPs and rsFC across subjects

The results presented in this study, consistent with previous studies, are generally inconclusive. In some subjects, certain rsFC metrics in certain frequency bands differed significantly between channels with and without CCEPs (Fig. 5.4) and/or correlated significantly with CCEP amplitude in the subset of channels with CCEPs (Fig. 5.5). Additionally, in all significant differences and correlations, recording sites with (larger magnitude) CCEPs were associated with stronger rsFC. However, the rsFC metrics and frequency bands that exhibited these relationships with CCEPs were not consistent across subjects. An initial prediction that rsFC in gamma and high gamma frequencies would be most strongly related to CCEPs since both are thought to reflect a correlate of summed local neural firing [18]. We also expected to see similarities in the relationship between rsFC and CCEPs in subjects who had stimulation in similar cortical areas. Neither of these hypotheses were borne out by the data and detailed analytical approach.

To our knowledge, no previous study has directly examined the relationship between phase-amplitude coupling and CCEPs (although a graph-based metric theoretically encompassing some aspects of PAC was used in [174]). Our findings suggest that, as with other rsFC metrics, PAC between two sites does not have a clear, consistent relationship with CCEPs evoked at one site by stimulation at another site (Fig. 5.3). PAC is a coupling metric which quantifies the capacity of specific phase elements of slow oscillations at one site to gate neuronal firing as indexed by high frequency amplitude estimates at another site [22]. PAC is generally 'loosely' considered to be a causal measure [184, 58]. CCEPs are a causal measurement of how neuronal firing at one site can engender neuronal firing at the other [99, 104]. Although these are distinct aspects of neural networks, both PAC and CCEPs are expected to pick up on directional, poly-synaptic pathways [99, 166]. We hypothesized that

PAC using low-frequency phase signals from stimulation site and high-frequency amplitude signals from the recording site would be stronger in recording sites with stronger CCEPs. This hypothesis was not borne out by the data. Additionally, results using the stimulation site for phase and using it for amplitude were generally quite similar. PAC results are discussed further in Section 5.4.2.

Observations in our data support certain specific findings from existing literature, but do not support others. For instance, while we saw more strong relationships between CCEPs and rsFC in cross-correlation than in Granger inference, as in [79], but our data are not consistent with their findings that Granger connectivity is over-represented in channels with CCEPs. Unlike [32], we did not see more correspondence between CCEP and rsFC networks in correlation than in cross-correlation. However, our data do support their observation that overlap in CCEP and coherence rsFC networks is greater at lower frequencies, as all significant coherence results were in delta, theta, and alpha bands (though the previous study saw differences through the beta and lower range of the gamma bands as well).

In general, however, our results suggest that CCEPs and rsFC are not clearly and consistently related across the human brain. This study presents data in the absence of rsFC thresholding, graph theoretical analysis, or distance-based metrics, and indicates that in the most fundamental sense, CCEPs and rsFC are measuring different aspects of brain networks.

5.4.2 Hypothesized explanations and consequences of CCEP-rsFC dissociation

It is clearly understood that effective and functional connectivity index different information arising from neural networks [62], especially when comparing undirected measures of functional connectivity to directional CCEPs. However, previous results comparing CCEPs and rsFC [86, 79, 174, 32, 96, 142, 98, 118, 188, 175] have suggested that these metrics may still be describing different facets of the same underlying functional circuitry. Our data do not directly support this hypothesis; nor do they directly refute it. While this limits interpretations on the network level, our data do potentially have utility in clarifying aspects of connectivity that CCEPs are unlikely to be measuring. Although CCEPs are used relatively broadly, the underpinnings of their circuit neurophysiology and functional correlates are broadly understudied. Therefore, the dissociation of CCEPs and rsFC is still, in and of itself, a significant contribution in our understanding of the neurophysiological contribution (or lack thereof) to the CCEP with the potential to shape the use of CCEPs in the future.

For instance, PAC is generally understood as a mechanism linking slow changes in large-scale networks to more instantaneous fluctuations in local processing circuitry [22] The result

that CCEPs do not have a clear relationship with the strength of PAC therefore may indicate that CCEPs are not reflective of this kind of spatiotemporal integration and instead measure circuits at only a single scale. The observation that CCEPs can be seen between spatially distant cortical sites [99] suggests they they are not just a product of only local computational circuits. Together, these observations support a hypothesis that CCEPs at a systems level are measuring spatially broad connections happening at a time scale faster than behavior but slower than that of a single synapse.

Overall, our results suggest that the dissociation between CCEP and rsFC need not be taken as a null or uninteresting result. Even in the absence of clear relationships between CCEP and rsFC networks, further comparative study is still warranted to better understand the physiological and functional meaning of CCEPs.

5.4.3 Limitations and future directions

The results presented here are, in many ways, limited. The number of subjects included is quite small, and we have only two subjects with stimulation in each cortical region for comparison. The CCEP stimulation sites for these and many other subjects were chosen largely irrespective of anatomy — 32 electrodes in general areas of anatomic interest were chosen for a brief stimulation test, but the electrode pairs for the full stimulation session were chosen based on whether these brief tests resulted in CCEPs elsewhere. A more focused study design in which 2-3 anatomical areas were targeted for CCEP measurement in each subject would allow for more thorough analytical comparison, both within and across subjects. An additional limitation is presented by the fact that even when stimulation sites were anatomically similar in multiple subjects, recording sites varied broadly, so we are not comparing the same brain regions in multiple subjects.

5.5 Conclusions

The analyses presented here, while limited in nature, demonstrate a lack of consistent relationships between connections measured with CCEPs and those measured with common rsFC metrics including correlation, coherence, and PAC. While some rsFC metrics in some frequency bands did have relationships with CCEPs, these were vastly inconsistent from subject to subject, even in subjects who had stimulation delivered at very anatomically similar sites. Despite this negative finding, we suggest that further in-depth comparisons of CCEP and rsFC networks using straightforward analytical approaches may be useful in elucidating the functional significance of CCEPs.

Chapter 6

Conclusions

In this dissertation, I explored cortico-cortical evoked potentials (CCEPs) as a metric for tracking changes in brain connectivity related to neuroplasticity. My focus was on the methodological considerations involved when recording and analyzing CCEPs, as well as techniques for contextualizing CCEPs with other brain activity and connectivity metrics to increase their interpretability. I will briefly review the findings from each of the chapters of the thesis, then consider the implications of these findings for future CCEP research.

6.1 Methodological considerations

In Chapter 2, I examined how data processing can impact CCEP results. As reviewed in Chapter 2 and, more thoroughly, in Appendix A, there is little standardization in processing strategies across CCEP research. I performed a systematic comparison of CCEP quantification using different filters, filter cutoffs, and re-referencing schemes. The choice of processing technique had a significant impact on some metrics of CCEP magnitude and morphology. However, I also demonstrated that without filtering, noise levels in the data can also impact results. This highlights the fact that data processing is necessary to address noise, but that it is vital that all data processing techniques be reported in studies, so that we can better synthesize results across literature.

Chapter 3 addresses four under-studied factors in the collection and analysis of CCEP data: (1) the number of trials needed to achieve stable quantification, (2) the effect of long CCEP data collection sessions on the CCEPs themselves, (3) the relative advantages and disadvantages of quantifying CCEPs at the trial level versus from the mean, and (4) the consistency of CCEPs over multiple days. These are basic questions that, primarily due to time constraints involved in human clinical research, have remained unaddressed even as CCEPs have become more broadly used.

Based on my findings, I concluded that approximately 50 CCEP trials should in most cases be sufficient for reliable results (factor 1) without risking habituation or even plasticity-inducing effects from the stimulation session (factor 2). Using 50 trials is also practically tractable — collecting 50 trials will take only 100s, so CCEPs could easily be measured at many different stimulation sites even with clinical time constraints. I demonstrated that, especially when very few trials are available or when comparing results across stimulation sessions or patients with very different numbers of trials, quantifying individual trials rather than a mean time series may be beneficial for drawing reliable conclusions (factor 3). Finally, in a small group of patients, I compared CCEPs recorded from each patient on two successive days. I demonstrated that many, though not all, of the CCEPs changed between the two stimulation days and that the nature of this change varied between subjects. Although far from conclusive, this pilot analysis suggests that further work will be needed to establish baseline changes in CCEPs in the absence of any clinical or stimulation interventions. This will be an important consideration when designing long-term studies of engineered neuroplasticity.

6.2 Contextualization

In Chapter 4, I departed from CCEPs and examined the evoked potentials (EPs) seen in the cortex after stimulating the subthalamic nucleus (STN) using deep brain stimulation (DBS)-like parameters. Using a new template-based artifact removal technique [1], I was able to measure ongoing EPs during this therapeutic-like stimulation, which is difficult to do in the presence of artifact. I also observed a second EP following the offset of this high-frequency stimulation. The during- and after-stimulation EPs had statistically different magnitudes and morphologies, suggesting they were the result of different neural circuitry and/or transmission mechanisms. This hypothesis was supported by the fact that only the end EP had a significant correlation with ongoing high gamma band (80-150Hz) activity. Although this work did not directly relate the EPs to clinical efficacy of DBS, by characterizing both EPs, I provide a possible biomarker for comparison to therapeutic outcomes.

The final chapter addressed the relationship between CCEPs and resting state functional connectivity (rsFC). The results of previous studies relating these two metrics of brain connectivity have been mixed [2–7]. Many of these analyses have used complex techniques for comparing CCEP and rsFC networks, but the most basic relationships between the measures remain incompletely understood. In this chapter, I did not see a clear, consistent, convincing relationship between CCEPs and rsFC. However, I argue that this negative result is interesting and important on its own, even in the absence of findings using more complex

computational comparisons. The fact that CCEPs and rsFC are dissociated may give us insight into the mechanisms underlying CCEPs and their functional significance. There is a large body of literature examining the mechanisms and functional correlates of different metrics of rsFC and knowing that CCEP networks do not follow the same pattern as rsFC networks indicates that CCEPs are likely arising from an entirely unique set of processes and revealing a different facet of brain connectivity than rsFC.

6.3 Synthesis and Impact: what have we learned about CCEPs?

The goals of this dissertation were to examine under-studied methodologies around CCEP data collection and analysis and to work towards contextualizing (CC)EPs using other metrics of brain activity and connectivity. Through this, I hoped to advance our understanding of the response of the brain to electrical stimulation, probe connectivity, and further develop a metric for use in long-term studies of engineered neuroplasticity.

This thesis is not — nor is it intended to be — a definitive perspective on how CCEPs can and should be used in the future. Rather, it provides common sense guidelines about how to assess basic aspects of CCEP methodology, including how to filter data and how many trials to collect. CCEPs are a metric that can and should be used in different ways depending on the focus of each research study. For instance, in Chapter 5, I chose to re-reference CCEP data to make CCEPs more directly comparable to functional connectivity metrics, while in other chapters I largely chose not to re-reference. My work in this area underlines the importance of reporting methodological choices in CCEP experiments to ensure that findings across the literature can be compared, synthesized, and built upon. It is important to understand how the methodology, not just the experimental variables, can influence results.

Again, my work comparing CCEPs to other metrics of brain activity and connectivity is far from conclusive. Further study is needed with more patients and stimulation across more brain areas. However, demonstrating the dissociation between CCEPs and rsFC, though a negative finding, can enhance our understanding of what CCEPs do and do not measure. This will help to guide evidence-based hypotheses about effective connectivity as measured by CCEPs, and potentially provide guidance about what it means to measure a change in a CCEP. This will be vital in studies of engineered neuroplasticity, in which change in CCEPs will be a metric of neuroplasticity but not of functional outcome. Linking neuroplasticity as measured by CCEPs to behavioral effects of neuroplasticity will help to strategically design neuroplasticity-inducing stimulation interventions.

Bibliography

[1] Filippo Agnesi et al. "Deep Brain Stimulation Imposes Complex Informational Lesions". In: *PLoS ONE* 8.8 (2013), pp. 1–12. ISSN: 19326203. DOI: 10.1371/journal.pone.0074462.

[2] Louise M. Allan et al. "Long-term incidence of depression and predictors of depressive symptoms in older stroke survivors". en. In: *British Journal of Psychiatry* 203.6 (Dec. 2013), pp. 453–460. ISSN: 0007-1250, 1472-1465. DOI: 10.1192/bjp.bp.113.128355.

[3] Anna Letizia Allegra Mascaro et al. "Combined Rehabilitation Promotes the Recovery of Structural and Functional Features of Healthy Neuronal Networks after Stroke". en. In: *Cell Reports* 28.13 (Sept. 2019), 3474–3485.e6. ISSN: 22111247. DOI: 10.1016/j.celrep.2019.08.062.

[4] Kunihiko Araki et al. "Bidirectional neural connectivity between basal temporal and posterior language areas in humans". en. In: *Clinical Neurophysiology* 126.4 (Apr. 1, 2015), pp. 682–688. ISSN: 1388-2457. DOI: 10.1016/j.clinph.2014.07.020.

[5] P. Ashby et al. "Neurophysiological effects of stimulation through electrodes in the human subthalamic nucleus". In: *Brain* 122.10 (1999), pp. 1919–1931. ISSN: 00068950. DOI: 10.1093/brain/122.10.1919.

[6] Kenneth B. Baker et al. "Subthalamic nucleus deep brain stimulus evoked potentials: Physiological and therapeutic implications". en. In: *Movement Disorders* 17.5 (2002), pp. 969–983. ISSN: 1531-8257. DOI: https://doi.org/10.1002/mds.10206.

[7] Lionel Barnett and Anil K. Seth. "The MVGC multivariate Granger causality toolbox: A new approach to Granger-causal inference". In: *Journal of Neuroscience Methods* 223 (Feb. 15, 2014), pp. 50–68. ISSN: 0165-0270. DOI: 10.1016/j.jneumeth.2013.10.018.

[8] Erol Basar. "A review of gamma oscillations in healthy subjects and in cognitive impairment". In: *International Journal of Psychophysiology* 90.2 (2013), pp. 99–117. ISSN: 01678760. DOI: 10.1016/j.ijpsycho.2013.07.005.

[9] André M. Bastos and Jan-Mathijs Schoffelen. "A Tutorial Review of Functional Connectivity Analysis Methods and Their Interpretational Pitfalls". In: *Frontiers in Systems Neuroscience* 9 (2016). [Online; accessed 2024-03-04]. ISSN: 1662-5137. URL: https://www.frontiersin.org/articles/10.3389/fnsys.2015.00175.

[10] Ishita Basu et al. "Consistent linear and non-linear responses to invasive electrical brain stimulation across individuals and primate species with implanted electrodes". English. In: *Brain Stimulation: Basic, Translational, and Clinical Research in Neuromodulation* 12.4 (July 1, 2019). publisher: Elsevier PMID: 30904423, pp. 877–892. ISSN: 1935-861X, 1876-4754. DOI: 10.1016/j.brs.2019.03.007.

[11] Bruce P. Bean. "The action potential in mammalian central neurons". eng. In: *Nature Reviews. Neuroscience* 8.6 (June 2007). PMID: 17514198, pp. 451–465. ISSN: 1471-003X. DOI: 10.1038/nrn2148.

[12] G Q Bi and M M Poo. "Synaptic modifications in cultured hippocampal neurons: dependence on spike timing, synaptic strength, and postsynaptic cell type." In: *The Journal of neuroscience : the official journal of the Society for Neuroscience* 18.24 (1998), pp. 10464–10472. ISSN: 0270-6474. DOI: 10.1038/25665.

[13] T. V. P. Bliss and G. L. Collingridge. "A synaptic model of memory: long-term potentiation in the hippocampus". en. In: *Nature* 361.6407 (Jan. 1993). number: 6407 publisher: Nature Publishing Group, pp. 31–39. ISSN: 1476-4687. DOI: 10.1038/361031a0.

[14] T. V. P. Bliss and T. Lømo. "Long-lasting potentiation of synaptic transmission in the dentate area of the anaesthetized rabbit following stimulation of the perforant path". In: *The Journal of Physiology* 232.2 (July 1973). PMID: 4727084 PMCID: PMC1350458, pp. 331–356. ISSN: 0022-3751.

[15] Svenja Borchers et al. "Direct electrical stimulation of human cortex - the gold standard for mapping brain functions?" eng. In: *Nature Reviews. Neuroscience* 13.1 (Nov. 30, 2011). PMID: 22127300, pp. 63–70. ISSN: 1471-0048. DOI: 10.1038/nrn3140.

[16] Sébastien Boulogne et al. "Cortico-cortical and motor evoked potentials to single and paired-pulse stimuli: An exploratory transcranial magnetic and intracranial electric brain stimulation study: Paired-Pulse Intracranial Direct Stimulation". en. In: *Human Brain Mapping* 37.11 (Nov. 2016), pp. 3767–3778. ISSN: 10659471. DOI: 10.1002/hbm.23274.

[17] György Buzsáki and Andreas Draguhn. "Neuronal Oscillations in Cortical Networks". en. In: *Science* 304.5679 (June 25, 2004), pp. 1926–1929. ISSN: 0036-8075, 1095-9203. DOI: 10.1126/science.1099745.

[18] György Buzsáki and Xiao-Jing Wang. "Mechanisms of Gamma Oscillations". In: *Annual review of neuroscience* 35 (2012). PMID: 22443509 PMCID: PMC4049541, pp. 203–225. ISSN: 0147-006X. DOI: 10.1146/annurev-neuro-062111-150444.

[19] D. J. Caldwell et al. "Signal recovery from stimulation artifacts in intracranial recordings with dictionary learning". In: *Journal of Neural Engineering* 17.2 (2020). ISSN: 17412552. DOI: 10.1088/1741-2552/ab7a4f.

[20] David Caldwell. "Engineering Direct Electrical Stimulation of Human Sensorimotor Cortex". en. PhD thesis. 2019. URL: https://digital.lib.washington.edu:443/researchworks/handle/1773/44050.

[21] Baruc Campos et al. "Rethinking Remapping: Circuit Mechanisms of Recovery after Stroke". en. In: *The Journal of Neuroscience* 43.45 (Nov. 8, 2023), pp. 7489–7500. ISSN: 0270-6474, 1529-2401. DOI: 10.1523/JNEUROSCI.1425-23.2023.

[22] Ryan T. Canolty and Robert T. Knight. "The functional role of cross-frequency coupling". In: *Trends in Cognitive Sciences* 14.11 (2010). publisher: Elsevier Ltd, pp. 506–515. ISSN: 1364-6613. DOI: 10.1016/j.tics.2010.09.001.

[23] Kaitlyn Casimo et al. "Spontaneous Variation in Electrocorticographic Resting-State Connectivity". In: *Brain Connectivity* 9.6 (July 2019). publisher: Mary Ann Liebert, Inc., publishers, pp. 488–499. ISSN: 2158-0014. DOI: 10.1089/brain.2018.0596.

[24] Vincent Castellucci et al. "Neuronal Mechanisms of Habituation and Dishabituation of the Gill-Withdrawal Reflex in Aplysia". In: *Science* 167.3926 (1970), pp. 1745–1748.

[25] Patrick Chauvel, Jorge Gonzalez-Martinez, and Juan Bulacio. "Chapter 3 - Presurgical intracranial investigations in epilepsy surgery". In: *Handbook of Clinical Neurology*. Ed. by Kerry H. Levin and Patrick Chauvel. Vol. 161. Clinical Neurophysiology: Diseases and Disorders. DOI: 10.1016/B978-0-444-64142-7.00040-0. Elsevier, Jan. 1, 2019, pp. 45–71. URL: https://www.sciencedirect.com/science/article/pii/B9780444641427000400.

[26] Andrei Ciuparu and Raul C. Mureşan. "Sources of bias in single-trial normalization procedures". en. In: *European Journal of Neuroscience* 43.7 (Apr. 2016). Ed. by Christoph M. Michel, pp. 861–869. ISSN: 0953816X. DOI: 10.1111/ejn.13179.

[27] Stuart F Cogan et al. “Tissue damage thresholds during therapeutic electrical stimulation”. In: *Journal of Neural Engineering* 13.2 (2016). DOI: 10.1088/1741-2560/13/2/021001.Tissue.

[28] “Concurrent Deep Brain Stimulation Reduces the Direct Cortical Stimulation Necessary for Motor Output”. In: (2020). ISSN: 1531-8257. DOI: https://doi.org/10.1002/mds.28255. URL: https://onlinelibrary.wiley.com/doi/abs/10.1002/mds.28255.

[29] Christopher R. Conner et al. “Anatomic and electro-physiologic connectivity of the language system: A combined DTI-CCEP study”. en. In: *Computers in Biology and Medicine*. Special Issue on Techniques for Measuring Brain Connectivity 41.12 (Dec. 1, 2011), pp. 1100–1109. ISSN: 0010-4825. DOI: 10.1016/j.compbiomed.2011.07.008.

[30] Eli J. Cornblath et al. “Quantifying trial-by-trial variability during cortico-cortical evoked potential mapping of epileptogenic tissue”. en. In: *Epilepsia* 64.4 (2023). _eprint: https://onlinelibrary.wiley.com/doi/pdf/10.1111/epi.17528, pp. 1021–1034. ISSN: 1528-1167. DOI: 10.1111/epi.17528.

[31] Otto D Creutzfeldt, Satoru Watanabe, and Hans D Lux. “Relations between EEG phenomena and potentials of single cortical cells. I. Evoked responses after thalamic and epicortical stimulation”. en. In: *Electroencephalography and Clinical Neurophysiology* 20.1 (Jan. 1966), pp. 1–18. ISSN: 00134694. DOI: 10.1016/0013-4694(66)90136-2.

[32] Britni Crocker et al. “Local and distant responses to single pulse electrical stimulation reflect different forms of connectivity”. en. In: *NeuroImage* 237 (Aug. 2021), p. 118094. ISSN: 10538119. DOI: 10.1016/j.neuroimage.2021.118094.

[33] J.A. Cronin et al. “Task-Specific Somatosensory Feedback via Cortical Stimulation in Humans”. In: *IEEE Transactions on Haptics* 9.4 (Oct. 2016). publisher: Institute of Electrical and Electronics Engineers, pp. 515–522. DOI: 10.1109/TOH.2016.2591952.

[34] Andrea L. Crowell et al. “Oscillations in sensorimotor cortex in movement disorders: An electrocorticography study”. In: *Brain* 135.2 (2012), pp. 615–630. ISSN: 14602156. DOI: 10.1093/brain/awr332.

[35] Lawrence J. Crowther et al. “A quantitative method for evaluating cortical responses to electrical stimulation”. In: *Journal of Neuroscience Methods* 311 (2019), pp. 67–75. ISSN: 2163684814. DOI: 10.1016/j.physbeh.2017.03.040.

[36] Olivier David et al. "Probabilistic functional tractography of the human cortex". en. In: *NeuroImage*. Mapping the Connectome 80 (Oct. 15, 2013), pp. 307–317. ISSN: 1053-8119. DOI: 10.1016/j.neuroimage.2013.05.075.

[37] Tyler S. Davis et al. "LeGUI: A Fast and Accurate Graphical User Interface for Automated Detection and Anatomical Localization of Intracranial Electrodes". In: *Frontiers in Neuroscience* 15 (Dec. 9, 2021). PMID: 34955721 PMCID: PMC8695687, p. 769872. ISSN: 1662-4548. DOI: 10.3389/fnins.2021.769872.

[38] Eran Dayan and Leonardo G. Cohen. "Neuroplasticity subserving motor skill learning". In: *Neuron* 72.3 (Nov. 3, 2011). PMID: 22078504 PMCID: PMC3217208, pp. 443–454. ISSN: 0896-6273. DOI: 10.1016/j.neuron.2011.10.008.

[39] Coralie De Hemptinne et al. "Exaggerated phase-amplitude coupling in the primary motor cortex in Parkinson disease". In: *Proceedings of the National Academy of Sciences of the United States of America* 110.12 (2013), pp. 4780–4785. ISSN: 00278424. DOI: 10.1073/pnas.1214546110.

[40] Coralie De Hemptinne et al. "Therapeutic deep brain stimulation reduces cortical phase-amplitude coupling in Parkinson's disease". In: *Nature Neuroscience* 18.5 (2015), pp. 779–786. DOI: 10.1038/nn.3997.Therapeutic.

[41] Rahul S. Desikan et al. "An automated labeling system for subdividing the human cerebral cortex on MRI scans into gyral based regions of interest". In: *NeuroImage* 31.3 (July 1, 2006), pp. 968–980. ISSN: 1053-8119. DOI: 10.1016/j.neuroimage.2006.01.021.

[42] Annaelle Devergnas and Thomas Wichmann. "Cortical potentials evoked by deep brain stimulation in the subthalamic area". In: *Frontiers in Systems Neuroscience* 5 (May 13, 2011). ISSN: 16625137. DOI: 10.3389/fnsys.2011.00030.

[43] Adam S. Dickey et al. "The Referential Montage Inadequately Localizes Corticocortical Evoked Potentials in SEEG". In: *Journal of clinical neurophysiology : official publication of the American Electroencephalographic Society* 39.5 (July 1, 2022). PMID: 33337663 PMCID: PMC10069706, pp. 412–418. ISSN: 0736-0258. DOI: 10.1097/WNP.0000000000000792.

[44] Michael A. Dimyan and Leonardo G. Cohen. "Neuroplasticity in the context of motor rehabilitation after stroke". en. In: *Nature Reviews Neurology* 7.2 (Feb. 2011), pp. 76–85. ISSN: 1759-4758, 1759-4766. DOI: 10.1038/nrneurol.2010.200.

[45] Sasha Dionisio et al. "Connectivity of the human insula: A cortico-cortical evoked potential (CCEP) study". en. In: *Cortex* 120 (Nov. 2019), pp. 419–442. ISSN: 00109452. DOI: 10.1016/j.cortex.2019.05.019.

[46] Yonglin Dou et al. "Identification of epileptic networks with graph convolutional network incorporating oscillatory activities and evoked synaptic responses". en. In: *NeuroImage* 284 (Dec. 2023), p. 120439. ISSN: 10538119. DOI: 10.1016/j.neuroimage.2023.120439.

[47] Agrita Dubey and Supratim Ray. "Cortical Electrocorticogram (ECoG) Is a Local Signal". In: *The Journal of Neuroscience* 39.22 (May 29, 2019). PMID: 30914446 PMCID: PMC6538865, pp. 4299–4311. ISSN: 0270-6474. DOI: 10.1523/JNEUROSCI.2917-18.2019.

[48] S. M. Dudek and M. F. Bear. "Homosynaptic long-term depression in area CA1 of hippocampus and effects of N-methyl-D-aspartate receptor blockade." en. In: *Proceedings of the National Academy of Sciences* 89.10 (May 15, 1992). publisher: National Academy of Sciences section: Research Article PMID: 1350090, pp. 4363–4367. ISSN: 0027-8424, 1091-6490. DOI: 10.1073/pnas.89.10.4363.

[49] Nicolás von Ellenrieder, Leandro Beltrachini, and Carlos H. Muravchik. "Electrode and brain modeling in stereo-EEG". In: *Clinical Neurophysiology* 123.9 (Sept. 1, 2012), pp. 1745–1754. ISSN: 1388-2457. DOI: 10.1016/j.clinph.2012.01.019.

[50] Rei Enatsu et al. "Connections of the limbic network: A corticocortical evoked potentials study". en. In: *Cortex*. Special issue: The clinical anatomy of the limbic lobe and connected structures 62 (Jan. 1, 2015), pp. 20–33. ISSN: 0010-9452. DOI: 10.1016/j.cortex.2014.06.018.

[51] Rei Enatsu et al. "Correlations between ictal propagation and response to electrical cortical stimulation: A cortico-cortical evoked potential study". en. In: *Epilepsy Research* 101.1 (Aug. 1, 2012), pp. 76–87. ISSN: 0920-1211. DOI: 10.1016/j.eplepsyres.2012.03.004.

[52] Rei Enatsu et al. "Cortical excitability varies upon ictal onset patterns in neocortical epilepsy: A cortico-cortical evoked potential study". en. In: *Clinical Neurophysiology* 123.2 (Feb. 1, 2012), pp. 252–260. ISSN: 1388-2457. DOI: 10.1016/j.clinph.2011.06.030.

[53] Andreas K. Engel et al. "Invasive recordings from the human brain: clinical insights and beyond". en. In: *Nature Reviews Neuroscience* 6.1 (Jan. 2005). publisher: Nature Publishing Group, pp. 35–47. ISSN: 1471-0048. DOI: 10.1038/nrn1585.

[54] Dario J. Englot and Edward F. Chang. "Rates and predictors of seizure freedom in resective epilepsy surgery: an update". en. In: *Neurosurgical Review* 37.3 (July 1, 2014), pp. 389–405. ISSN: 1437-2320. DOI: 10.1007/s10143-014-0527-9.

[55] László Entz et al. "Evoked effective connectivity of the human neocortex". en. In: *Human Brain Mapping* 35.12 (Dec. 2014), pp. 5736–5753. ISSN: 10659471. DOI: 10.1002/hbm.22581.

[56] Siobhan Ewert et al. "Toward defining deep brain stimulation targets in MNI space: A subcortical atlas based on multimodal MRI, histology and structural connectivity". In: *NeuroImage* 170 (2018), pp. 271–282. ISSN: 10959572. DOI: 10.1016/j.neuroimage.2017.05.015.

[57] Kazuhisa Ezure and Tomokazu Oshima. "Lateral Spread of Neuronal Activity within the Motor Cortex Investigated with Intracellular Responses to Distant Epicortical Stimulation". In: *The Japanese Journal of Physiology* 35.2 (1985), pp. 223–249. DOI: 10.2170/jjphysiol.35.223.

[58] L. Fontolan et al. "The contribution of frequency-specific activity to hierarchical information processing in the human auditory cortex". en. In: *Nature Communications* 5.1 (Sept. 2, 2014). publisher: Nature Publishing Group, p. 4694. ISSN: 2041-1723. DOI: 10.1038/ncomms5694.

[59] Kieran C. R. Fox et al. "Intrinsic network architecture predicts the effects elicited by intracranial electrical stimulation of the human brain". en. In: *Nature Human Behaviour* 4.10 (Oct. 2020). Bandiera_abtest: a Cg_type: Nature Research Journals number: 10 Primary_atype: Research publisher: Nature Publishing Group Subject_term: Cognitive neuroscience;Neurology Subject_term_id: cognitive-neuroscience;neurology, pp. 1039–1052. ISSN: 2397-3374. DOI: 10.1038/s41562-020-0910-1.

[60] Jean A. Frazier et al. "Structural Brain Magnetic Resonance Imaging of Limbic and Thalamic Volumes in Pediatric Bipolar Disorder". In: *American Journal of Psychiatry* 162.7 (July 2005). publisher: American Psychiatric Publishing, pp. 1256–1265. ISSN: 0002-953X. DOI: 10.1176/appi.ajp.162.7.1256.

[61] U. Frey, Y.-Y. Huang, and E. R. Kandel. "Effects of cAMP Simulate a Late Stage of LTP in Hippocampal CA1 Neurons". en. In: *Science* 260.5114 (June 11, 1993), pp. 1661–1664. ISSN: 0036-8075, 1095-9203. DOI: 10.1126/science.8389057.

[62] Karl J Friston. "Functional and effective connectivity: a review". In: *Brain Connectivity* 1.1 (2011), pp. 13–36. ISSN: 2158-0014. DOI: 10.1089/brain.2011.0008.

[63] Leonardo A. Frizon et al. "Deep Brain Stimulation for Pain in the Modern Era: A Systematic Review". eng. In: *Neurosurgery* 86.2 (Feb. 1, 2020). PMID: 30799493, pp. 191–202. ISSN: 1524-4040. DOI: 10.1093/neuros/nyy552.

[64] Masafumi Fukuda et al. "Pallidal stimulation for parkinsonism: Improved brain activation during sequence learning". In: *Annals of Neurology* 52.2 (2002), pp. 144–152. ISSN: 03645134. DOI: 10.1002/ana.10261.

[65] Ron Gadot et al. "Efficacy of deep brain stimulation for treatment-resistant obsessive-compulsive disorder: systematic review and meta-analysis". en. In: *Journal of Neurology, Neurosurgery & Psychiatry* 93.11 (Nov. 1, 2022). publisher: BMJ Publishing Group Ltd section: Neuropsychiatry PMID: 36127157, pp. 1166–1173. ISSN: 0022-3050, 1468-330X. DOI: 10.1136/jnnp-2021-328738.

[66] Sidney Goldring et al. "Direct Response of Human Cerebral Cortex". In: *Archives of Neurology* 4.6 (June 1, 1961), pp. 590–598. ISSN: 0003-9942. DOI: 10.1001/archneur.1961.00450120004002.

[67] Hannah E Goldstein et al. "Risk of seizures induced by intracranial research stimulation: analysis of 770 stimulation sessions". In: *Journal of neural engineering* 16.6 (Nov. 11, 2019). PMID: 31509808 PMCID: PMC8381291, p. 066039. ISSN: 1741-2560. DOI: 10.1088/1741-2552/ab4365.

[68] Jill M. Goldstein et al. "Hypothalamic Abnormalities in Schizophrenia: Sex Effects and Genetic Vulnerability". In: *Biological Psychiatry* 61.8 (Apr. 15, 2007), pp. 935–945. ISSN: 0006-3223. DOI: 10.1016/j.biopsych.2006.06.027.

[69] Romain Grandchamp and Arnaud Delorme. "Single-Trial Normalization for Event-Related Spectral Decomposition Reduces Sensitivity to Noisy Trials". en. In: *Frontiers in Psychology* 2 (2011). [Online; accessed 2021-04-29]. ISSN: 1664-1078. DOI: 10.3389/fpsyg.2011.00236. URL: http://journal.frontiersin.org/article/10.3389/fpsyg.2011.00236/abstract.

[70] Warren M. Grill, Andrea N. Snyder, and Svjetlana Miocinovic. "Deep brain stimulation creates an informational lesion of the stimulated nucleus". In: *NeuroReport* 15.7 (2004), pp. 1137–1140. ISSN: 09594965. DOI: 10.1097/00001756-200405190-00011.

[71] D. J. Guggenmos et al. "Restoration of function after brain damage using a neural prosthesis". en. In: *Proceedings of the National Academy of Sciences* 110.52 (Dec. 24, 2013), pp. 21177–21182. ISSN: 0027-8424, 1091-6490. DOI: 10.1073/pnas.1316885110.

[72] Zhi-hao Guo et al. "Epileptogenic network of focal epilepsies mapped with cortico-cortical evoked potentials". en. In: *Clinical Neurophysiology* 131.11 (Nov. 1, 2020), pp. 2657–2666. ISSN: 1388-2457. DOI: 10.1016/j.clinph.2020.08.012.

[73] C. J. Hartmann et al. "Distinct cortical responses evoked by electrical stimulation of the thalamic ventral intermediate nucleus and of the subthalamic nucleus". In: *NeuroImage: Clinical* 20.November (2018), pp. 1246–1254. ISSN: 22131582. DOI: 10.1016/j.nicl.2018.11.001.

[74] Takao Hashimoto, Christopher M Elder, and Jerrold L Vitek. "A template subtraction method for stimulus artifact removal in high-frequency deep brain stimulation". en. In: *Journal of Neuroscience Methods* 113.2 (Jan. 30, 2002), pp. 181–186. ISSN: 0165-0270. DOI: 10.1016/S0165-0270(01)00491-5.

[75] Mark A. Hays et al. "Cortico-cortical evoked potentials in response to varying stimulation intensity improves seizure localization". en. In: *Clinical Neurophysiology* (Sept. 11, 2022). [Online; accessed 2022-12-07]. ISSN: 1388-2457. DOI: 10.1016/j.clinph.2022.08.024. URL: https://www.sciencedirect.com/science/article/pii/S1388245722008768.

[76] Mark A. Hays et al. "Effects of stimulation intensity on intracranial cortico-cortical evoked potentials: A titration study". en. In: *Clinical Neurophysiology* 132.11 (Nov. 1, 2021), pp. 2766–2777. ISSN: 1388-2457. DOI: 10.1016/j.clinph.2021.08.008.

[77] Mark A. Hays et al. "Towards optimizing single pulse electrical stimulation: High current intensity, short pulse width stimulation most effectively elicits evoked potentials". In: *Brain Stimulation* 16.3 (May 1, 2023), pp. 772–782. ISSN: 1935-861X. DOI: 10.1016/j.brs.2023.04.023.

[78] D. O. Hebb. *The organization of behavior; a neuropsychological theory.* The organization of behavior; a neuropsychological theory. page: xix, 335. Oxford, England: Wiley, 1949.

[79] Jurgen Hebbink et al. "A Comparison of Evoked and Non-evoked Functional Networks". In: *Brain Topography* 32.3 (2019). publisher: Springer US, pp. 405–417. ISSN: 0123456789. DOI: 10.1007/s10548-018-0692-1.

[80] Henk T. Hendricks et al. "Motor recovery after stroke: A systematic review of the literature". en. In: *Archives of Physical Medicine and Rehabilitation* 83.11 (Nov. 2002), pp. 1629–1637. ISSN: 00039993. DOI: 10.1053/apmr.2002.35473.

[81] Jose L. Herrero et al. "Inducing neuroplasticity through intracranial theta-burst stimulation in the human sensorimotor cortex". In: *Journal of Neurophysiology* 126.5 (Nov. 1, 2021). publisher: American Physiological Society, pp. 1723–1739. ISSN: 0022-3077. DOI: 10.1152/jn.00320.2021.

[82] Jeffrey A. Herron et al. "Chronic electrocorticography for sensing movement intention and closed-loop deep brain stimulation with wearable sensors in an essential tremor patient". In: *Journal of Neurosurgery* 127.3 (2017), pp. 580–587. ISSN: 19330693. DOI: 10.3171/2016.8.JNS16536.

[83] Okihide Hikosaka et al. "Central mechanisms of motor skill learning". eng. In: *Current Opinion in Neurobiology* 12.2 (Apr. 2002). PMID: 12015240, pp. 217–222. ISSN: 0959-4388. DOI: 10.1016/s0959-4388(02)00307-0.

[84] Andreas Horn and Andrea A. Kühn. "Lead-DBS: A toolbox for deep brain stimulation electrode localizations and visualizations". In: *NeuroImage* 107 (2015), pp. 127–135. ISSN: 10959572. DOI: 10.1016/j.neuroimage.2014.12.002.

[85] Mark Huang et al. "Cortical Stimulation for Upper Limb Recovery Following Ischemic Stroke: A Small Phase II Pilot Study of a Fully Implanted Stimulator". In: *Topics in Stroke Rehabilitation* 15.2 (Mar. 1, 2008). publisher: Taylor & Francis _eprint: https://doi.org/10.1310/tsr1502-160 PMID: 18430685, pp. 160–172. ISSN: 1074-9357. DOI: 10.1310/tsr1502-160.

[86] Yuhao Huang et al. "Intracortical Dynamics Underlying Repetitive Stimulation Predicts Changes in Network Connectivity". en. In: *Journal of Neuroscience* 39.31 (July 31, 2019). publisher: Society for Neuroscience section: Research Articles PMID: 31182638, pp. 6122–6135. ISSN: 0270-6474, 1529-2401. DOI: 10.1523/JNEUROSCI.0535-19.2019.

[87] I. H. Hyde. "A Micro-Electrode and Unicellular Stimulation". In: *Biological Bulletin* 40.3 (1921). publisher: Marine Biological Laboratory, pp. 130–133. ISSN: 0006-3185. DOI: 10.2307/1536534.

[88] Takeshi Inoue et al. "Engagement of cortico-cortical and cortico-subcortical networks in a patient with epileptic spasms: An integrated neurophysiological study". en. In: *Clinical Neurophysiology* 131.9 (Sept. 1, 2020), pp. 2255–2264. ISSN: 1388-2457. DOI: 10.1016/j.clinph.2020.04.167.

[89] T.A. Ishankulov et al. "Prediction of Postoperative Speech Dysfunctions in Neurosurgery Based on Cortico-Cortical Evoked Potentials and Machine Learning Technology". In: *Modern Technologies in Medicine* 14.1 (2022). PMID: 35992997 PMCID: PMC9376754, pp. 25–32. ISSN: 2076-4243. DOI: 10.17691/stm2022.14.1.03.

[90] Masaki Iwasaki et al. "Accentuated cortico-cortical evoked potentials in neocortical epilepsy in areas of ictal onset". en. In: *Epileptic Disorders* 12.4 (Dec. 1, 2010), pp. 292–302. ISSN: 1950-6945. DOI: 10.1684/epd.2010.0334.

[91] Andrew Jackson, Jaideep Mavoori, and Eberhard E. Fetz. "Long-term motor cortex plasticity induced by an electronic neural implant". In: *Nature* 444.7115 (2006), pp. 56–60. ISSN: 1476-4687 (Electronic). DOI: 10.1038/nature05226.

[92] Kara A. Johnson et al. "Deep brain stimulation for refractory major depressive disorder: a comprehensive review". en. In: *Molecular Psychiatry* (Jan. 30, 2024). publisher: Nature Publishing Group, pp. 1–13. ISSN: 1476-5578. DOI: 10.1038/s41380-023-02394-4.

[93] L. A. Johnson et al. "Direct electrical stimulation of the somatosensory cortex in humans using electrocorticography electrodes: A qualitative and quantitative report". In: *Journal of Neural Engineering* 10.3 (2013). DOI: 10.1088/1741-2560/10/3/036021.

[94] Golnoosh Kamali et al. "Transfer Function Models for the Localization of Seizure Onset Zone From Cortico-Cortical Evoked Potentials". en. In: *Frontiers in Neurology* 11 (Dec. 10, 2020), p. 579961. ISSN: 1664-2295. DOI: 10.3389/fneur.2020.579961.

[95] Aya Kanno et al. "Location and Threshold of Electrical Cortical Stimulation for Functional Brain Mapping". en. In: *World Neurosurgery* 119 (Nov. 1, 2018), e125–e130. ISSN: 1878-8750. DOI: 10.1016/j.wneu.2018.07.059.

[96] C. J. Keller et al. "Corticocortical Evoked Potentials Reveal Projectors and Integrators in Human Brain Networks". en. In: *Journal of Neuroscience* 34.27 (July 2, 2014), pp. 9152–9163. ISSN: 0270-6474, 1529-2401. DOI: 10.1523/JNEUROSCI.4289-13.2014. URL: http://www.jneurosci.org/cgi/doi/10.1523/JNEUROSCI.4289-13.2014 (visited on 09/10/2020).

[97] C. J. Keller et al. "Induction and Quantification of Excitability Changes in Human Cortical Networks". en. In: *The Journal of Neuroscience* 38.23 (June 6, 2018), pp. 5384–5398. ISSN: 0270-6474, 1529-2401. DOI: 10.1523/JNEUROSCI.1088-17.2018.

[98] C. J. Keller et al. "Intrinsic functional architecture predicts electrically evoked responses in the human brain". In: *Frontiers in Neuroinformatics* 108.41 (2011).

[99] C. J. Keller et al. "Mapping human brain networks with cortico-cortical evoked potentials". eng. In: *Philosophical Transactions of the Royal Society of London. Series B, Biological Sciences* 369.1653 (Oct. 5, 2014). PMID: 25180306 PMCID: PMC4150303. ISSN: 1471-2970. DOI: 10.1098/rstb.2013.0528.

[100] Katsuya Kobayashi et al. "High frequency activity overriding cortico-cortical evoked potentials reflects altered excitability in the human epileptic focus". In: *Clinical Neurophysiology* 128.9 (2017). publisher: International Federation of Clinical Neurophysiology, pp. 1673–1681. DOI: 10.1016/j.clinph.2017.06.249.

[101] Stjepana Kovac et al. "Invasive epilepsy surgery evaluation". en. In: *Seizure* 44 (Jan. 2017), pp. 125–136. ISSN: 10591311. DOI: 10.1016/j.seizure.2016.10.016.

[102] Pawel Kudela and William S. Anderson. "Computational Modeling of Subdural Cortical Stimulation: A Quantitative Spatiotemporal Analysis of Action Potential Initiation in a High-Density Multicompartment Model". eng. In: *Neuromodulation: Journal of the International Neuromodulation Society* 18.7 (Oct. 2015). PMID: 26245183 PMCID: PMC4615525, 552–564, discussion 564–565. ISSN: 1525-1403. DOI: 10.1111/ner.12327.

[103] Andrea A. Kühn et al. "High-frequency stimulation of the subthalamic nucleus suppresses oscillatory beta activity in patients with Parkinson's disease in parallel with improvement in motor performance". In: *Journal of Neuroscience* 28.24 (2008), pp. 6165–6173. ISSN: 02706474. DOI: 10.1523/JNEUROSCI.0282-08.2008.

[104] Takeharu Kunieda et al. "New Approach for Exploring Cerebral Functional Connectivity: Review of Cortico-cortical Evoked Potential". en. In: *Neurologia medico-chirurgica* 55.5 (2015), pp. 374–382. ISSN: 0470-8105, 1349-8029. DOI: 10.2176/nmc.ra.2014-0388.

[105] Bradley Lega et al. "Cortico-cortical evoked potentials for sites of early versus late seizure spread in stereoelectroencephalography". en. In: *Epilepsy Research* 115 (Sept. 1, 2015), pp. 17–29. ISSN: 0920-1211. DOI: 10.1016/j.eplepsyres.2015.04.009.

[106] Jean-Didier Lemaréchal et al. "A brain atlas of axonal and synaptic delays based on modelling of cortico-cortical evoked potentials". In: *Brain* 145.5 (May 1, 2022), pp. 1653–1667. ISSN: 0006-8950. DOI: 10.1093/brain/awab362.

[107] Robert Levy et al. "Cortical stimulation for the rehabilitation of patients with hemiparetic stroke: a multicenter feasibility study of safety and efficacy". en. In: *Journal of Neurosurgery* 108.4 (Apr. 2008), pp. 707–714. ISSN: 0022-3085, 1933-0693. DOI: 10.3171/JNS/2008/108/4/0707.

[108] Guangye Li et al. "Optimal referencing for stereo-electroencephalographic (SEEG) recordings". en. In: *NeuroImage* 183 (Dec. 1, 2018), pp. 327–335. ISSN: 1053-8119. DOI: 10.1016/j.neuroimage.2018.08.020.

[109] Stephen Luck. *An Introduction to the Event-Related Potential Technique*. Cambridge: MIT Press, 2014.

[110] Dian Lyu et al. "Causal evidence for the processing of bodily self in the anterior precuneus". en. In: *Neuron* 111.16 (Aug. 2023), 2502–2512.e4. ISSN: 08966273. DOI: 10.1016/j.neuron.2023.05.013.

[111] Nikos Makris et al. "Decreased volume of left and total anterior insular lobule in schizophrenia". In: *Schizophrenia Research* 83.2 (Apr. 1, 2006), pp. 155–171. ISSN: 0920-9964. DOI: 10.1016/j.schres.2005.11.020.

[112] Nicolas Mallet et al. "Disrupted dopamine transmission and the emergence of exaggerated beta oscillations in subthalamic nucleus and cerebral cortex". In: *Journal of Neuroscience* 28.18 (2008), pp. 4795–4806. ISSN: 02706474. DOI: 10.1523/JNEUROSCI.0123-08.2008.

[113] Emmanuel Mandonnet, Peter A. Winkler, and Hugues Duffau. "Direct electrical stimulation as an input gate into brain functional networks: principles, advantages and limitations". eng. In: *Acta Neurochirurgica* 152.2 (Feb. 2010). PMID: 19639247, pp. 185–193. ISSN: 0942-0940. DOI: 10.1007/s00701-009-0469-0.

[114] Lorea Mar-Barrutia et al. "Deep brain stimulation for obsessive-compulsive disorder: A systematic review of worldwide experience after 20 years". eng. In: *World Journal of Psychiatry* 11.9 (Sept. 19, 2021). PMID: 34631467 PMCID: PMC8474989, pp. 659–680. ISSN: 2220-3206. DOI: 10.5498/wjp.v11.i9.659.

[115] Valeria Mariani et al. "Intraoperative Corticocortical Evoked Potentials for Language Monitoring in Epilepsy Surgery". en. In: *World Neurosurgery* 151 (July 1, 2021), e109–e121. ISSN: 1878-8750. DOI: 10.1016/j.wneu.2021.03.141.

[116] Marcello Massimini et al. "Triggering sleep slow waves by transcranial magnetic stimulation". In: *Proceedings of the National Academy of Sciences of the United States of America* 104.20 (2007), pp. 8496–8501. DOI: 10.1073/pnas.0702495104.

[117] Pedro Mateos-Aparicio and Antonio Rodríguez-Moreno. "The Impact of Studying Brain Plasticity". In: *Frontiers in Cellular Neuroscience* 13 (Feb. 27, 2019). PMID: 30873009 PMCID: PMC6400842, p. 66. ISSN: 1662-5102. DOI: 10.3389/fncel.2019.00066.

[118] Teppei Matsui et al. "Direct Comparison of Spontaneous Functional Connectivity and Effective Connectivity Measured by Intracortical Microstimulation: An fMRI Study in Macaque Monkeys". In: *Cerebral Cortex* 21.10 (Oct. 1, 2011), pp. 2348–2356. ISSN: 1047-3211. DOI: 10.1093/cercor/bhr019.

[119] Riki Matsumoto, Takeharu Kunieda, and Dileep Nair. "Single pulse electrical stimulation to probe functional and pathological connectivity in epilepsy". English. In: *Seizure - European Journal of Epilepsy* 44 (Jan. 1, 2017). publisher: Elsevier PMID: 27939100, pp. 27–36. ISSN: 1059-1311, 1532-2688. DOI: 10.1016/j.seizure.2016.11.003.

[120] Riki Matsumoto et al. "Functional connectivity in human cortical motor system: A cortico-cortical evoked potential study". In: *Brain* 130.1 (2007), pp. 181–197. DOI: 10.1093/brain/awl257.

[121] Riki Matsumoto et al. "Functional connectivity in human cortical motor system: A cortico-cortical evoked potential study". In: *Brain* 130.1 (2007), pp. 181–197. DOI: 10.1093/brain/awl257.

[122] Riki Matsumoto et al. "Functional connectivity in the human language system: a cortico-cortical evoked potential study". en. In: *Brain* 127.10 (Oct. 2004), pp. 2316–2330. ISSN: 1460-2156, 0006-8950. DOI: 10.1093/brain/awh246.

[123] Riki Matsumoto et al. "Interareal connectivity in the human language system: a cortico-cortical evoked potential study". en. In: *International Congress Series*. Unveiling the Mystery of the Brain: Neurophysiological Investigation of the Brain Function 1278 (Mar. 1, 2005), pp. 397–400. ISSN: 0531-5131. DOI: 10.1016/j.ics.2004.11.128.

[124] Riki Matsumoto et al. "Parieto-frontal network in humans studied by cortico-cortical evoked potential". en. In: *Human Brain Mapping* 33.12 (2012), pp. 2856–2872. DOI: 10.1002/hbm.21407.

[125] Cameron C. McIntyre et al. "Electric field and stimulating influence generated by deep brain stimulation of the subthalamic nucleus". In: *Clinical Neurophysiology* 115.3 (2004), pp. 589–595. ISSN: 13882457. DOI: 10.1016/j.clinph.2003.10.033.

[126] Manuel R. Mercier et al. "Advances in human intracranial electroencephalography research, guidelines and good practices". en. In: *NeuroImage* 260 (Oct. 2022), p. 119438. ISSN: 10538119. DOI: 10.1016/j.neuroimage.2022.119438.

[127] Kai J. Miller, Klaus-Robert Müller, and Dora Hermes. "Basis profile curve identification to understand electrical stimulation effects in human brain networks". en. In: *PLOS Computational Biology* 17.9 (Sept. 2, 2021). publisher: Public Library of Science, e1008710. ISSN: 1553-7358. DOI: 10.1371/journal.pcbi.1008710.

[128] Kai J. Miller et al. "Canonical Response Parameterization: Quantifying the structure of responses to single-pulse intracranial electrical brain stimulation". en. In: (Aug. 5, 2022). page: 2022.08.05.502944 section: New Results. DOI: 10.1101/2022.08.05.502944. URL: https://www.biorxiv.org/content/10.1101/2022.08.05.502944v1.

[129] Svjetlana Miocinovic et al. "Computational analysis of subthalamic nucleus and lenticular fasciculus activation during therapeutic deep brain stimulation". In: *Journal of Neurophysiology* 96.3 (2006), pp. 1569–1580. ISSN: 00223077. DOI: 10.1152/jn.00305.2006.

[130] Svjetlana Miocinovic et al. "Cortical Potentials Evoked by Subthalamic Stimulation Demonstrate a Short Latency Hyperdirect Pathway in Humans". In: *Journal of Neuroscience* 38.43 (2018), pp. 9129–9141. DOI: 10.1523/JNEUROSCI.1327-18.2018.

[131] K. Monakow, K. Akert, and H. Künzle. "Projections of the precentral motor cortex and other cortical areas of the frontal lobe to the subthalamic nucleus in the monkey." In: *Frontiers in Systems Neuroscience* 5.2011 (1978), p. 30.

[132] Chet T. Moritz. "Now is the Critical Time for Engineered Neuroplasticity". en. In: *Neurotherapeutics* 15.3 (July 1, 2018), pp. 628–634. ISSN: 1878-7479. DOI: 10.1007/s13311-018-0637-0.

[133] V. N. Murthy and E. E. Fetz. "Oscillatory activity in sensorimotor cortex of awake monkeys: synchronization of local field potentials and relation to behavior". eng. In: *Journal of Neurophysiology* 76.6 (Dec. 1996). PMID: 8985892, pp. 3949–3967. ISSN: 0022-3077. DOI: 10.1152/jn.1996.76.6.3949.

[134] V. N. Murthy and E. E. Fetz. "Synchronization of neurons during local field potential oscillations in sensorimotor cortex of awake monkeys". eng. In: *Journal of Neurophysiology* 76.6 (Dec. 1996). PMID: 8985893, pp. 3968–3982. ISSN: 0022-3077. DOI: 10.1152/jn.1996.76.6.3968.

[135] Sadegh Nabavi et al. "Engineering a memory with LTD and LTP". In: *Nature* 511.7509 (2014), pp. 348–352. DOI: 10.1038/nature13294.

[136] Surendar S. Nathan et al. "Determination of current density distributions generated by electrical stimulation of the human cerebral cortex". en. In: *Electroencephalography and Clinical Neurophysiology* 86.3 (Mar. 1, 1993), pp. 183–192. ISSN: 0013-4694. DOI: 10.1016/0013-4694(93)90006-H.

[137] R. J. Nudo and G. W. Milliken. "Reorganization of movement representations in primary motor cortex following focal ischemic infarcts in adult squirrel monkeys". en. In: *Journal of Neurophysiology* 75.5 (May 1, 1996), pp. 2144–2149. ISSN: 0022-3077, 1522-1598. DOI: 10.1152/jn.1996.75.5.2144.

[138] Randolph J. Nudo et al. "Neural substrates for the effects of rehabilitative training on motor recovery after ischemic infarct". In: *Science* 272.5269 (June 1996). publisher: American Association for the Advancement of Science, pp. 1791–1794. DOI: 10.1126/science.272.5269.1791.

[139] E. S. Nurse et al. "Consistency of Long-Term Subdural Electrocorticography in Humans". In: *IEEE Transactions on Biomedical Engineering* 65.2 (Feb. 2018). event-title: IEEE Transactions on Biomedical Engineering, pp. 344–352. ISSN: 1558-2531. DOI: 10.1109/TBME.2017.2768442.

[140] G.M.S Nys et al. "Early cognitive impairment predicts long-term depressive symptoms and quality of life after stroke". en. In: *Journal of the Neurological Sciences* 247.2 (Sept. 2006), pp. 149–156. ISSN: 0022510X. DOI: 10.1016/j.jns.2006.04.005.

[141] Justin O'Hare, Nicole Calakos, and Henry H Yin. "Recent insights into corticostriatal circuit mechanisms underlying habits". In: *Current Opinion in Behavioral Sciences*. Habits and Skills 20 (Apr. 1, 2018), pp. 40–46. ISSN: 2352-1546. DOI: 10.1016/j.cobeha.2017.10.001.

[142] Irina Oane et al. "Cingulate cortex function and multi-modal connectivity mapped using intracranial stimulation". en. In: *NeuroImage* 220 (Oct. 2020), p. 117059. ISSN: 10538119. DOI: 10.1016/j.neuroimage.2020.117059.

[143] Bente Pakkenberg and Hans Jørgen G. Gundersen. "Neocortical neuron number in humans: Effect of sex and age". en. In: *Journal of Comparative Neurology* 384.2 (1997), pp. 312–320. ISSN: 1096-9861. DOI: 10.1002/(SICI)1096-9861(19970728)384:2{\textless}312::AID-CNE10{\textgreater}3.0.CO;2-K.

[144] Bente Pakkenberg et al. "Aging and the human neocortex". In: *Experimental Gerontology*. Proceedings of the 6th International Symposium on the Neurobiology and Neuroendocrinology of Aging 38.1 (Jan. 1, 2003), pp. 95–99. ISSN: 0531-5565. DOI: 10.1016/S0531-5565(02)00151-1.

[145] Christopher S. Parker et al. "Structural and effective connectivity in focal epilepsy". en. In: *NeuroImage: Clinical* 17 (Jan. 1, 2018), pp. 943–952. ISSN: 2213-1582. DOI: 10.1016/j.nicl.2017.12.020.

[146] S. Parmigiani et al. "Simultaneous stereo-EEG and high-density scalp EEG recordings to study the effects of intracerebral stimulation parameters". en. In: *Brain Stimulation* 15.3 (May 2022), pp. 664–675. ISSN: 1935861X. DOI: 10.1016/j.brs.2022.04.007.

[147] Paul Pauli et al. "Brain potentials during mental arithmetic: effects of extensive practice and problem difficulty". en. In: *Cognitive Brain Research* 2.1 (July 1994), pp. 21–29. ISSN: 09266410. DOI: 10.1016/0926-6410(94)90017-5.

[148] Angelique C. Paulk et al. "Local and distant cortical responses to single pulse intracranial stimulation in the human brain are differentially modulated by specific stimulation parameters". en. In: *Brain Stimulation* 15.2 (Mar. 2022), pp. 491–508. ISSN: 1935861X. DOI: 10.1016/j.brs.2022.02.017.

[149] W. Penfield and E. Boldrey. "Somatic motor and sensory representation in the cerebral cortex of man as studied by electrical stimulation". In: *Brain: A Journal of Neurology* 60 (1937). publisher-place: United Kingdom publisher: Oxford University Press, pp. 389–443. ISSN: 1460-2156(Electronic),0006-8950(Print). DOI: 10.1093/brain/60.4.389.

[150] Andrea Pigorini et al. "Bistability breaks-off deterministic responses to intracortical stimulation during non-REM sleep". en. In: *NeuroImage* 112 (May 2015), pp. 105–113. ISSN: 10538119. DOI: 10.1016/j.neuroimage.2015.02.056.

[151] David Prime et al. "Comparing connectivity metrics in cortico-cortical evoked potentials using synthetic cortical response patterns". In: *Journal of Neuroscience Methods* 334 (2020).

[152] David Prime et al. "Considerations in performing and analyzing the responses of cortico-cortical evoked potentials in stereo-EEG". In: *Epilepsia* 59.1 (2017), pp. 16–26. ISSN: 15281167. DOI: 10.1111/epi.13939.

[153] David Prime et al. "Quantifying volume conducted potential using stimulation artefact in CCEP". In: *Journal of Neuroscience Methods* 337 (2020).

[154] D. P. Purpura et al. "Observations on evoked dendritic potentials of human cortex". en. In: *Electroencephalography and Clinical Neurophysiology* 9.3 (Aug. 1, 1957), pp. 453–459. ISSN: 0013-4694. DOI: 10.1016/0013-4694(57)90034-2.

[155] Dominick P. Purpura, Martin Girado, and Harry Grundfest. "Components of evoked potentials in cerebral cortex". In: *Electroencephalography and Clinical Neurophysiology* 12.1 (Feb. 1, 1960), pp. 95–110. ISSN: 0013-4694. DOI: 10.1016/0013-4694(60)90064-X.

[156] Supratim Ray et al. “Neural correlates of high-gamma oscillations (60-200 Hz) in macaque local field potentials and their potential implications in electrocorticography”. In: *Journal of Neuroscience* 28.45 (2008), pp. 11526–11536. ISSN: 02706474. DOI: 10.1523/JNEUROSCI.2848-08.2008.

[157] Karin Rosenkranz, Aleksandra Kacar, and John C. Rothwell. “Differential Modulation of Motor Cortical Plasticity and Excitability in Early and Late Phases of Human Motor Learning”. In: *The Journal of Neuroscience* 27.44 (Oct. 31, 2007). PMID: 17978047 PMCID: PMC6673358, pp. 12058–12066. ISSN: 0270-6474. DOI: 10.1523/JNEUROSCI.2663-07.2007.

[158] Olivier Rossel et al. “Short-range axono-cortical evoked-potentials in brain tumor surgery: Waveform characteristics as markers of direct connectivity”. In: *Clinical Neurophysiology* 153 (Sept. 1, 2023), pp. 189–201. ISSN: 1388-2457. DOI: 10.1016/j.clinph.2023.05.011.

[159] Beth K. Rush et al. “Behavioral Symptoms in Long-Term Survivors of Ischemic Stroke”. en. In: *Journal of Stroke and Cerebrovascular Diseases* 19.4 (July 2010), pp. 326–332. ISSN: 10523057. DOI: 10.1016/j.jstrokecerebrovasdis.2009.09.009.

[160] Hyeon Seo, Donghyeon Kim, and Sung Chan Jun. “Computational Study of Subdural Cortical Stimulation: Effects of Simulating Anisotropic Conductivity on Activation of Cortical Neurons”. en. In: *PLOS ONE* 10.6 (June 9, 2015). publisher: Public Library of Science, e0128590. ISSN: 1932-6203. DOI: 10.1371/journal.pone.0128590.

[161] Hossein Shahabi et al. “Effective connectivity differs between focal cortical dysplasia types I and II”. en. In: *Epilepsia* 62.11 (2021). _eprint: https://onlinelibrary.wiley.com/doi/pdf/10.11 pp. 2753–2765. ISSN: 1528-1167. DOI: 10.1111/epi.17064.

[162] Nour Shaheen et al. “Deep brain stimulation for chronic pain: a systematic review and meta-analysis”. In: *Frontiers in Human Neuroscience* 17 (Nov. 30, 2023). PMID: 38098761 PMCID: PMC10719838, p. 1297894. ISSN: 1662-5161. DOI: 10.3389/fnhum.2023.1297894.

[163] Maxwell A. Sherman et al. “Neural mechanisms of transient neocortical beta rhythms: Converging evidence from humans, computational modeling, monkeys, and mice”. eng. In: *Proceedings of the National Academy of Sciences of the United States of America* 113.33 (Aug. 16, 2016). PMID: 27469163 PMCID: PMC4995995, E4885–4894. ISSN: 1091-6490. DOI: 10.1073/pnas.1604135113.

[164] Seijiro Shimada et al. “Impact of volume-conducted potential in interpretation of cortico-cortical evoked potential: Detailed analysis of high-resolution electrocorticography using two mathematical approaches”. In: *Clinical Neurophysiology* 128.4 (2017). publisher: International Federation of Clinical Neurophysiology, pp. 549–557. DOI: 10.1016/j.clinph.2017.01.012.

[165] Brian H. Silverstein et al. “Dynamic tractography: Integrating cortico-cortical evoked potentials and diffusion imaging”. en. In: *NeuroImage* 215 (July 15, 2020), p. 116763. ISSN: 1053-8119. DOI: 10.1016/j.neuroimage.2020.116763.

[166] Nirvik Sinha et al. “Cross-Frequency Coupling in Descending Motor Pathways: Theory and Simulation”. In: *Frontiers in Systems Neuroscience* 13 (2020). [Online; accessed 2024-03-04]. ISSN: 1662-5137. URL: https://www.frontiersin.org/articles/10.3389/fnsys.2019.00086.

[167] Katja Stefan et al. “Temporary Occlusion of Associative Motor Cortical Plasticity by Prior Dynamic Motor Training”. en. In: *Cerebral Cortex* 16.3 (Mar. 1, 2006), pp. 376–385. ISSN: 1460-2199, 1047-3211. DOI: 10.1093/cercor/bhi116.

[168] M Steriade and F Amzica. “Intracortical and corticothalamic coherency of fast spontaneous oscillations.” In: *Proceedings of the National Academy of Sciences* 93.6 (Mar. 19, 1996). publisher: Proceedings of the National Academy of Sciences, pp. 2533–2538. DOI: 10.1073/pnas.93.6.2533.

[169] Verne Strudwick Caviness et al. “MRI-based brain volumetrics: emergence of a developmental brain science”. In: *Brain and Development* 21.5 (July 1, 1999), pp. 289–295. ISSN: 0387-7604. DOI: 10.1016/S0387-7604(99)00022-4.

[170] Samantha Sun et al. “Human intracortical responses to varying electrical stimulation conditions are separable in low-dimensional subspaces”. In: ISSN: 2577-1655. Oct. 2022, pp. 2663–2668. DOI: 10.1109/SMC53654.2022.9945369.

[171] Yukie Tamura et al. “Passive language mapping combining real-time oscillation analysis with cortico-cortical evoked potentials for awake craniotomy”. en. In: *Journal of Neurosurgery* 125.6 (Dec. 1, 2016). publisher: American Association of Neurological Surgeons section: Journal of Neurosurgery, pp. 1580–1588. ISSN: 1933-0693, 0022-3085. DOI: 10.3171/2015.4.JNS15193.

[172] Darren Tanner, Kara Morgan-Short, and Steven J. Luck. “How inappropriate high-pass filters can produce artifactual effects and incorrect conclusions in ERP studies of language and cognition”. In: *Psychophysiology* 52.8 (Aug. 2015). PMID: 25903295 PMCID: PMC4506207, pp. 997–1009. ISSN: 0048-5772. DOI: 10.1111/psyp.12437.

[173] Edward Taub, Gitendra Uswatte, and Thomas Elbert. "New treatments in neurorehabiliation founded on basic research". en. In: *Nature Reviews Neuroscience* 3.3 (Mar. 2002), pp. 228–236. ISSN: 1471-003X, 1471-0048. DOI: 10.1038/nrn754.

[174] Siddhi Tavildar et al. "Inferring Cortical Connectivity From ECoG Signals Using Graph Signal Processing". In: *IEEE Access* 7 (2019). event-title: IEEE Access, pp. 109349–109362. ISSN: 2169-3536. DOI: 10.1109/ACCESS.2019.2934490.

[175] Masaya Togo et al. "Distinct connectivity patterns in human medial parietal cortices: Evidence from standardized connectivity map using cortico-cortical evoked potential". en. In: *NeuroImage* 263 (Nov. 1, 2022), p. 119639. ISSN: 1053-8119. DOI: 10.1016/j.neuroimage.2022.119639.

[176] Simon Tousseyn et al. "Connectivity in ictal single photon emission computed tomography perfusion: a cortico-cortical evoked potential study". en. In: *Brain* 140.7 (July 1, 2017), pp. 1872–1884. ISSN: 0006-8950, 1460-2156. DOI: 10.1093/brain/awx123.

[177] Qing-zhang Tuo, Shu-ting Zhang, and Peng Lei. "Mechanisms of neuronal cell death in ischemic stroke and their therapeutic implications". en. In: *Medicinal Research Reviews* 42.1 (2022). _eprint: https://onlinelibrary.wiley.com/doi/pdf/10.1002/med.21817, pp. 259–305. ISSN: 1098-1128. DOI: 10.1002/med.21817.

[178] Julian Unterweger et al. "ECoG Beta Suppression and Modulation During Finger Extension and Flexion". In: *Frontiers in Neuroscience* 14.February (2020), pp. 1–10. ISSN: 1662453X. DOI: 10.3389/fnins.2020.00035.

[179] Lorena Vega-Zelaya et al. "Intraoperative Cortico-Cortical Evoked Potentials for Monitoring Language Function during Brain Tumor Resection in Anesthetized Patients". en. In: *Journal of Integrative Neuroscience* 22.1 (Jan. 13, 2023), p. 17. ISSN: 0219-6352. DOI: 10.31083/j.jin2201017.

[180] Marion Vincent et al. "Electrophysiological brain mapping: Basics of recording evoked potentials induced by electrical stimulation and its physiological spreading in the human brain". en. In: *Clinical Neurophysiology* 128.10 (Oct. 2017), pp. 1886–1890. ISSN: 13882457. DOI: 10.1016/j.clinph.2017.07.402.

[181] Marion Vincent et al. "The difference between electrical microstimulation and direct electrical stimulation - towards new opportunities for innovative functional brain mapping?" eng. In: *Reviews in the Neurosciences* 27.3 (Apr. 1, 2016). PMID: 26646021, pp. 231–258. ISSN: 2191-0200. DOI: 10.1515/revneuro-2015-0029.

[182] Daniel A Wagenaar and Steve M Potter. "Real-time multi-channel stimulus artifact suppression by local curve fitting". en. In: *Journal of Neuroscience Methods* 120.2 (Oct. 2002), pp. 113–120. ISSN: 01650270. DOI: 10.1016/S0165-0270(02)00149-8.

[183] Harrison C. Walker et al. "Short latency activation of cortex during clinically effective subthalamic deep brain stimulation for Parkinson's disease". In: *Movement Disorders* 27.7 (June 2012), pp. 864–873. ISSN: 08853185. DOI: 10.1002/mds.25025.

[184] Kurt E. Weaver et al. "Directional patterns of cross frequency phase and amplitude coupling within the resting state mimic patterns of fMRI functional connectivity". In: *NeuroImage* 128 (2016). publisher: Elsevier Inc., pp. 238–251. DOI: 10.1016/j.neuroimage.2015.12.043.

[185] Thomas Wichmann and Mahlon R. DeLong. "Deep Brain Stimulation for Movement Disorders of Basal Ganglia Origin: Restoring Function or Functionality?" In: *Neurotherapeutics* 13.2 (2016), pp. 264–283. ISSN: 18787479. DOI: 10.1007/s13311-016-0426-6.

[186] Peter R. Wilkinson et al. "A Long-term Follow-up of Stroke Patients". In: *Stroke* 28.3 (Mar. 1997). publisher: American Heart Association, pp. 507–512. DOI: 10.1161/01.STR.28.3.507.

[187] Dan Wilson and Jeff Moehlis. "Clustered Desynchronization from High-Frequency Deep Brain Stimulation". In: *PLoS Computational Biology* 11.12 (2015), pp. 1–26. ISSN: 15537358. DOI: 10.1371/journal.pcbi.1004673.

[188] Di Wu et al. "Human anterior thalamic stimulation evoked cortical potentials align with intrinsic functional connectivity". en. In: *NeuroImage* 277 (Aug. 2023), p. 120243. ISSN: 10538119. DOI: 10.1016/j.neuroimage.2023.120243.

[189] Youliang Wu et al. "Deep Brain Stimulation in Treatment-Resistant Depression: A Systematic Review and Meta-Analysis on Efficacy and Safety". In: *Frontiers in Neuroscience* 15 (Apr. 1, 2021). PMID: 33867929 PMCID: PMC8047101, p. 655412. ISSN: 1662-4548. DOI: 10.3389/fnins.2021.655412.

[190] Yukihiro Yamao et al. "Intraoperative Brain Mapping by Cortico-Cortical Evoked Potential". In: *Frontiers in Human Neuroscience* 15 (2021). [Online; accessed 2022-11-30]. ISSN: 1662-5161. URL: https://www.frontiersin.org/articles/10.3389/fnhum.2021.635453.

[191] Azadeh Yazdan-Shahmorad, Daryl R. Kipke, and Mark J. Lehmkuhle. "High gamma power in ECoG reflects cortical electrical stimulation effects on unit activity in layers V/VI". en. In: *Journal of Neural Engineering* 10.6 (Oct. 2013). publisher: IOP Publishing, p. 066002. ISSN: 1741-2552. DOI: 10.1088/1741-2560/10/6/066002.

[192] Stavros Zanos et al. "Phase-Locked Stimulation during Cortical Beta Oscillations Produces Bidirectional Synaptic Plasticity in Awake Monkeys". en. In: *Current Biology* 28.16 (Aug. 2018), 2515–2526.e4. ISSN: 09609822.

[193] F. M. Zauli et al. "The web of laughter: frontal and limbic projections of the anterior cingulate cortex revealed by cortico-cortical evoked potential from sites eliciting laughter". In: *Philosophical Transactions of the Royal Society B: Biological Sciences* 377.1863 (Nov. 7, 2022). publisher: Royal Society, p. 20210180. DOI: 10.1098/rstb.2021.0180.

[194] Nan Zhang et al. "The effectiveness of cortico-cortical evoked potential in detecting seizure onset zones". en. In: *Neurological Research* 40.6 (June 3, 2018), pp. 480–490. ISSN: 0161-6412, 1743-1328. DOI: 10.1080/01616412.2018.1454092.

[195] Cui Zhao et al. "Localization of epileptogenic zone based on cortico-cortical evoked potential (CCEP): A feature extraction and graph theory approach". In: *Frontiers in Neuroinformatics* 13.April (2019), pp. 1–9. DOI: 10.3389/fninf.2019.00031.

[196] Ulf Ziemann et al. "Learning Modifies Subsequent Induction of Long-Term Potentiation-Like and Long-Term Depression-Like Plasticity in Human Motor Cortex". In: *The Journal of Neuroscience* 24.7 (Feb. 18, 2004). PMID: 14973238 PMCID: PMC6730462, pp. 1666–1672. ISSN: 0270-6474. DOI: 10.1523/JNEUROSCI.5016-03.2004.

[197] Andrew J. Zimnik et al. "Movement-related discharge in the macaque globus pallidus during high-frequency stimulation of the subthalamic nucleus". In: *Journal of Neuroscience* 35.9 (2015), pp. 3978–3989. ISSN: 15292401. DOI: 10.1523/JNEUROSCI.4899-14.2015.

Appendices

Appendix A

Literature Review of CCEP Pre-Processing Methods

We surveyed 62 CCEP studies to gather pre-processing methods used. All papers included were: (1) published after 2010, (2) used ECoG, high-density ECoG, and/or sEEG electrodes in humans, (3) collected CCEP data extra-operatively (as opposed to intra-operatively), (4) did not focus on spectral characteristics of CCEPs. Intra-operative CCEP studies were excluded as intra-operative data collection may pose unique noise concerns that are not faced in typical extra-operative environments. Studies that focused on time-frequency analysis were excluded because filter cutoffs depended heavily on frequency bands of interest.

Table A.1: Table of Methods Across Literature.

Authors	General		Recording			Offline Pre-Processing						
	modality	**metrics**	**sampling rate (Hz)**	**recording reference**	**hardware filter**	**subsequent digital filtering**	**re-referencing**	**baseline correction**	**normalization**	**artifact mitigation techniques**	**epileptiform activity**	**other pre-processing**
Araki et al. (2015)	ECoG	p2t	5000-10000	subdural	BPF 10 to 2000-5000Hz					bipolar stim		
Arihara et al. (2021)	ECoG, sEEG	amp	2000		BPF 0.016 to 600Hz	BPF 5 to 600Hz				excl. artifactual period	excl. bad channels	
Basu et al. (2019)	sEEG	amp, AUC, lat	2000 (DS to 1000)	EEG (CZ or C2)	BPF 0.5 to 500Hz		BP	z-scored to BL (500ms pre-stim)			excl. bad channels & trials	subtracted signal BPF at line noise freq & harmonics

Boulogne et al. (2016)	sEEG	lat, p2t	1024				BP	amp measured relative to BL	excl. first 10ms	excl. bad trials	
Conner et al. (2011)	ECoG	amp, lat	1000	average of >20 low noise/artifact/ CCEP chans	BPF 0.2 to 300 Hz	HPF 1Hz			excl. first 8ms	excl. bad trials	
Cornblath et al. (2023)	sEEG	amp	512-1024	usually skull screw		compared none, LPF 30Hz	BP	z-scored to BL (-500 to -30ms)	manually validated artifact rejection; excluded first 15ms	no epileptic spike excl.	detrended
David et al., (2013)	sEEG	binary, lat	256 or 512	WM contact	BPF 0.1 to 90 or BPF 0.1 to 200Hz	BPF 1 to 45Hz		BL corrected (-100 to 0ms)	cubic spine interpolated; excluded first 5ms	excl. bad trials (cumulative amp. threshold), excl. bad channels (vis. examination)	
Dickey et al. (2022)	sEEG	RMS	1000 or 2000	extracranial		none	compared none, CAR, BP, Laplacian	BL corrected (-100 to -1ms)	excl. first 10ms		
Dionisio et al. (2019)	sEEG	RMS	1000			BPF 1 to 300Hz, notch 60Hz			kurtosis-based artifact rem. (w/ visual inspection); excl. first 10ms	excl. bad channels	
Donos et al. (2016a, b)	sEEG	amp, RMS	4096		none				excl. first 10ms	excl. bad channels	
Dou et al. (2023)	sEEG	amp, binary	2000 (DS to 500)		BPF 0.1 to 300 Hz		BP		excl. first 10ms		
Enatsu et al. (2012a, b)	ECoG	lat, p2t	1000 or 2000	scalp	BPF 1 to 300 or 800Hz				excl. artifactual period		
Enatsu et al. (2013a, b)	ECoG, sEEG	lat, p2t, RMS	1000	scalp	BPF 0.08 to 300Hz	BPF 1 to 300Hz			excl. first 10ms		
Enatsu et al. (2015, 2016)	sEEG	RMS	1000			BPF 1 to 300Hz			excl. first 15ms		
Entz et al. (2014)	ECoG, sEEG	abs. amp	1000 or 2000	skull or mastoid				z-scored to BL (-200 to -50ms)	excl. first 10ms	excl. bad trials & channels (vis. inspection)	

Guo et al. (2020, 2021)	sEEG	amp, RMS	1000 or 2000 (DS to 1000)			notch line noise & harmonics, BPF 1 to 300Hz	BP	BL corrected (-500 to -10ms; 2020 paper only)	excl. first 10ms or 15ms		
Hays et al. (2021, 2022, 2023)	ECoG, sEEG	amp, lat, RMS	1000		BPF 0.3 to 7500Hz; AAF	LPF 50Hz	BP	z-scored to BL (-500 to -10ms)	replaced artifact w/ reversed, tapered copies of pre/post data; excl. first 10ms	excl. bad trials (vis. inspection)	
Hebbink et al. (2019)	ECoG	binary	512 or 2048	extracranial			none			excl. bad trials (reference noise)	
Herrero et al. (2021)	ECoG, sEEG	binary	512Hz or 3000	subdural or skull	BPF 0.01 to 250Hz		BP	BL corrected (-200 to -25ms) t-transformed	excl. first 10ms		
Huang et al. (2019)	ECoG, sEEG	amp	512 or 2048			notch 60 or 50Hz	BP (sEEG), or CAR (ECoG)	z-scored to BL (-150 to -50ms)	replaced artifact w/ reversed, tapered copies of pre/post data; excl. first 10ms		
Inoue et al. (2020, 2021)	ECoG	amp, binary	2000	extracranial	BPF 0.08 to 600Hz			[95ms before stim onset]	excl. first 10ms		
Iwasaki et al. (2010)	ECoG	amp,lat	1000	scalp	BPF 1 to 300 or 800Hz				visually separated artifact		
Kamali et al. (2020)	sEEG	amp, binary	1000 or 2000						replaced with linearly spaced vector	excl. bad channels (st. dev. threshold)	
Kanno et al. (2018)	ECoG	lat, p2t	5000	scalp	BPF 0.5 to 1500Hz				visually separated artifact		
Keller et al. (2011)	ECoG	amp, binary				LPF 30Hz		BL corrected, z-scored to BL (-500 to -50ms)	interested in later response	excl. bad trials (voltage threshold)	
Keller et al. (2014)	ECoG, sEEG	amp, binary	2000	skull screw	BPF 0.1 to 1000Hz	notch 60Hz	CAR	z-scored to BL (-500 to -5ms)	excl. first 10ms	excl. bad channels (within 1.5cm of stim)	
Keller et al. (2018)	ECoG, sEEG	amp, AUC, lat, p2t				notch 60Hz		BL corrected (-50 to -10ms)	excl. first 10ms	excl. bad channels (amp. threshold)	

Kubota et al. (2013)	sEEG	lat, RMS	1000	scalp		BPF 1 to 300Hz				exc. first 20ms		
Lega et al. (2015)	sEEG	RMS	1000			notch 60Hz, BPF 1 to 300Hz				kurtosis-based artifact rejection		
Lemaréchal et al. (2022)	sEEG	lat	F-TRACT dataset, parameters varied			BPF 1 to 45Hz	BP		z-scored to BL (-200 to -10ms)	piecewise cubic Hermite inter-polation	excl. bad channels (high inter-ictal spiking as identified in ML ap-proach & vis. in-spection)	
Lyu et al. (2023)	sEEG	binary	1000			notch 60Hz & harmonics	BP		normalized to pre-stim BL	excl. first15ms	excl. bad trials (thresh-olding); excl. bad channels (HFO, WM, channels near stim)	
Matsumoto et al. (2012, 2017)	ECoG	amp (adj)	1000-5000	scalp	BPF 0.08-1 to 300-2500Hz					visual rejection		
Matsuzaki et al. (2013)	ECoG	abs. amp, amp	1000	avg. of 2 electrodes	BPF 0.08 to 300Hz	BPF 1 to 300Hz	CAR			rejected sites <2cm from stim		
Mouthaan et al. (2016)	ECoG	amp, lat	2048 or 512	extracranial	AAF (538 or 134Hz)	LPF 500Hz (only data recorded at 2048Hz)	none	[-1000 to -200ms]		Wiener filtering	excl. bad channels	
Parker et al. (2018)	sEEG	amp, lat	512 or 1024	avg. of 2 electrodes		LPF 110Hz		[-500 to -15ms]		ICA-based art-ifact reduction, visual excl., excl. first 12ms	excl. bad trials (vis. inspection)	
Parmigiani et al. (2022)	sEEG	amp, lat	1000	two WM contacts		BPF 0.5 to 300Hz	BP	z-scored to BL (-300 to -50ms)		Tukey-windowed median filtering	excl. bad trials & channels (vis. inspection)	linear detrended
Pigorini et al. (2015)	sEEG	amp	1000	WM contact		BPF 0.5 to 300Hz	BP	[-300 to -50ms]		Tukey-windowed median filtering		linear detrended; excl. WM contacts

Paulk et al. (2022)	ECoG, sEEG	abs. amp, amp, RMS	2000	EEG (CZ or C2, chest) or internal			BP	demeaned & z-scored to BL	Tukey-windowed median filter	excl. bad channels (vis. inspection & automoatic), excl. bad trials (amp. threshold)	
Prime et al. (2020)	sEEG	RMS	1000		HPF 0.08Hz	BPF 1 to 300Hz, notch 49-51Hz	none	BL subtracted (avg. of 2 samps before stim)	excl. first 10ms	excl. bad trials (vis. inspection)	* focus on artifact
Rossel et al. (2023)	ECoG	morph	38400	ipsilesional mastoid	none	BPF 1 to 1000Hz		[10 or 100ms pre-stim]	interpolation		subtracted signal BPF at 50Hz
Seguin et al. (2023)	sEEG	amp, binary	F-TRACT dataset, parameters varied					z-scored to baseline (-400 to -10ms)	template regression	excl. bad trials (automatic)	
Shahabi et al. (2021)	sEEG	lat, RMS		scalp			none, BP		excl. first 10ms	excl. bad trials (vis. inspection)	
Shimada et al. (2017)	hECoG	morph, RMS	2000	dura-facing electrode	BPF 0.016 to 600Hz			BL corrected (655-950ms post-stim)	excl. first 5ms	excl. bad trials	linear detrended
Silverstein et al. (2020)	ECoG	amp, lat, velocity	1000	avg. of 2 electrodes	BPF 0.016 to 300Hz	BPF 1 to 45Hz	CAR	BL corrected (-200 to -20ms)	excl. first 10ms	excl. bad channels (inc. channels within 25mm of stim)	
Takeyama et al. (2019)	ECoG	amp, lat, binary	1000 or 2000	scalp	BPF 0.08 to 300 or 600Hz			[-100ms to -5ms]	excl. first 5ms		
Togo et al. (2022)	ECoG, sEEG	amp (adj)	1000 or 2000		BPF 0.08 to 300 or 600Hz	z-scored to BL (-100 to -5ms)					
Tousseyn et al. (2017)	sEEG	RMS	1000			notch 60Hz, BPF 1 to 300Hz		t-transformed to BL (-200 to -20ms)	excl. first 20ms		
Usami et al. (2015)	ECoG	AUC, lat	1000 or 2000	scalp	BPF 0.08 to 300 or 600Hz			[-300 to -100ms]		excl. bad trials (vis. inspection)	
Veit et al. (2021)	sEEG	amp, lat, morph	1000		BPF 0.08 to 300Hz		BP	normalized to BL (-25 to -5)		excl. bad channels (WM, sub-cortical, on same shaft as stim channel)	

Wang et al. (2021)	ECoG, hECoG, sEEG	amp, lat	1000-30000 (DS to 1000)	intracranial	AAF		CAR (per grid, strip, or sEEG probe)	z-scored to BL (-500 to -10ms)	excl. first 10ms		
Yu et al. (2019)	sEEG	binary			BPF 0.5 to 2000Hz						
Zauli et al. (2022)	sEEG	lat	1000	WM contact		HPF 0.5Hz	BP	BL corrected (-300 to -20ms)	Tukey filter, excl. first 5ms	excl. bad trials (automatic)	
Zhang et al. (2018)	sEEG	RMS	2000		BPF 0.5 to 300Hz				excl. first 7ms		
Zhao et al. (2019)	ECoG	amp	1024					BL drift elim. (-100 to -5ms)	normalized amp	excl. first 16ms	

Table key:

Modality: ECoG, sEEG, and/or hECoG (high-density ECoG).

Metrics: the primary quantification method used in the paper. They are indicated as amp (amplitude; adj indicates adjusted form of amplitude), abs. amp (absolute value of amplitude), binary (1/0 indication of CCEP presence/absence), AUC (area under the curve), lat (latency), morph (descriptive measures of CCEP morphology), p2t (peak-to-trough), PCA (principal component analysis-based metric), RMS (root mean square).

Filters: HPF (highpass filter), BPF (bandpass filter), LPF (lowpass filter), AAF (anti-alias lowpass filter) and notch filters are given with cutoffs in Hz.

Re-referencing: CAR (common average reference), BP (bipolar reference), or other.

Baseline: brackets indicate that a baseline was noted in the paper but its use was unspecified.

Other abbreviations: EEG (extracranial electroencephalography), WM (white matter), DS (downsampled).

Overall note: empty cells indicate that the reviewer could not find information about this method in the paper. When "none" is indicated, the papers specifically noted that they did not use this method.

Appendix B

Validating Noise Quantification

As schematized in B.1, we designed metrics to analyze the relative noise levels in all channels. These metrics are described in detail below. We also validate the metrics by inserting more noise into an example channel and demonstrate that the metrics increase commensurately.

B.1 Low frequency noise

Normalized signals without baseline subtraction (units U_o) were used to measure relative slow drift and DC offset between channels. The average amplitude during the baseline period (0.4 to 0.1s prior to stimulation onset) was computed for each trial over all channels. Then, for each channel, this baseline average was fit to a linear model with time of stimulation relative to the start of the stimulation session as the predictor variable. Nonzero y-intercept was used as a measure of DC offset and nonzero slope was used as a measure of signal drift over the course of the session.

To confirm that this method captured low frequency noise, we added additional low frequency (0.0001 Hz) noise at a high amplitude relative to baseline (50 or $100U_o$, for an amplitude gain of 0.5 or $1U_o$ over 100s). This introduced additional baseline drift which was captured by linear modeling (B.1A).

B.2 Line noise

The Welch power spectral density from 1 to 200 Hz (MATLAB's built-in pwelch function with 1s Hanning windows and 50% overlap) was computed from individual and averaged trials of the overall normalized, baseline corrected signal (units U_{o-bl}). The result was converted to dB/Hz and normalized power at 60Hz and harmonics (120, 180Hz) was extracted. Addi-

tionally, using MATLAB's built-in findpeaks function, the presence or absence of a narrow peak at each of these frequencies, consistent with the bandlimited power increases caused by line noise, was noted. Finally, the baseline periods were Fast Fourier Transformed (FFT; using MATLAB's fft function) to extract the relative amplitudes of line noise oscillations for a given trial or CCEP average. The maximum amplitude value in a frequency window ± 5 Hz from 60Hz and harmonics was taken.

To confirm the efficacy of our methods of measuring 60Hz noise, we measured power and frequency in the same signal after adding additional 60 Hz oscillations at an amplitude of 1 or $2U_{o-bl}$ (B.1B). Commensurate changes in power spectral density and amplitude were seen with these increases in noise.

B.3 High frequency noise

We took the FFT of the baseline period using MATLAB's fft function. The sum and RMS of amplitudes for frequencies between 250Hz and 2000Hz were computed. To confirm that this was an effective metric of the high-frequency components of white noise, we added Gaussian white noise at signal-to-noise ratios of 10 and 5 (with lower signal-to-noise ratios indicating higher noise contribution; using the agwn function in MATLAB's Communications toolbox). Commensurate changes in the sum and RMS of high frequencies of the FFT were seen alongside these increases in noise (B.1C).

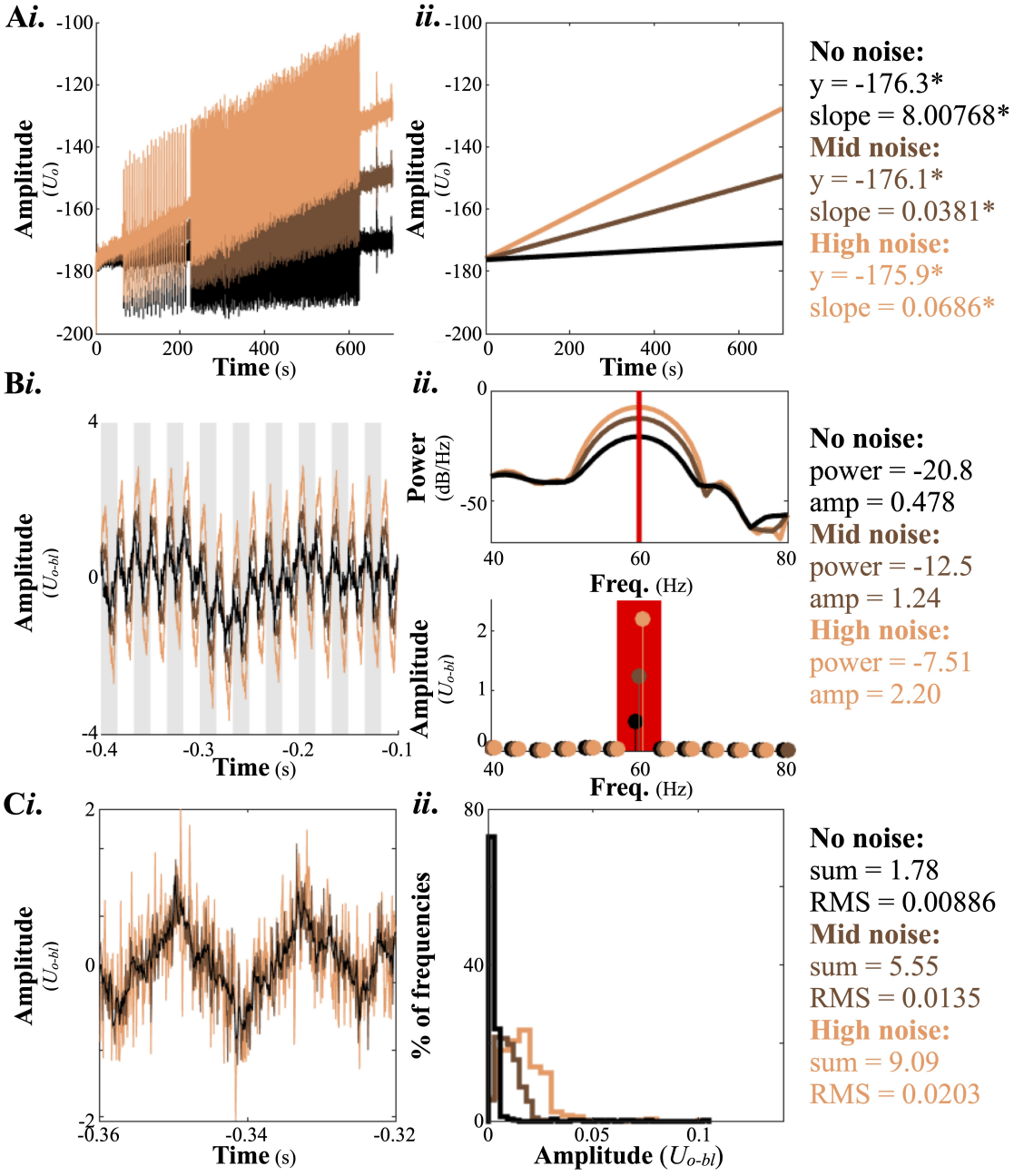

Figure B.1: Electrode placement. ECoG (A) and DBS (B) electrode locations shown for the 6 subjects in MNI space. For ECoG strips, electrode 1 was the most posterior and electrode 8 was the most anterior. The 4 gray bands on each DBS contact (B) represent the contacts, with electrode 0 the deepest and electrode 3 the most superficial (Medtronic naming conventions). GPe, globus pallidus external segment; GPi, globus pallidus internal segment; STN, subthalamic nucleus.